

8-26-2010

Submarine Groundwater Discharge: Its Measurement and Implications For Nutrient Inputs and Biogeochemical Processes in the Nearshore Coastal Zone

Benjamin M. Mwashote
Florida State University

Recommended Citation

Mwashote, Benjamin M., "Submarine Groundwater Discharge: Its Measurement and Implications For Nutrient Inputs and Biogeochemical Processes in the Nearshore Coastal Zone" (2010). *Electronic Theses, Treatises and Dissertations*. Paper 2154. <http://diginole.lib.fsu.edu/etd/2154>

This Dissertation - Open Access is brought to you for free and open access by the The Graduate School at DigiNole Commons. It has been accepted for inclusion in Electronic Theses, Treatises and Dissertations by an authorized administrator of DigiNole Commons. For more information, please contact mvandegrift@fsu.edu.

THE FLORIDA STATE UNIVERSITY
COLLEGE OF ARTS AND SCIENCES

SUBMARINE GROUNDWATER DISCHARGE: ITS MEASUREMENT AND
IMPLICATIONS FOR NUTRIENT INPUTS AND BIOGEOCHEMICAL PROCESSES
IN THE NEARSHORE COASTAL ZONE

By

BENJAMIN MKOJI MWASHOTE

A Dissertation Submitted to the
Department of Earth, Ocean and Atmospheric Science
in Partial Fulfillment of the
Requirements for the Degree of
Doctor of Philosophy

Degree Awarded:
Fall Semester, 2010

The members of the Committee approve the dissertation of Benjamin Mkoji Mwashote successfully defended; August 26, 2010.

William C. Burnett
Professor Directing Dissertation

Xiaolong (Bill) Hu
University Representative

Jeffrey P. Chanton
Committee Member

William M. Landing
Committee Member

Joel E. Kostka
Committee Member

Approved:

Lynn Dudley, Chair, Department of Earth, Ocean and Atmospheric Science
The Graduate School has verified and approved the above named Committee Members

DEDICATION

To my beloved dad, the late Abel Mwashote Aaron, who passed while this work was in progress. Its success serves as a tribute to his consistent Godly counsel and deep fear of God (Proverbs 1: 7; 10: 27) during his entire earthly sojourn. This precious impartation has undoubtedly remained a constant source of inspiration to me...

ACKNOWLEDGEMENTS

I am sincerely grateful to Bill Burnett for the opportunity to work with him over the years on research projects comprising this dissertation. His unmatched professional capacity to constantly keep track of the work – literally on a 24/7 basis, even through email, phone and courier services whenever he was away on overseas research, is a virtue I have found worthy emulating. Jeff Chanton is much appreciated for his ever willingness to help whenever any type of help was needed – especially in furnishing handy, yet appropriate creative solutions. Bill Landing, Joel Kostka and Bill Hu who also ably served as members in my committee, are greatly appreciated for their invaluable support that contributed immensely to the success of this work.

I am thankful to the various research colleagues with whom I have worked at field, laboratory and interacted variously during the course of this study. Specific mention of this, as well as the various sources of research funding, are appropriately included at the end of each chapter. Guebuem Kim is appreciated for providing the initial special temperature sensors that were utilized during preliminary work on development of the innovative continuity - SGD measuring device, VoST, which is still undergoing further research (Appendix B).

The Florida State University (FSU) Department of Geology (now part of EOAS), is particularly acknowledged for availing use of their cold room facility (the Antarctic Marine Geology Research Facility) for conducting special low temperature seepmeter calibrations. Anne Womack, Stephanie Brimm and Fran Bollmann are sincerely appreciated for insuring constant supply of all research needs during the study, while Michaela Lupiani is appreciated for ably taking care of all academic administrative aspects. William Dewar, Susan Stetson and Diane Grubbs are cordially acknowledged for their all round support in diverse departmental administrative matters during the study.

I am especially thankful to Bishop John E. Baker and the wonderful spiritual family at New Hope International Outreach Ministries (NHIOM). This is a special Church home where my family and I have been spiritually nourished ever since arriving in Tallahassee.

Special gratitude is to my home country's research institution, the Kenya Marine and Fisheries Research Institute, for granting me the necessary extended study leave that will enable me accomplish what it takes to become an invaluable scientific asset. My sincere gratitude goes to the IFP-Ford Foundation for the PhD Fellowship award that enabled me undertake the PhD program at FSU. I also greatly appreciate the significant financial support I received from FSU through Teaching and Graduate Assistantships which went a long way in complementing my program.

Last but not least, I would like to deeply thank my dear wife Shainance and our lovely children Charity and David for their constant faith, prayer and unwavering support throughout the study, even when they had to put up with long hours, often days, of my absence from home during the numerous fieldworks that characterized this study.

TABLE OF CONTENTS

LIST OF FIGURES	ix
LIST OF TABLES.....	xiii
ABSTRACT.....	xiv
CHAPTER 1: INTRODUCTION TO THE DISSERTATION.....	1
Submarine Groundwater Discharge and its Significance.....	1
SGD Quantification.....	3
Research Objectives.....	4
Dissertation Format.....	5
CHAPTER 2: CALIBRATION AND USE OF CONTINUOUS HEAT-TYPE AUTOMATED SEEPAGE METERS FOR SUBMARINE GROUNDWATER DISCHARGE MEASUREMENTS.....	7
Introduction.....	8
Materials and Methods.....	12
Study Area.....	12
Bench Calibration.....	13
Field Measurements.....	16
Results and Discussion.....	16
Calibration.....	16
Salinity and Temperature Effects on Seepmeter - Measurements.....	19
Field Measurements.....	22
Comparison With Other SGD Methods.....	26
Conclusions.....	32
CHAPTER 3: ASSESSMENT AND REDUCTION OF ENVIRONMENTALLY INDUCED ARTIFACTS IN SUBMARINE GROUNDWATER DISCHARGE SEEPAGE METER MEASUREMENTS.....	34
Introduction.....	35
Materials and Methods.....	36
Study Area.....	36
Field Measurements.....	38
Results and Discussion.....	40
Relationship Between SGD_{seep} Measurements - and Sea level, Wind Speed and Direction.....	41
Relationship Between SGD_{rad} Measurements - and Sea Level, Wind Speed and Direction.....	48
Effect of Burying (Submerging) the Seepmeter - Benthic Chamber in Sediment and Application -	

of Blanks on SGD_{seep} Estimations.....	50
Comparison Between SGD_{seep} and SGD_{rad} - Estimates.....	57
Conclusions.....	63

CHAPTER 4: SUBMARINE GROUNDWATER DISCHARGE IN THE
SARASOTA BAY SYSTEM: ITS ASSESSMENT AND
IMPLICATIONS FOR THE NEARSHORE COASTAL
ENVIRONMENT..... 65

Introduction.....	66
Background.....	66
Significance and Objectives of Study.....	68
Study Area: Description of the Sarasota - Bay System.....	69
Materials and Methods.....	74
General Approach.....	74
Radon Measurements.....	74
^{222}Rn - Bottle Technique.....	74
Sediment Equilibration Experiments.....	76
^{222}Rn and ^{226}Ra Calculations.....	77
Continuous ^{222}Rn - Mode (CRM) Surveys... ..	78
SGD Estimates from ^{222}Rn	78
Estimation of ^{222}Rn from Diffusion.....	80
Methane Measurements.....	81
Seepage Meter Measurements.....	82
Resistivity Survey.....	85
Nutrient Measurements.....	86
SB System Flushing (Residence) Time Estimations. .	87
Results.....	87
Radon Determinations.....	87
Grab Samples.....	87
Continuous ^{222}Rn Mode (CRM) Surveys.....	88
Methane (CH_4).....	88
Continuous ^{222}Rn Mode (CRM) Fixed - Station Estimates.....	93
^{222}Rn End Member Estimates and Diffusive - Fluxes.....	95
Resistivity Surveys.....	99
Seepage Meter Measurements.....	105
Nutrient Concentrations.....	107
Discussion.....	110
SGD, Water Volumes and Residence Times.....	110
^{222}Rn Model and Seepage Meter SGD - Estimates.....	112

Relationship Between ^{222}Rn and CH_4	120
Resistivity Survey.....	121
Nutrient Fluxes in the SB System.....	123
Conclusions.....	128
CONCLUSION.....	130
APPENDIX A.....	132
APPENDIX B.....	137
DEVELOPMENT OF THE CONTINUITY DEVICE, VoST, AND ITS - APPLICATION IN THE QUANTIFICATION OF SUBMARINE - GROUNDWATER DISCHARGE	137
Derivation of Steady State Volume-Salinity-Temperature (VoST) - SGD Model Equation.....	137
Principle and Assumptions.....	137
Derivation.....	138
Recommendations for Further Developmental Research on VoST...	141
REFERENCES.....	144
BIOGRAPHICAL SKETCH.....	155

LIST OF FIGURES

Fig 2.1: Continuous heat-type automated seepage meter (Taniguchi and Iwakawa 2001), referred to in this paper simply as “seepmeter.”	11
Fig. 2.2: Diagrammatic representation of a typical seepmeter calibration set up. CCS stands for Constant Current Supply, an important current regulating unit (device) which is part of the seepmeter sensor - datalogger circuitry.....	14
Fig. 2.3: Sensor response at different flow rates (each held constant for ~30 mins) for seepmeter M3 (seepmeter tube flow rate range: 3.5 - 50 mL/min or ~2.0 to 28 cm/day). The error bars represent standard deviations on the voltage scale.....	17
Fig. 2.4: (A) Comparison between freshwater (FW) of salinity ~ 0, and seawater (SW) of ambient salinity ~ 35, seepmeter calibrations. The figure shows that the two plots are in agreement within 95% confidence interval (shown as red dotted outline, which was plotted for the FW plot). This shows that there is no significant difference between SGD seepmeter measurements taken in FW and SW within the same ambient environmental conditions. (B) Comparison between seepmeter calibrations conducted at low (cold room) temperature (LT: 1.1 - 3.3 °C) and at ambient (room) temperature (RT: 25 - 27 °C). The 95% confidence interval for the RT plot is shown as red a dotted outline.....	20
Fig. 2.5: Long term time series variations with water level of: (A) SGD, (B) Wind Speed and (C) Precipitation, during the period, 03 - 17 April 2007.....	23
Fig. 2.6: Long term time series variations with water level of: (A) SGD, (B) Wind Speed and (C) Precipitation, during the period, 06 - 13 March 2007.....	25
Fig. 2.7: Effect of the length of deployment duration periods, on seepmeter (q_s) and Lee-type (manual) meter (q_m) SGD relative estimates, expressed as a ratio (q_s/q_m). This is an example of a dawn to dusk deployment (including the initial ~ 4 h waiting period for stabilization of the seepage chambers following the deployments). Diamonds and squares represent two manual meters, M1 and M3 respectively. These were deployed next to the seepmeter benthic chambers.....	26
Fig. 2.8: Measurement of concurrent SGD variations with water level by: (A) seepmeter, and (B) an electromagnetic (EM) seepage meter, at FSUCML during the period: July 24-26, 2006 (notice close agreement in SGD trend and magnitude). The capability of an EM seepage meter to measure negative fluxes is evident (B). The two meters were deployed in close proximity. During deployment, specific conductivity decreased gradually (C)...	28
Fig. 3.1: Map showing the study area at FSUCML. The site location (N 29°55', W 84°31') is indicated in the map by an open triangular shape (index map source: http://www.mapquest.com/beta/maps).....	37

Fig. 3.2: Seepmeter benthic chamber deployment: (A) Unburied benthic chamber (typical normal deployment mode), (B) Buried benthic chamber.....	39
Fig. 3.3: Relationship between SGD_{seep} variations with: (A) Sea level, (B) Wind speed and (C) Wind direction, Θ (where, $\Theta = 180 - \text{actual angle}$, in degrees), for the period: 08 - 12 July'07. Buried chambers (the blank chamber was deployed inside a child's plastic play pool).....	42
Fig. 3.4: Relationship between SGD_{seep} variations with: (A) Sea level, (B) Wind speed and (C) Wind direction, Θ (where, $\Theta = 180 - \text{actual angle}$, in degrees), for the period: 05 - 11 August'07. Buried chambers (the blank chamber was deployed inside a child's plastic play pool).....	44
Fig. 3.5: Relationship between SGD_{seep} variations with: (A) Sea level, (B) Wind speed and (C) Wind direction, Θ (where, $\Theta = 180 - \text{actual angle}$, in degrees), for the period: 29 - 31 May'07. Unburied chambers.....	46
Fig. 3.6: Relationship between Sea Level and Wind speed for the period: 29 - 31 May'07.....	48
Fig. 3.7: Relationship between SGD_{rad} variations with: (A) Sea level, (B) Wind speed and (C) Wind direction, Θ (where, $\Theta = 180 - \text{actual angle}$, in degrees), for the period: 29 - 31 May'07.....	49
Fig. 3.8: Relationship between SGD_{blank}/SGD_{seep} ratio variations with: (A) Sea level, (B) Wind speed and (C) Wind direction, Θ (where, $\Theta = 180 - \text{actual angle}$, in degrees), for the period: 08 - 12 July'07.....	54
Fig. 3.9: Relationship between SGD_{blank}/SGD_{seep} ratio variations with: (A) Sea level, (B) Wind speed and (C) Wind direction, Θ (where, $\Theta = 180 - \text{actual angle}$, in degrees), for the period: 05 - 11 August'07.....	55
Fig. 3.10: Average long-term relationship between SGD_{seep} and SGD_{rad} with: (A) P1 Well water-level and (B) Monthly Rainfall. Error bars represent 1σ (standard deviation).....	58
Fig. 3.11: Average correlations between P1 well water - level and: (A) SGD_{seep} and (B) SGD_{rad} measurements. Each data point represents average monthly measurements from May'06 through February'07. Error bar represents 1σ (standard deviation).....	61
Fig. 4.1: Study area showing sampling sites for radon grab (bottle) samples, continuous radon monitor (CRM) transects and seepmeter SGD measurements within the Sarasota Bay system. For purposes of the study, the area was divided into three regions: North Region (NR, water volume $\approx 80\%$), Middle Region (MR, water volume $\approx 12\%$) and South Region (SR, water volume $\approx 8\%$). This is also the region referred to Sarasota Bay (SB). The assumed 200 m SGD regime area within the SB system is $\sim 7.8 \text{ km}^2$ ($\sim 8\%$ of the total SB area). The North Bay region lies on latitudes $\geq 27.3444^\circ \text{ N}$. Middle Bay	

(MB) is found within latitudes 27.3047 - 27.3444° N, while the South Bay region lies within latitudes 27.1250 - 27.3047° N.....	70
Fig. 4.2: Monthly rainfall variation around the Sarasota Bay region, July '02 - January'05 (Note that places with arrows indicate sampling periods). <i>Rainfall data source: Southwest Florida Water Management District, 2005</i>	73
Fig. 4.3: Conceptual box model for ²²² Rn model (Burnett and Dulaiova 2003).....	80
Fig. 4.4: Lee - type, manual seepmeter (Lee 1977; Taniguchi et al. 2003a). When water seeps into the chamber it displaces that is forced into a plastic bag attached to a tube in the top of the drum. The change in volume over a measured time interval provides the seepage rate.....	83
Fig. 4.5: Field manual seepage meter and “bottle” (²²² Rn) sampling (grab sampling using a peristaltic pump), within the Sarasota Bay system during: (A) Low tide and (B) High tide.....	84
Fig. 4.6: Summary of ²²² Rn and CH ₄ concentration distributions in the Sarasota Bay system during the period July'02 to July' 04. Each plotted point is derived from averaging five different points, representing five different time periods (or samples); n = 5.....	89
Fig. 4.7: Relationship between ²²² Rn and CH ₄ concentrations in the Sarasota Bay system, July'02, November'02 and March'03.....	90
Fig. 4.8: Scatter plots for ²²² Rn (CRM) survey transects conducted within the Sarasota Bay system showing salinity variations for two different periods (A) 27 - 28 May'03 and (B) 18-19 August 2004. In both periods, the plots clearly depict lowest salinities, coinciding with the highest ²²² Rn concentration levels in the South Region relative to the other regions.....	92
Fig. 4.9: Variations over time of seawater ²²² Rn concentrations (dpm/L) and water level at two fixed stations: (A) Roberts Bay, RB - Middle Bay (Mean concentration = 39.4 ± 7.3 dpm/L) and (B) at the New College, NC - North Bay (Mean concentration = 38.9 ± 7.2 dpm/L), within the Sarasota Bay system during a time series monitoring, 8 - 12 January 2003.....	94
Fig. 4.10: Depth ²²² Rn concentration profiles (based on piezometer sampling) from the Sarasota Bay System: (A) North Bay region (NC site) and (B) Mid Bay region (RB site). Values shown by arrows are mean bottom water ²²² Rn concentrations. The shaded band indicate the margin for the equivalent equilibrium concentration zone (390 ± 180 dpm/L).....	98
Fig. 4.11: Map showing location of resistivity surveys and dates of acquisition. Inverted resistivity values within the water column (one meter below water surface).....	100

Fig. 4.12a: Location of resistivity Lines A and B. Blue dots show path of seismic profile acquisition (May'03).....	101
Fig. 4.12b: Locations of resistivity lines F, G, and H run at location of seismic line within the Sarasota Bay system (May'03).....	102
Fig. 4.13: Sample line segments for resistivity survey taken from the northern Sarasota Bay system near New College.....	103
Fig. 4.14: Line sections (as indicated in Fig. 4.12) in the southern bay (Little Sarasota Bay) showing resistivities that decrease around ten meters depth. The 3 different resistivity surveys were run over the location of the seismic surveys at essentially the same time.....	104
Fig. 4.15: Variations over time of estimated advection rate (cm/day) with water level at fixed sites: (A) at the New College, NC - North Bay (Mean advection = 43 ± 20 cm/day) and (B) at Roberts Bay, RB - Middle Bay (mean advection = 46 ± 21 cm/day), within the Sarasota Bay system during a time series monitoring, 8-12 January 2003. Groundwater end member used was 390 ± 180 dpm/L.....	114
Fig. 4.16: A scatter plot of synchronized ^{222}Rn - SGD (cm/day) estimates (CRM) at the two time series sites, NC (North) and RB (Middle) within the Sarasota Bay system, 8 - 12 January 2003.....	116
Fig. 4.17: Average advection (^{222}Rn model) within the Sarasota Bay system, July'02, November'02 and March'03.....	117
Fig. B.1: Field temperature measurements using VoST device: Temperature sensors installed inside benthic chamber without bottom barrier.....	142
Fig. B.2: Field temperature measurements using VoST device: Temperature sensors installed inside benthic chamber with bottom barrier.....	142

LIST OF TABLES

Table 2.1: Comparison between mean seepmeter SGD rates and those derived via the radon model for selected months, FSUCML research site.....	30
Table 2.2: Comparison of SGD rates between this study and other studies.....	31
Table 3.1: Summary of correlation analysis between SGD measurements and environmental variables.....	51
Table 3.2: Comparison of SGD measurements obtained from buried and unburied benthic seepmeter chambers and relative difference between SGD_{seep} and SGD_{rad}	59
Table 4.1: Estimates of physical characteristics of the Sarasota Bay system (SBEP 2006; FGS open file report 10 Geology of Sarasota Co. 1985).....	72
Table 4.2: Average seawater ^{222}Rn and CH_4 concentrations in the Sarasota Bay system during the period July'02 to July'04 for bottle samples; 18 - 19 August'03 for CRM survey.....	91
Table 4.3: Results of sediment equilibration experiments from the Sarasota Bay system, May03 – March'04.....	96
Table 4.4: Quantitative estimations of SGD and nutrient fluxes within the different regions of the Sarasota Bay System.....	106
Table 4.5: Seawater nutrient concentration levels in the Sarasota Bay system. Sampling conducted on 04 January and 04 March'04 for all the SB system regions (North, Middle and South).....	108
Table 4.6: Average groundwater nutrient concentrations in wells found within the vicinity of the SB system.....	109
Table 4.7: SGD - advection and diffusive flux estimations using different approximation approaches within the Sarasota Bay system.....	111
Table 4.8: Comparison of nutrient flux rates and N/P ratios between this study and other studies.....	127
Table A.1: Groundwater $NO_2 + NO_3$ concentrations (μM) in wells in vicinity of SB system.....	132
Table A.2: Groundwater PO_4 concentrations (μM) in wells in vicinity of SB system...	133
Table A.3: Groundwater NH_4 concentrations (μM) in wells in vicinity of SB system...	135

ABSTRACT

Submarine groundwater discharge (SGD) assessments conducted both in the laboratory and at a field site in the northeastern Gulf of Mexico, using a continuous-heat type automated seepage meter (seepmeter) have shown that the device has the potential of providing long-term, high-resolution measurements of SGD. The improvements on the device using a simple inexpensive laboratory set up, have shown that: (1) connecting an extension cable to the seepmeter has a negligible effect on its measuring capability and, (2) influence of very low temperature ($\leq 3\text{ }^{\circ}\text{C}$) on seepmeter measurements can be accounted for by conducting calibrations at such temperatures prior to field deployments and, (3) salinity had no significant effect on the performance of the seepmeter. Calibration results from fresh water and sea water showed close agreement at a 95% confidence level significance between the data sets from the two media ($R^2 = 0.98$).

The observed artifacts on seepmeter measurements associated with Bernoulli-induced flow, the vertically directed flow arising due to water movement across topographic features can significantly be reduced by burying (or submerging) the seepmeter to nearly the same level as the sediment topography. While the study revealed that in general wind speeds $> 6\text{ m/s}$ were associated with enhanced SGD measurements in seepmeters with buried and unburied benthic chambers, the influence was greater in the unburied meters, and more pronounced for SGD rates $< 2\text{ cm/day}$. Comparatively, the seepmeter SGD measurements provided data that are comparable to manually-operated seepage meters, the radon geochemical tracer approach, and an electromagnetic (EM) seepage meter.

Study of the Sarasota Bay (SB) system revealed SGD advection rates ranging from 0.7 to 24.0 cm/day, except for rare isolated hot spot occurrences where higher rates were observed. In general, SGD estimates were relatively higher in the middle and south regions (5.9 – 24.0 cm/day) compared to the north region (0.7 – 5.9 cm/day). Although no obvious seawater nutrient concentration trend was revealed, the average N/P ratio was higher in the north compared to the middle and south regions of the SB system. The importance of SGD was evident in that about 40% of the regional nutrient fluxes were

observed in the north while ~ 60% occurred in the middle and south regions combined. The latter two regions also had the highest overall nutrient flux per water volume ratio, compared to the north region, thus making them potentially more vulnerable to eutrophic conditions. On average, we estimate about 27% of total dissolved N in the SB system was derived via SGD.

CHAPTER 1

INTRODUCTION TO THE DISSERTATION

Submarine Groundwater Discharge and its Significance

Exchange between submarine groundwater discharge (SGD) and overlying surface waters is recognized as being important due to potential impacts resulting from anthropogenic land uses. The most general definition of groundwater is water in the saturated zone of geologic material (Visser 1980; Fetter 1988). Water in the pores of submerged sediments or rock is, therefore, “groundwater” since the geological material below the seafloor will be saturated. In view of the foregoing considerations, the latest generalized definition of SGD that has been modified from an earlier version (Burnett et al. 2003) is thus,

...the flow of water through continental margins from the seabed to the coastal ocean, with scale lengths of meters to kilometers, regardless of fluid composition or driving force (Moore 2010).

Groundwater discharge originates inland and carries with it contaminants or nutrients, dissolved or colloidal, that have the potential to impact the chemical budget of surface water ecosystems. This impact, both chemical and physical may be heightened in smaller bodies of water such as embayments or lagoons due to their limited volume and restricted fluid exchange with the open ocean. In addition to these freshwater inputs, groundwater discharge occurs as saltwater re-circulation induced by tides and other driving forces.

SGD can vary widely over time and space. Short period water waves stir or agitate pore water without, necessarily, producing any net flow. This has been referred to as ‘wave pumping’ or “wave stirring” (Harrison et al. 1983). If the density of the ocean water increases above that of pore water for any reason, pore water can float out of the sediment by gravitational convection in an exchange with denser seawater, without net

discharge. The process has been referred to as “floating” (Thorstenson and Mackenzie 1974) or “salt fingering” (Gorsink and Baker 1990). SGD has also been referred to as “flushing.” This generally involves a continuous replacement of pore water involving a discharge driven by the hydraulic gradients on shore or pressure gradients in the coastal ocean. Gradients may be due to wave set-up at the shore (Li et al. 1999), tidal pumping at the shore (Nielsen 1990; Santos et al. 2009), or differences in tidal elevations across narrow reefs or barrier islands (Reich et al. 2002).

Groundwater in any aquifer typically flows from areas of high hydraulic head defined as the elevation to which water rises in a well to areas of low hydraulic head under the force of gravity. Although groundwater flows downhill, it often follows a tortuous path through small pores in the aquifer material, typically slowing its flow to a crawl. Unlike surface waters that move at noticeably rapid rates, groundwater may only move a few centimeters in a day. Ultimately, it flows into the coastal ocean through seeps and springs, thus completing the continuous water cycle between land, ocean, and atmosphere.

In general the driving forces for groundwater flow and its eventual seepage in the coastal zone include hydraulic gradients, buoyant forces and biological forces (McKenna and Martin 2004). SGD occurrence is a result of a hydraulic connection and a positive pressure gradient between shallow or deep coastal aquifers and the sea and occurs as diffuse seepage along the shoreline, offshore seepage or spring discharge. Near-shore diffuse seepage is typical for shallow, unconsolidated, coarse-grained aquifers (Portnoy et al. 1998; Valiela et al. 1990) or in the sand, clay and limestone mixtures of shallow aquifers in Florida (Cable et al. 1997). The magnitude of this type of seepage generally decreases with increasing water depth and distance from the coast (Cable et al. 1997; Giblin and Gaines 1990 and Taniguchi et al. 2002). Typically coastal aquifers are classified depending on their hydrology, either as shallow - local flow systems, or deep - intermediate or regional flow systems (Toth 1963). Long term data (Australian Bureau of Meteorology 2001) reveal that shallow aquifers are characterized by high rates of recharge (0 – 0.35 m/yr) and high rates of groundwater flow (1 – 100 m/yr). Rates of recharge and water levels respond rapidly to individual precipitation events (Santos et al.

2009). Deep aquifers on the other hand, are much less connected with the surface and generally associated with lower rates of recharge (0.01–1 cm/yr) with concomitant low flow velocities (0.1–1 m/yr) in general (Lovely and Chapelle 1995).

Although SGD is a potentially important source of nutrients and other dissolved components to the coastal ocean, it has so far remained poorly quantified (Burnett et al. 2001; Johannes 1980; Moore 1999). An accurate insight into the magnitude and controls of these components, especially the nutrient fluxes (nitrogen, N and phosphorus, P) associated with SGD is necessary if we are to clearly understand the functioning of the coastal ocean and how it responds to anthropogenic and natural perturbations. Apart from the amounts of N and P entering the coastal ocean through SGD, it is also important to evaluate the potential effect of SGD on the ratio of N and P in coastal waters, because this ratio determines which nutrient is limiting phytoplankton growth (Howarth 1988). For instance, in rivers the flux ratio of dissolved inorganic nitrogen (DIN) and dissolved inorganic phosphorus (DIP) has been found to be variable within a range of at least two orders of magnitude (Caraco 1995; Meybeck 1993).

SGD Quantification

In general, three principle approaches are used to estimate the SGD magnitude. These include: (1) direct measurement using manual or automated seepage meters, (2) a suite of isotopic techniques that use geochemical tracers to compute the rate or amount of SGD present in the water column above the sea bed, and (3) hydrogeologic modeling.

Of the above available approaches however, SGD has traditionally often been measured using the first type of method (both manual and automated), by employing the open cut-off end of a 55-gallon steel drum that is pushed into the bottom sediment (Israelsen and Reeve 1944; Lee 1977). The groundwater head of the adjacent upland area induces the groundwater to seep into the drum funnel, and for the case of the manual seepage meter, a plastic bag attached to a tube in the top of the drum catches the seepage. After a period of time, the bag is removed from the tube and the cumulative discharge is measured. This

conventional bag method has been applied in various hydrogeologic settings, including lakes, reservoirs, rivers, estuaries and coasts, but subsequent studies have revealed several limitations inherent of this method (Taniguchi and Fukuo 1993; Cable et al. 1997; Burnett et al. 2003; Mwashote et al. 2010).

In an attempt to alleviate complications encountered with the conventional bag method of measuring SGD, a host of different automated seepage meters have recently been developed (Taniguchi and Iwakawa 2001; Taniguchi and Fukuo 1993; Krupa et al. 1998; Paulsen et al. 2001; Sholkovitz et al. 2003; Rosenberry & Morin 2004). There are also other approaches for SGD estimation that are based on geochemical tracers (Rn and Ra) that have been found to provide internally consistent results and modeling (Moore 1996, 1999, 2010; Burnett et al. 2002; Burnett and Dulaiova 2003).

Research Objectives

The thrust of this research work hinged around SGD quantification with a view to assessing as well as improving the continuous heat-type automated seepage meter (seepmeter) SGD measuring method to enable it become more reliable and achieve wider application in SGD study. The main objectives were to:

- (1) design and construct an in-house calibration system for the seepmeter with a view to improving its SGD measurement capability in a practical sense;
- (2) assess the effects and reduction of artifacts induced by environmental factors (variations in seawater level, wind speeds and wind direction) on seepmeter SGD measurements ;
- (3) assess the relative significance of SGD to the nearshore coastal environment via a case study using Sarasota Bay, Florida

(4) assess on comparative terms, the reliability of seepmeter SGD measurements relative to those obtained independently using manual seepage meters, geochemical tracers, an electromagnetic seepage meter and sub-seaflow resistivity measurements.

Dissertation Format

In **Chapter 2**, the first objective of this research was addressed. This chapter describes a detailed study conducted in the laboratory and at a study site in the northeastern Gulf of Mexico next to the Florida State University Coastal and Marine Laboratory (FSUCML). The study which was just published in the Journal of Estuarine, Coastal and Shelf Science (Mwashote et al. 2010), reports important findings on the functioning and improvements carried out on the seepmeter. This study describes a simple calibration method for the seepmeter and results using the calibrated devices in SGD measurements in the field. In particular, results of SGD measurements are described for seepmeters in which a 76.2 m (250 ft) electrical extension cables are connected. The results of effects of salinity and low temperature on seepmeter SGD measurements are also discussed. Finally, the seepmeter SGD estimations are compared with those made using the radon geochemical tracer technique, manual seepage meters, and an EM seepage meter.

Chapter 3 presents the results of a study conducted to assess the influence of environmentally induced (Bernoulli-related flow) artifacts in SGD seepmeter measurements (SGD_{seep}), and the practical ways of reducing these artifacts to enable benthic chamber based seepage meters to remain viable tools in SGD measurements. This detailed study addresses the second research objective. The study analyzes the relationship between SGD_{seep} estimations and environmentally induced sea level (tidal) and wind speed variations. The effects of burying (submerging) seepmeter benthic chambers into the sediment and use of blank chambers to evaluate artifacts in SGD_{seep} estimations were also assessed. Additionally, comparative long-term SGD_{seep} obtained by direct seepmeter measurements with those obtained via the ^{222}Rn geochemical tracer approach (SGD_{rad}), are described in this chapter.

Chapter 4 describes the detailed results of the of SGD measurements in Sarasota Bay and its significance to the overall water and nutrient budgets of the bay system. This study covered the third research objective. In this chapter, detailed findings of the comparative assessment of three independent approaches in the SGD measurements are reported. These independent approaches included the manual seepage meters, geochemical tracers (^{222}Rn , CH_4) and a relatively new technology for sub-seafloor resistivity measurements, which was used to locate and characterize subsurface salinities within the bay system.

CHAPTER 2

CALIBRATION AND USE OF CONTINUOUS HEAT-TYPE AUTOMATED SEEPAGE METERS FOR SUBMARINE GROUNDWATER DISCHARGE MEASUREMENTS

Publication Status:

B. M. Mwashote; W. C. Burnett; J. Chanton; I. R. Santos; N. Dimova; P. W. Swarzenski. 2010. Calibration and use of continuous heat-type automated seepage meters for submarine groundwater discharge measurements, *Estuarine Coastal and Shelf Science*, 87: 1 – 10.

Abstract

Submarine groundwater discharge (SGD) assessments were conducted both in the laboratory and at a field site in the northeastern Gulf of Mexico, using a continuous-heat type automated seepage meter (seepmeter). The functioning of the seepmeter is based on measurements of a temperature gradient in the water between downstream and upstream positions in its flow pipe. The device has the potential of providing long-term, high-resolution measurements of SGD. Using a simple inexpensive laboratory set up, we have shown that connecting an extension cable to the seepmeter has a negligible effect on its measuring capability. Similarly, the observed influence of very low temperature (≤ 3 °C) on seepmeter measurements can be accounted for by conducting calibrations at such temperatures prior to field deployments. Compared to manual volumetric measurements, calibration experiments showed that at higher water flow rates (> 28 cm/day or $\text{cm}^3/\text{cm}^2\cdot\text{day}$) an analog flow meter overestimated flow rates by $\geq 7\%$. This was apparently due to flow resistance, turbulence and formation of air bubbles in the seepmeter water flow tubes. Salinity had no significant effect on the performance of the seepmeter. Calibration results from fresh water and sea water showed close agreement at a 95% confidence level significance between the data sets from the two media ($R^2 =$

0.98). Comparatively, the seepmeter SGD measurements provided data that are comparable to manually-operated seepage meters, the radon geochemical tracer approach, and an electromagnetic (EM) seepage meter.

Introduction

One of the most challenging areas for investigating submarine groundwater discharge (SGD) is properly quantifying its diffuse and ephemeral nature. Much research has therefore focused on this aspect, with an overall aim of developing reproducible and reliable groundwater discharge rates. Numerous studies continue to be conducted to estimate the magnitude of SGD in various types of coastal environments, using varied techniques and methods. For instance, Taniguchi et al. (2002) presented a review of studies that have attempted to estimate the magnitude of SGD or have indicated that SGD is significant. Some of the methods available in this respect include: seepage meters, piezometers, geochemical or geophysical tracers and modeling (Lee 1977; Robinson et al. 1998; Burnett and Dulaiova 2003; Sholkovitz et al. 2003).

Conventionally, SGD has often been measured using a manually-operated seepage meter. This is usually an open, cut-off end of a 55-gallon steel drum (of base cross section area 2550 cm^2) that is pushed into the bottom sediment (Israelsen and Reeve 1944; Lee 1977). The groundwater head of the adjacent upland area or some tidal processes can then induce groundwater to seep into the drum (i.e., funneling). A plastic bag attached to a tube above the drum can collect the displaced water. After a set period of time, the bag is periodically removed from the tube and the cumulative discharge can be measured. This conventional bag method has been applied in various hydrogeologic settings, including lakes, reservoirs, rivers, estuaries, and coastal areas (Lee 1977; Shaw and Prepas 1989; Shinn et al. 2002).

Subsequent studies however, have shown that this method may have some limitations (Taniguchi and Fukuo 1993; Cable et al. 1997; Shinn et al. 2002). First, it is cumulative and therefore it cannot provide information on the temporal evolution of seepage during

the collection period (typically 30 minutes to several hours). Second, it cannot accurately measure reverse flow or resolve small fluctuations in seepage, such as those induced by tides. Third, measurement artifacts can readily arise from frictional resistance along the internal boundary of the meter, attachment tube and reservoir bags.

The short-term influx of water after the plastic bags have been attached to the seepage meter has also been reported as a common draw back associated with manual seepage meters (Shaw and Prepas 1989, 1990a,b; Shinn et al. 2002). In their detailed study of this particular problem, Shaw and Prepas (1989) have shown that the problem is not caused by fluctuations in seepage rates due to hydrological process but rather, it is directly associated with mechanical properties of the plastic bags themselves. Their study further showed that the short-term influx problem can be alleviated by pre-filling the plastic bag with one liter of water before attaching it to the manual seepage meter. In addition to all the confounding factors mentioned above in using the conventional bag method, it is also very labor intensive (Taniguchi and Iwakawa 2001; Shinn et al. 2002; Cable et al. 2004).

In an attempt to address some of these difficulties, a number of different types of seepage meters have been developed. These include, heat pulse meters (Taniguchi and Fukuo 1993; Krupa et al.1998), the continuous automated heat-type seepage meter as used here (Taniguchi and Iwakawa 2001), ultrasonic groundwater seepage meters (Paulsen et al. 2001), dye-dilution meters (Sholkovitz et al. 2003), and the autonomous electromagnetic (EM) seepage meter (Rosenberry and Morin 2004; Swarzenski et al. 2004). These automated approaches are able to detect low levels of flow rates, in addition to providing higher sampling frequency and resolving artifacts associated with the plastic bags, but not other artifacts. Despite the potential errors and detection limits inherent in the manual devices field evaluations of the "Lee-type" manual meters showed that consistent results can be obtained if one takes these potential problems into account (Cable et al. 2004; Taniguchi and Iwakawa 2001).

The continuous heat-type automated seepage meter (Fig. 2.1), referred to here simply as seepmeter, is based on the "Granier" method commonly used in sap flow meters that are

intended to measure water flux in trees (Granier 1985; Taniguchi and Iwakawa 2001). The method is based on the effect of water flow velocity on a temperature gradient established along a flow tube. The temperature difference between two points in the tube is at a maximum under no-flow conditions and progressively decreases with increasing water flow velocity. As originally designed, the seepmeter has the potential of providing long-term and high-resolution SGD measurements.

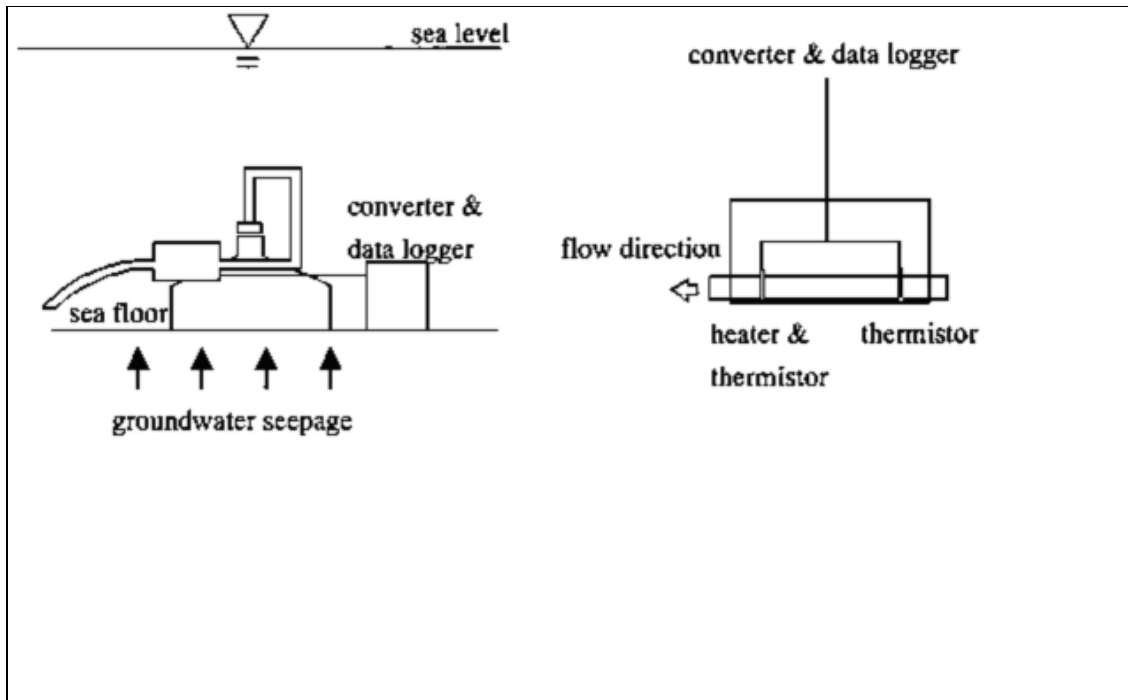


Fig 2.1: Continuous heat-type automated seepage meter (Taniguchi and Iwakawa 2001), referred to in this paper simply as “seepmeter.”

Due to lengthy field work necessary for SGD measurements, there has been the need to modify the seepmeter to improve the datalogger robustness, and make the whole set up easier and more user friendly. Normally when such meters are used for field measurements, it is necessary to employ the services of a boat, anchored next to the site where measurements are to be conducted. The anchored boat serves to accommodate the associated accessories for the seepmeter, namely, the datalogger and batteries. With frequent use of seepmeters for our SGD work however, we have increasingly found this practice not only expensive and cumbersome, but also jeopardizes the safety of the seepmeter accessories that are anchored in the boat, including the laptop computer used for the required frequent downloading of data. For example, the equipment has often

been drenched with seawater during stormy sea or rainy weather conditions. Even when working during non stormy, calm and dry weather, the typical saturated humidity conditions are usually not conducive to long storage of any electronic equipment during extended deployment periods that are of interest in most field seepmeter measurements. Therefore we explored the possibility of modifying the seepmeter by attaching a suitable length of electrical cable that would enable the datalogger, batteries and other accessories to be controlled from the seashore during deployments in the sea. This is a potentially feasible solution since most seepmeter SGD measurements are conducted at nearshore areas where SGD is known to be most prevalent. This arrangement offers a robust set up with considerable advantages, especially for long-term deployments. It is a viable less expensive alternative to using a boat or waterproof equipment casements in the sea.

The purpose of this study was to devise a simple calibration method for the seepmeter and test the calibrated devices in SGD measurements in the field. Specifically, we planned to: (1) set up and test an inexpensive calibration approach for the seepmeters (2) assess the effect on seepmeter measurements, of introducing a 76.2 m (250 ft) electrical extension cable to the seepmeter to facilitate its positioning and handling in the field. (3) assess the effect of salinity and low temperature on seepmeter measurements and (4) compare field seepmeter SGD measurements with those made using the radon geochemical tracer technique, manual seepage meters, and an EM seepage meter.

Materials and Methods

Study Area

Field measurements were carried out at a study site located in the northeastern coastal Gulf of Mexico, an area known for the presence of seepage and submarine springs (Cable et al. 1997; Burnett 1999). The area (N 29° 55' W 84S 31') lies within the Woodville Karst Plain, which extends from about 80 km inland to the coastal zone where the Florida State University Coastal and Marine Laboratory (FSUCML) is located at Turkey Point, Franklin County, Florida. The horizontal hydraulic conductivity of the unconfined aquifer (within the depth of 0 – 6 m) in the study area is estimated from slug tests to range from

1.2×10^{-5} to 2.9×10^{-2} cm/s (Li et al. 2009). A more detailed description of the study area is given elsewhere (Bugna et al. 1996; Santos et al. 2008, 2009).

Bench Calibration

A series of bench calibration experiments were conducted with a total of five seepmeters (M1, M3, M4, M5, M6). In these experiments, controlled and constant water flow rates were provided to the seepmeter from a constant head reservoir (Fig. 2.2). An analog flowmeter (Key Instruments, FR4000 Series) was mounted in series to monitor and control the flow rate. The outflow water through the seepmeter was periodically collected into a measuring cylinder to quantitatively determine the actual flow rates. The laboratory set up consisted of the horizontally submerged seepmeter being tested, in a continuously overflowing tank of water fed from a constant head reservoir. The continuously overflowing water tank precluded any local temperature artifacts from developing around the submerged seepmeter.

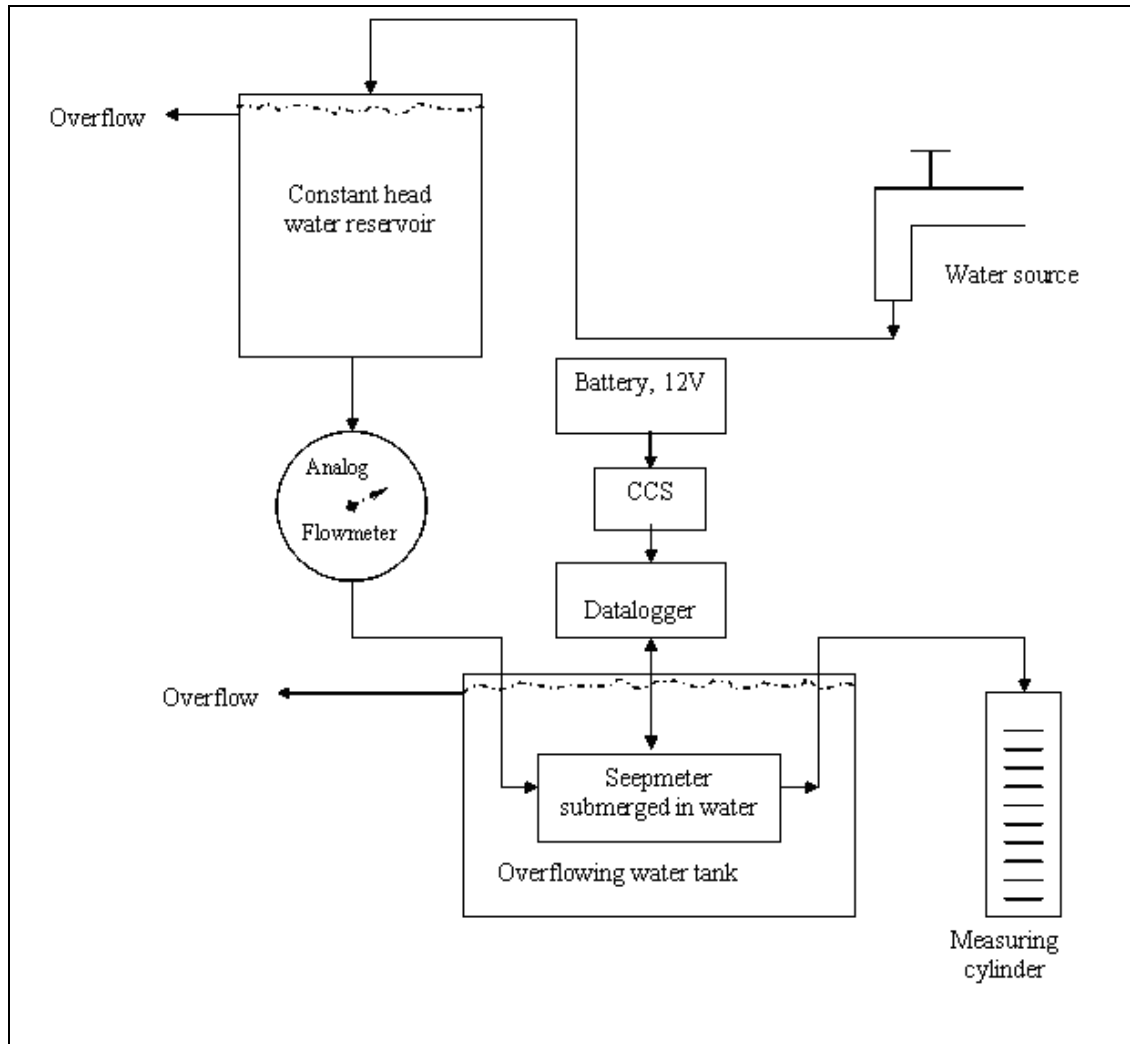


Fig. 2.2: Diagrammatic representation of a typical seepmeter calibration set up. CCS stands for Constant Current Supply, an important current regulating unit (device) which is part of the seepmeter sensor – datalogger circuitry.

The seepmeter functions by measuring the temperature difference between two points by means of thermistor probes (seepmeter sensor). At one point in the flow tube there is a small heating element that creates a temperature gradient between the two probes. The temperature difference between the heating point and the downstream probe is recorded as a voltage change and used to calculate the rate of seepage flow (Taniguchi and Iwakawa 2001). Theoretically, if the water were to flow infinitely fast, the two probes would be at exactly the same temperature. The frequency and sampling durations are all

programmed into a data logger (Data Hog 2, Skye Instruments Limited, UK). During calibration, the datalogger captures and stores measurements of various flow rates in voltage units.

Flow rates determined volumetrically are more reliable compared to relying on the flow meter readings which are often subject to factors such as internal flow resistance and bubble formation that take place within the seepmeter flow tube (Taniguchi and Iwakawa 2001). The volume collected divided by the time of collection gives the accurate discharge rate, while the seepmeter provided a continuous record of voltages via the datalogger.

In order to investigate the effect of attaching a 76.2 m extension cable to a seepmeter on the seepmeter measurements, calibrations were run with and without the extension cable connected. Calibration tests were conducted in the laboratory at several selected constant flow rates, ranging from 0 to ~7000 cm/h (equivalent to field seepage rates of 0 to ~ 85 cm/day), for an uninterrupted period of time of half to one hour (Fig. 2.2). Sampling intervals were set at every two minutes and logged every ten minutes to the datalogger.

Further laboratory investigations were also conducted to test whether salinity and low temperatures can affect SGD seepmeter measurements. The former test was done by running simultaneous calibrations using seawater and freshwater, while the latter experiment was performed by running calibrations at both low (1 – 3 °C; cold room) and ambient (25 – 27 °C; room) temperatures, respectively. Measurements using the seepmeter in the field are based on the commonly used technique (Fig. 2.1) of placing an open ended benthic chamber into the seabed to capture SGD (Taniguchi and Iwakawa 2001).

The laboratory computation of flow rate, in cm/h, is done by dividing the volume (cm³) of water that flows through the seepmeter and collected in the measuring cylinder, by the seepmeter tube cross-section area (cm²), then dividing this result by the time taken, t (h) for the volume of water collected (i. e., cm³/cm².h). Field SGD seepage rates (cm/day)

can subsequently be computed from the above relationship after taking into account the area ratio of the seepmeter chamber (2550 cm²) to the flow tube (1.327 cm²), since all the seepage water (SGD) that comes through the seepmeter tube in the field is collected over the entire area that is covered by the seepmeter benthic chamber at the deployment site.

Field Measurements

In the field, the seepmeters were deployed on top of cutoff sections of 55-gallon drums as used for Lee-type seepage meters (Lee 1977). Each seepmeter deployment for SGD measurements at the study site were conducted after prior laboratory calibrations were conducted with an extension cable attached. In addition, comparison experiments were also conducted to compare seepmeter SGD rate measurements with those obtained through the manual or Lee-type seepage meters. For the manual meters, seepage bags were pre-filled with 1 L ambient seawater before deploying them on the drum chambers which had been left for at least the initial ~ 4 h of deployment (preferably overnight), to achieve equilibration at the deployed site (Shaw and Prepas 1990). Net measured water volumes, collected in the bag after every ~ 1 h over the seepage chamber on a known area (2550 cm²), yielded the seepage rate (cm/day). Other comparison SGD measurements were conducted at the same study site via the radon geochemical tracer model (Santos et al. 2009) and the EM seepage meter. Detailed description and use of these two respective techniques are found elsewhere (Burnett and Dulaiova 2003; Rosenberry and Morin 2004; Swarzenski et al. 2004).

Results and Discussion

Calibration

Experiments on sensor response with changing flow rates indicated a sharp and rapid response with respect to the time interval used (Fig. 2.3). The time interval used for data logging was 10 minutes, with a 2 minute sampling time. The datalogger takes readings five times within a period of 10 minutes, averages them and stores the averaged reading. Practical resolutions for the datalogger voltage equivalence of the flow rates were achievable up to at least a single digit minute level (in other words, it is possible to

distinguish flow rates within a short interval of up to within less than ten minutes). The observed relatively high seepage resolution capability is an excellent feature that makes the seepmeter especially suited for SGD measurements (Taniguchi and Iwakawa 2001). The uncertainties in the datalogger voltage equivalence for the flow rates used during the calibration averaged about 0.3%.

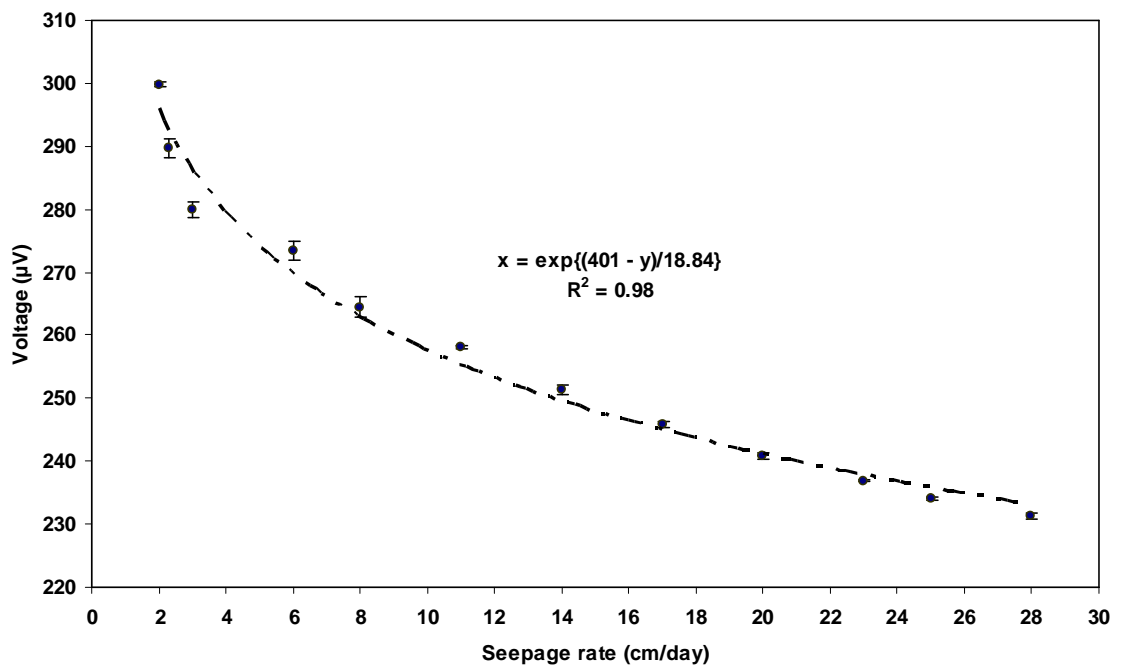


Fig. 2.3: Sensor response at different flow rates (each held constant for ~30 mins) for seepmeter M3 (seepmeter tube flow rate range: 3.5 –50 mL/min or ~2.0 to 28 cm/day). The error bars represent standard deviations on the voltage scale.

At constant flow conditions, calibration experiments revealed that for higher flow rates the analog flow meter readings were consistently higher than the flow rates quantitatively determined by cumulative collection of water discharged through the seepmeter flow tubes into a measuring cylinder (Fig. 2.2). Experiments revealed that the analog flow meter overestimated the flow rates by about 7 - 10 % at higher flows, especially flow rates > 2300 cm/h (equivalent to field rates of > 28 cm/day), compared to the volumetric manual flow measurements. According to the laboratory observations, it was clear that

beyond the upper calibration limit in our experiment (> 28 cm/day), the disparity between concurrent flow rate measurements obtained through the analog flow meter and those estimated through the manual approach progressively increased. The physical implication of this is that at higher flowrates (> 28 cm/day) the general laminar flows are lost making the flow rate measurements unreliable. As a result, better calibrations are more probable when the flowrates are determined directly by manually collecting the outflow water at the end of the seepmeter flow pipe over known time intervals.

Thus, based on the disparity between the two laboratory flow rate observations, on average the most consistent and practical seepmeter SGD measurement range using either of the laboratory flow rate approaches would be from about 2 to 28 cm/day, within an experimental maximum allowable 10% error limit. The observed effect (apparent disparity between the two flowrate measurement approaches) could be attributable to various factors, ranging from accuracy level of the analog flow meter to flow resistance related factors within the seepmeter flow tubes (Shaw and Prepas 1989, 1990a; Taniguchi and Iwakawa 2001; Hornberger et al. 1998).

The best-fit relationship between output voltage due to the temperature gradient between upstream and downstream positions of the seepmeter sensors and the flow rate of water through the flow tube is shown in Fig. 2.3. This is typically what is obtained from the bench calibration work in the laboratory before deployments are made for field measurements. In the calibration equation:

$$x = \exp\{((401.38 \pm 2.59) - y)/(18.84 \pm 0.50)\}$$

Where, y is the output voltage (μV) and x is the flow velocity (cm/h) through the flow tube.

The laboratory experiments show that the use of an extension cable on the seepmeter by 76.2 m (250 ft) had a negligible effect on the reliability of the device, as long as prior appropriate calibrations were made on the seepmeter with the extension cable connected.

The net effect of an extension cable uniformly introduced a near constant overall positive offset on the sensor output voltage with respect to the suitable flow rate calibration range used. The offset voltage was approximately 71 μV for seepmeter M3. This offset is an inherent property of each individual seepmeter and the actual value varies slightly between individual seepmeters and likely between different cable lengths. Seepmeter calibrations thus need to be device-and cable length-specific. Since this near constant positive voltage shift is uniformly observed at every flow rate, the new calibration equation that results after the cable connection sufficiently compensates for the apparent voltage offset and the overall seepmeter measurements derived from the modified set up are essentially unaffected.

Overall, the presence of the extension cable is therefore advantageous to the seepmeter. While it serves to increase its physical operation range, it also enables easy handling and control of the associated seepmeter accessories (i.e. datalogger, battery and laptop computer) from the seashore. With the extension cable attached, it is possible for SGD measurements at nearshore coastal environments to be conducted in a cheaper, safer and more convenient manner, without having to employ the use of a boat or expensive waterproof enclosures to shelter the seepmeter accessories such as was the practice previously. It is also especially desirable for conducting long term time series SGD seepmeter measurements.

Salinity and Temperature Effects on Seepmeter Measurements

The experimental results on the effect of salinity on SGD measurements are shown in Fig. 2.4A. A close agreement (within the 95% confidence interval) is evident between measurements done in the two media within the range of flow rates considered. This was statistically (Stratigraphics Plus Version 5.1, 2001) supported by a t-test ($p = 0.12$, $\alpha = 0.05$), performed on data set pairs ($n = 5$) on the two media under similar conditions.

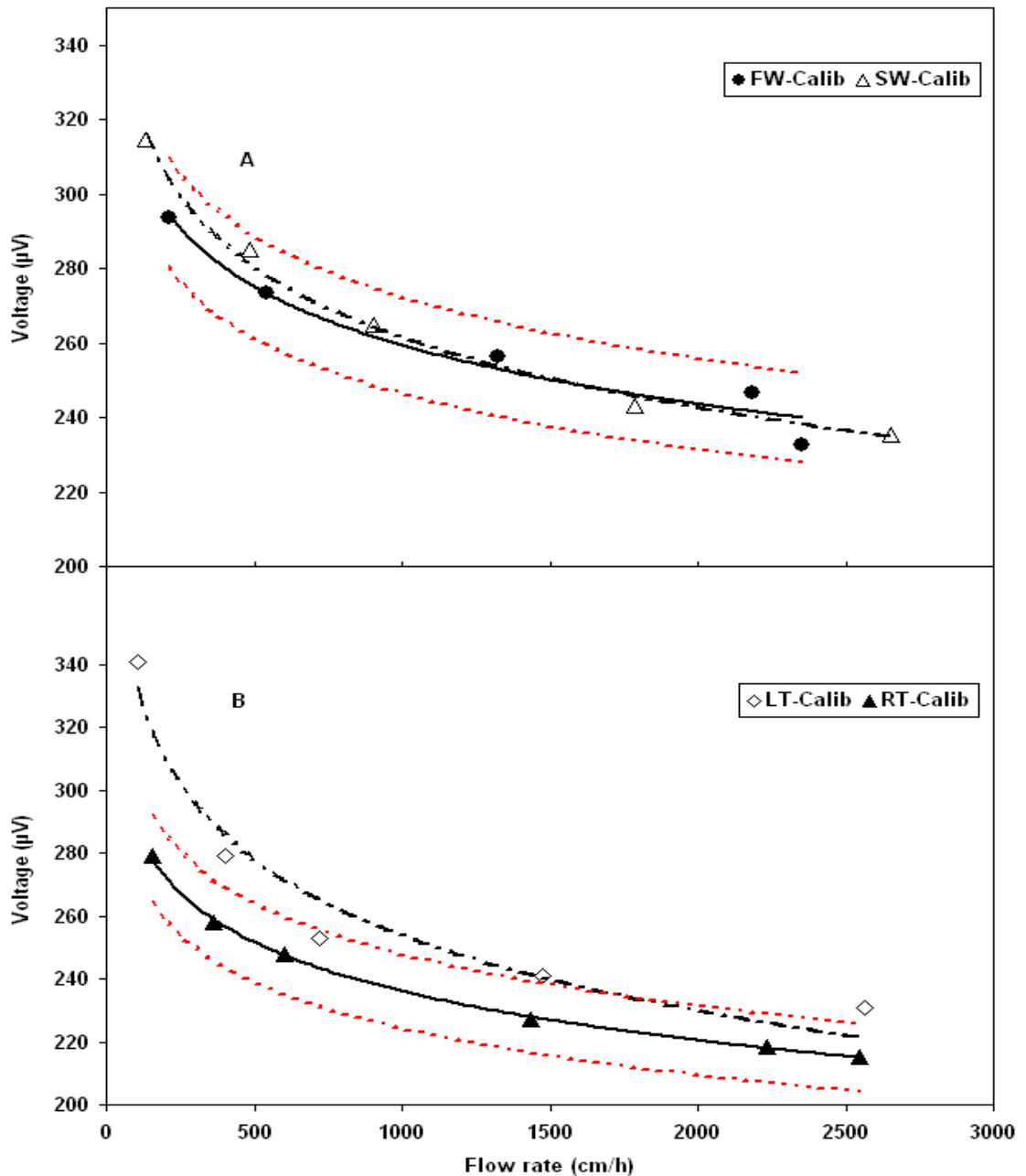


Fig. 2.4: (A) Comparison between freshwater (FW) of salinity ~ 0 , and seawater (SW) of ambient salinity ~ 35 , seepmeter calibrations. The figure shows that the two plots are in agreement within 95% confidence interval (shown as red dotted outline, which was plotted for the FW plot). This shows that there is no significant difference between SGD seepmeter measurements taken in FW and SW within the same ambient environmental conditions. (B) Comparison between seepmeter calibrations conducted at low (cold room) temperature (LT: 1.1 - 3.3 °C) and at ambient (room) temperature (RT: 25 - 27 °C). The 95% confidence interval for the RT plot is shown as red a dotted outline.

The SGD experimental results conducted at low temperatures (1 – 3 °C), and at room temperature (25 - 27 °C) are shown on Fig 2.4B. It is apparent that low temperatures introduced a voltage offset on the seepmeter sensor voltage output, similar to the one observed with the extension cable. Again, this offset is most likely as a result of changing electrical resistance of the electrical conductors of the seepmeter, especially between the sensor and the datalogger. However, since this is a uniform physical characteristic inherent in most electrical conductors under such conditions the apparent observed effect could similarly be easily accounted for by carrying out calibrations at the desired low temperature.

The electrical resistance, R , is an extrinsic property of a device which is represented by the equation, $R = \rho/l/A$, where A is the cross-section area and l the length. The resistivity, ρ , of materials is simply the inverse of conductivity, σ , that is, $\rho = 1/\sigma$. The linear relationship between resistivity and temperature, T , is often represented by the empirical relationship, $\rho = \rho_0 + \alpha T$, where ρ_0 is the resistivity at a reference temperature (usually ambient or room temperature) and α is the temperature coefficient, a material specific constant (CRC 1985). Therefore, it is reasonable to deduce that the physical influence of the apparent linear effects on seepmeter measurements due to the extension cable and low temperatures can sufficiently be taken care of by appropriate prior calibrations before conducting the field deployments.

Generally, as long as there are no extreme drastic temperature changes (such as those considered here, i.e. < 5 °C) during the period of field seepmeter measurements, any possible effect related to temperature variations on the measurements can be assumed to be negligible. Under normal circumstances, the average temperature variations during the deployment period is usually not more than a few degrees. For instance, a change of ~ 20 °C for our case, resulted to an approximate change in calibration of about 11%.

Field Measurements

Long-term continuous deployments showed that seepmeters are capable of providing internally consistent SGD rate measurements over an extended time period (at least for 1 week continuously) without recourse to recharging the battery power source (Table 2.1). However, due to the seepmeter's detector being particularly sensitive to the functioning of the "constant current supply" (CCS) unit within its power module (Fig. 2.2), it is important to ensure that no voltage supply fluctuation occurs on the seepmeter during its entire deployment period to obtain consistent and reliable SGD measurements. Since the normal functioning of the seepmeter sensor and datalogger were designed to operate with a 12 V-DC power supply, it is recommended that the power source (12V battery) be regularly replenished on at least a weekly basis for extended deployment periods. With regular replenishment of the power source however and by using an extension cable, it is possible to attain continuous uninterrupted seepmeter SGD measurements that can last for weeks or months (Taniguchi and Iwakawa 2001).

Some long-term field time-series field seepmeter data are displayed in Fig. 2.5 and 2.6. It is evident that the SGD and water level (tide) relationships are complex, as also observed from long-term SGD tracer measurements (Santos et al. 2009). There are times during the long deployment periods (Fig. 2.5) when the highest SGD coincided with the highest water level peaks, such as on April 4, 8, 13, 14 and 15. There are also periods when the highest SGD peaks coincided with the highest falling water level rate (for example on April 11 and 14). In numerous other instances during the same deployment period, SGD variations seemed to remain largely unaffected over the normal periodic water level (tidal) variations (April 9 and 10). These complex variations between SGD and water level at this site suggest that it is probable that other factors besides the water level variations play a role in modulating SGD over time.

There is a coincidental major maximum SGD and water level peaks that occurred on April 15 (at ~ 03:30) as shown in Fig. 2.5. This was also a time of heavy downpour (hourly precipitation of > 4 mm) and wind speeds were at their maximum (> 10 m/s). Thus in addition to water level variations, the SGD variation trends can also be

significantly influenced by a combination of environmental factors such as precipitation and wind speeds that are likely to enhance current velocities.

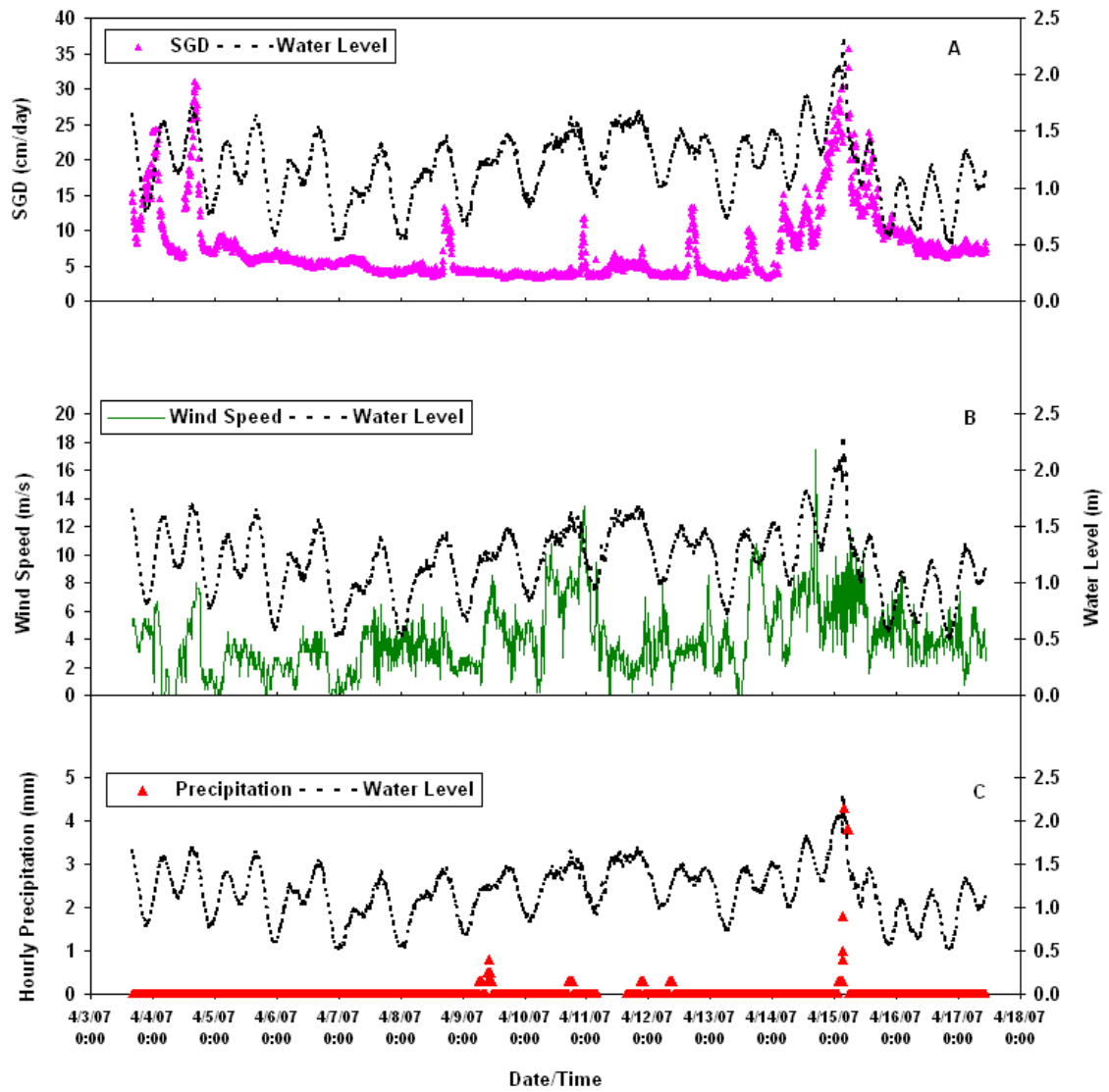


Fig. 2.5: Long term time series variations with water level of: (A) SGD, (B) Wind Speed and (C) Precipitation, during the period, 03 – 17 April 2007.

At the maximum SGD peak (~ 35 cm/day), the wind speeds were generally about double the average speeds experienced during the entire deployment period. Similar SGD

variation trends have also been observed in previous studies. For example, at Flamengo Bay, Brazil, decoupling of SGD and tide were observed on the same day in which rain occurred (Taniguchi et al. 2008). While it was thought that rainfall played a role in these observations, the hydrogeologic setting at that field site (fractured crystalline rocks) may have facilitated rapid flushing of meteoric water as SGD.

The SGD distribution depicted in Fig. 2.6, displays a slightly different trend compared to that depicted in Fig 2.5. While during the former there was a heavy downpour and the accompanying wind speeds were elevated, this was not the case with the latter seepmeter deployment. The SGD peaks tended to line up very well with the diurnal wind peaks during the first few days of this record. These fairly consistent trends in SGD and tide variations are in agreement with numerous previous similar studies including for instance that of Burnett et al. (2007), who attributed the observed SGD variations to sea level changes altering the hydraulic gradients and tidal pumping that tend to induce recirculation of porewater fluids at the Upper Gulf of Thailand.

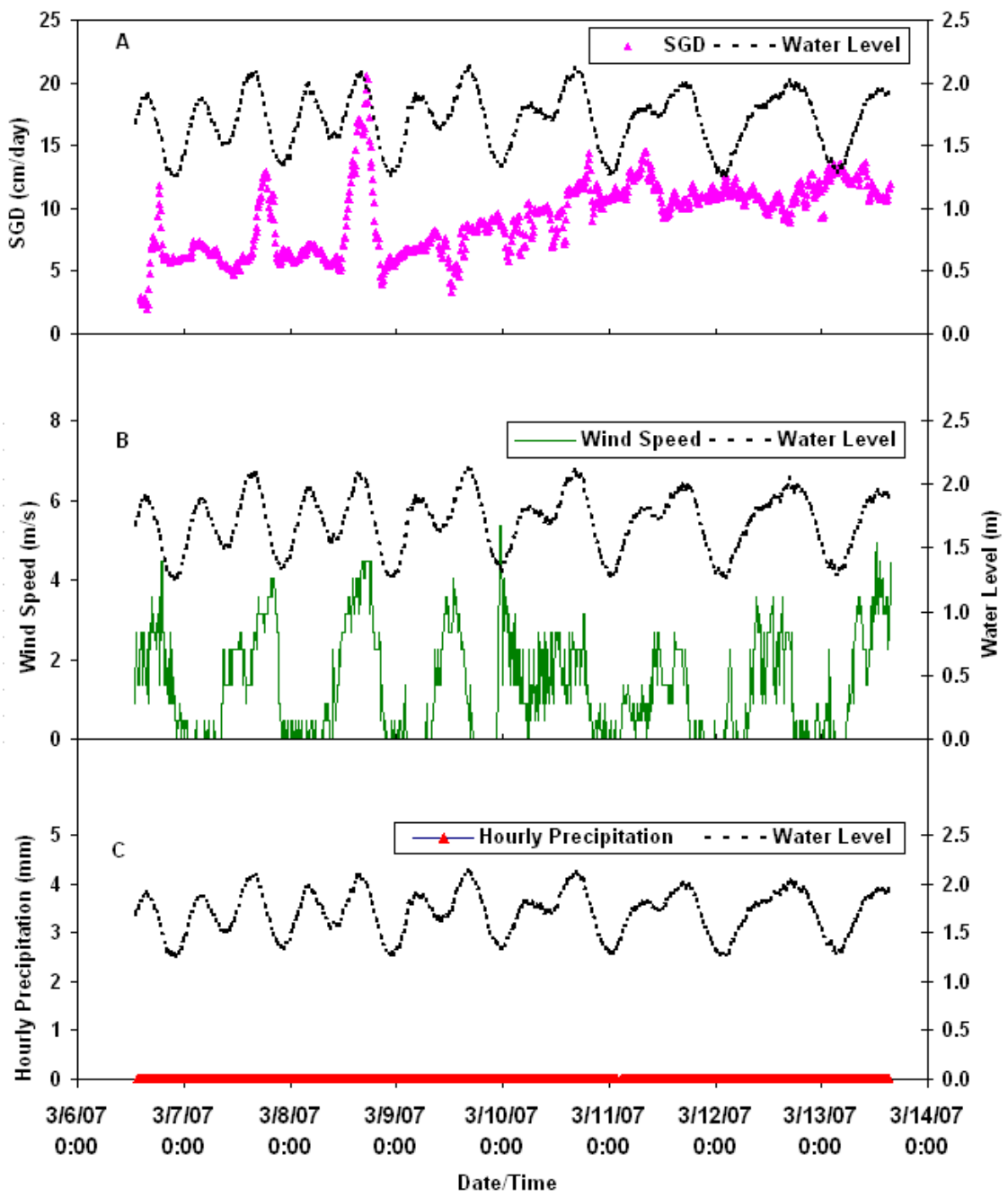


Fig. 2.6: Long term time series variations with water level of: (A) SGD, (B) Wind Speed and (C) Precipitation, during the period, 06 – 13 March 2007.

Comparison With Other SGD Methods

There is compelling evidence that the average SGD seepmeter measurements are in close agreement in magnitude with those obtained from different approaches. The evidence include the concurrent independent SGD measurements conducted during this study period (Figs. 2.7 and 2.8, Table 2.1), radon-derived SGD rates obtained concurrently with our seepmeter deployments (Santos et al. 2009), and those done previously at this and other sites (Table 2.2). The estimated mean SGD values in the study area, for the three months shown in Table 2.1, were 8.5 ± 6.4 cm/day by the seepmeters, while the radon model provided an estimate of 10.2 ± 8.4 cm/day. It should be noted that these standard deviations are not uncertainty limits but rather a measure of the actual variability of seepage during the measurement period.

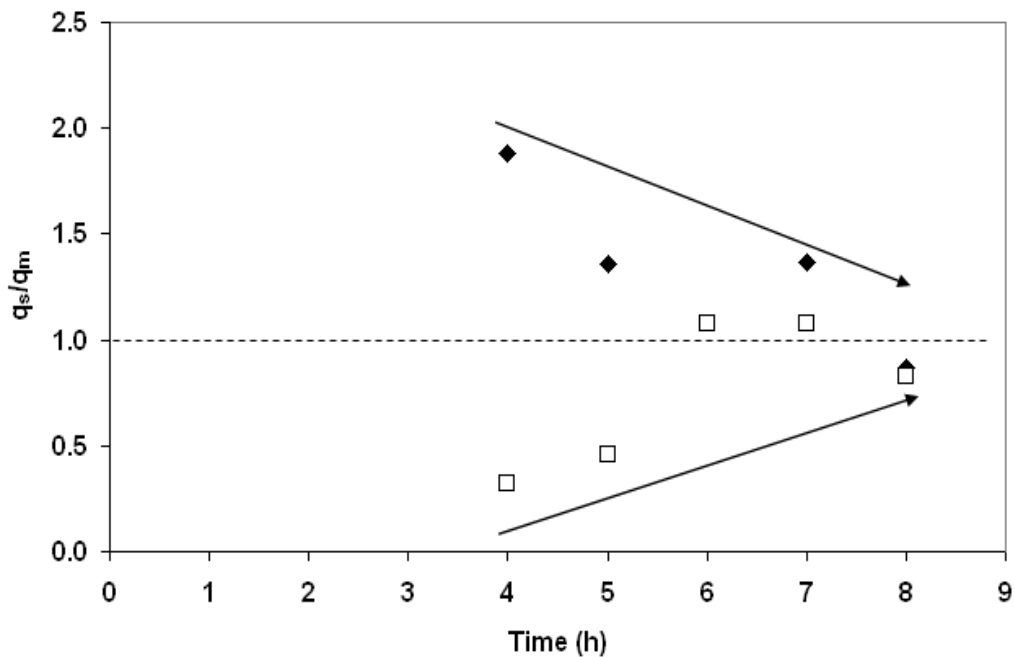


Fig. 2.7: Effect of the length of deployment duration periods, on seepmeter (q_s) and Lee- type (manual) meter (q_m) SGD relative estimates, expressed as a ratio (q_s/q_m). This is an example of a dawn to dusk deployment (including the initial ~ 4 h waiting period for stabilization of the seepage chambers following the deployments). Diamonds and squares represent two manual meters, M1 and M3 respectively. These were deployed next to the seepmeter benthic chambers.

The comparison shown in Fig. 2.8 does reveal a good temporal trend agreement between SGD estimates obtained through the application of two independent approaches, the seepmeter and EM seepage meter, deployed just a few meters apart during the same period. The average SGD rates in Fig 2.8 were 11.2 ± 9.4 and 4.2 ± 3.9 , cm/day, for the heat-type seepmeter and EM seepage meter respectively. Quantitatively, the average computed SGD rates for the covered study site via the two different approaches during the deployment period (July 24 – 26, 2006) were of similar order of magnitude when one integrates the flow over time. They were: $(11.17 \pm 0.04) \times 10^{-2}$ and $(4.31 \pm 0.02) \times 10^{-2}$ $\text{m}^3/\text{m}^2 \cdot \text{day}$ for the seepmeter and EM respectively. While trends in the two approaches agree very well, the absolute values for the seepmeter estimates were on average higher than those of the EM seepage meter during many intervals. This may have been due to a combination of various factors, such as the fact that the EM is capable of reverse flow measurements unlike the case with the seepmeter. Additionally, these differences are attributed to the fact that the two techniques rely solely on direct seepage measurements emanating from specific sites where the respective benthic chambers are placed within the seafloor. Similar variations have also been commonly observed in other studies (Taniguchi et al. 2003a). The other potential factors that may result to these individual differences are likely related to the sediment composition, compactness as well as the presence of various benthic biota at the deployment sites. This problem is characteristic to all benthic chamber based approaches, thus making geochemical tracer techniques better suited for regional, larger-scale SGD estimations (Burnett and Dulaiova 2003). However, the application of the former approach is still useful where actual benthic SGD rates are desired. These different approaches are a means of providing better SGD estimations when applied in a complimentary manner. It is interesting to note how conductivity measurements continued to decrease with time within the benthic chamber during SGD measurements in the case of EM seepage meter deployment (Fig. 2.8, Tables 2.1 and 2.2). The capability of EM seepage meter to detect both positive and negative SGD fluxes was also evident during this deployment period.

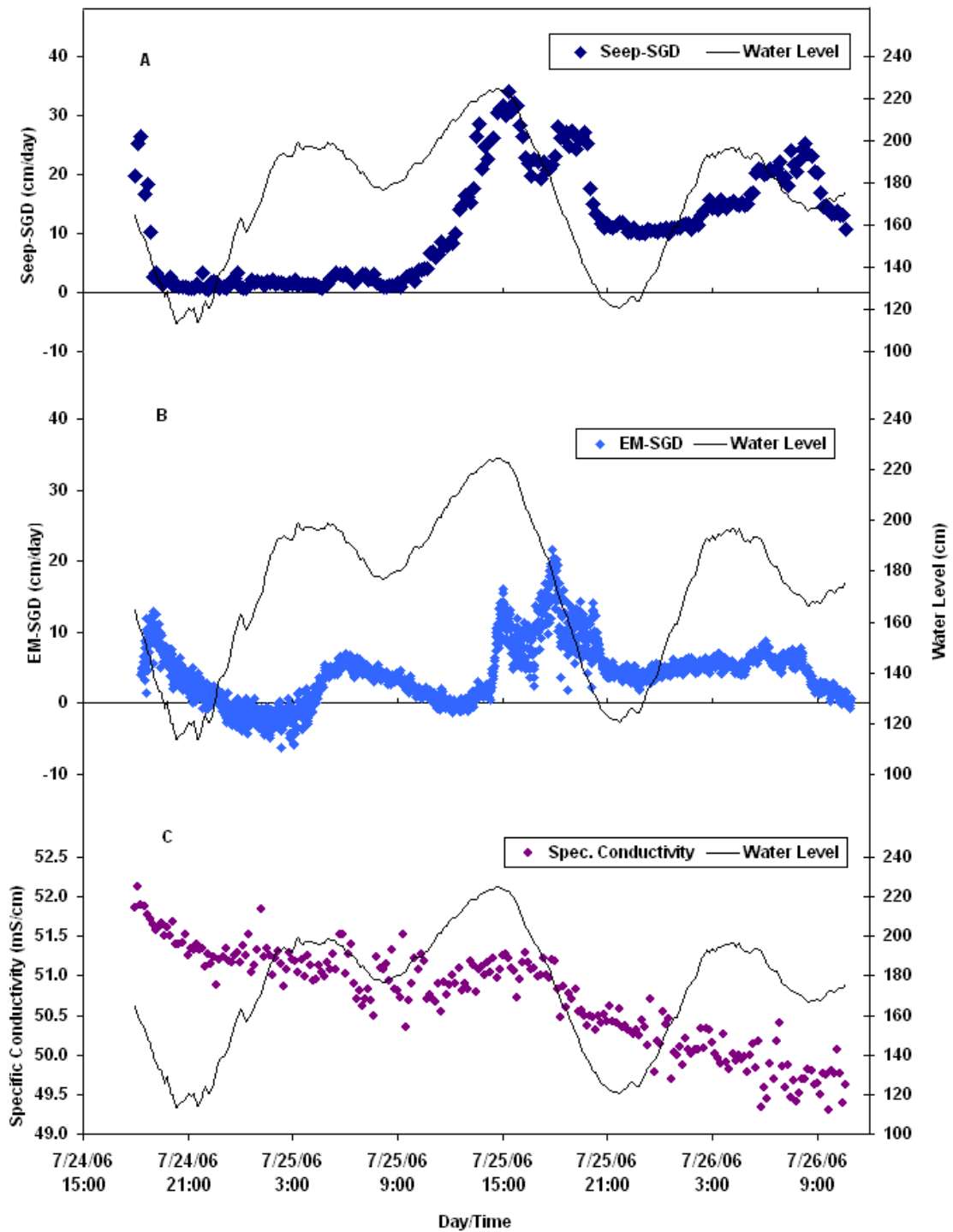


Fig. 2.8: Measurement of concurrent SGD variations with water level by: (A) seepmeter, and (B) an electromagnetic (EM) seepage meter, at FSUCML during the period: July 24-26, 2006 (notice close agreement in SGD trend and magnitude). The capability of an EM seepage meter to measure negative fluxes is evident (B). The two meters were deployed in close proximity. During deployment, specific conductivity decreased gradually (C).

In order to assess how different deployment duration periods in the field affect the overall averaged SGD estimations, we compared the ratio of estimated SGD using seepmeter, q_s , and rates measured using manual (Lee-type) meters that were deployed nearby, q_m (Fig. 2.8, Table 2.1). This comparison confirms results of a similar study previously conducted by Taniguchi et al. (2003a) in the same environment. It is evident that short deployment duration periods for SGD estimation by seepage meters may result in significant underestimations or overestimations. Our measurements revealed variations between 29% and 171% of the averaged SGD rates within a period of about 10 hours. Most underestimations or overestimations are more likely to occur at the lower time duration periods.. SGD variations also tend to increase the further the measurement site is from the shore, and variations from 30% to 230% have been reported previously (Taniguchi et al. 2003a). Since our observations are in agreement with those that had been made in this previous study, it is unlikely that they are a function of the cable length since the previous study had not employed the extension cable. We speculate that the most probable reason for the observed variation is the fact that the general SGD distribution tends to taper off the further offshore compared to nearshore (Taniguchi et al. 2008).

Table 2.1: Comparison between mean seepmeter SGD rates and those derived via the radon model for selected months, FSUCML research site.

Year Month Date	2006 May (01 – 04)	2006 July (24-26)	2006 December (14-18)	2007 March (06-13)	2007 April (03-17)
<i>Means for ^aseepmeter SGD</i>					
Mean (cm/day)	3.3 ± 3.1	11.2 ± 9.4	10.9 ± 6.7	9.2 ± 2.9	8.8 ± 3.8
n	165	233	188	1019	2009
Maximum distance from shore (m)	65	138	62	62	62
<hr/>					
<i>Means for radon model SGD</i>					
Mean (cm/day)	7.2 ± 5.6	10.9 ± 8.6	12.4 ± 11.1	-	-
n	72	78	340	-	-

The results of ^aseepmeter SGD rates in the table were averaged from the five different seepmeters that were deployed during the study.

Table 2.2: Comparison of SGD rates between this study and other studies.

Study Site	Seepmeter (cm.day ⁻¹)	Manual meter (cm.day ⁻¹)	²²² Radon Model (cm.day ⁻¹)	EM (cm.day ⁻¹)
^b Turkey Point, FL (FSUCML) - <i>previous study</i>	13	11.5 – 18	12.2 – 18	-
^c Banana River Lagoon, FL	-	3.6 - 6.9	3.5	-
^d Town Cove, Cape Pod, MS	-	2.4 - 7.2	-	-
^e Cockburn Sound, N. Australia	13.7 - 16.3	-	-	-
Turkey Point, FL (FSUCML) - <i>present study</i>	3.3 - 11.3 (8.5 ± 6.4)	7 - 14 (10 ± 2)	7.2 - 12.4 (10.2 ± 8.4)	-6.2 - 21.7 (4.2 ± 3.9)

^bBurnett et al. (2002); ^cCable et al. (2004); ^dGiblin and Gaines (1990); ^eTaniguchi et al. (2003b)

Elsewhere, using manual seepage meters (Lee 1977), seepage rates ranging from 1 to 12 cm/day have been reported in the Indian River Lagoon system (Cable et al. 2006). While using both automated and manual seepage meters, Taniguchi et al. (2003a), measured SGD rates that ranged from 13.7 to 16.3 cm/day at Cockburn Sound, Western Australia. All of these values attest to the usefulness of these approaches in studying SGD in various nearshore coastal environments. Based on the results of these measurements, when viewed in relation to the other SGD measuring techniques, our data confirm the applicability of seepmeters in SGD studies.

Conclusions

The continuous heat-type automated seepage meter can provide reliable, long-term SGD rate measurements. The seepmeter measurements provided data that agreed both in trend and magnitude with other independent SGD techniques, including the manual seepage meter, radon as a geochemical tracer, and an electromagnetic seepmeter.

Laboratory experiments have shown that connecting a 76.2 m extension cable to the continuous heat-type automated seepage meter has negligible effects on its SGD measuring capability, as long as calibrations are made with the extension cable connected. Similarly, the apparent effect of low temperature (at least a net difference of > 20 °C below the typical ambient temperature) on sensor output voltage (as recorded in the datalogger) can also be effectively accounted for by conducting calibrations at the anticipated temperatures. These observed calibration effects are attributed to the linear changes in electrical resistance in the seepmeter sensor connectors as a result of the extension cable and extreme temperature changes, respectively.

Salinity was found to have no significant effect on the continuous heat-type automated seepage meter measurements as the calibration results from fresh water and sea water agreed to within the 95% confidence level.

Acknowledgements

The authors express their sincere thanks to the FSUCML director and staff for logistical support during field work. Peter Fuleki, Rick Peterson, Peter Lazarevich, Eric Howarth, Dave Oliff and Alan Michels are much appreciated for their invaluable technical suggestions during calibration work. Special thanks are to Jack Winchester and Marcus Huettel whose overall creativity and constructive criticism greatly enhanced the successful completion of this study. We are indebted to three anonymous reviewers for their insightful and constructive comments. The project was jointly funded through an NSF research grant (OCE05-20723) to Bill Burnett and Jeff Chanton, and an IFP-Ford Foundation PhD Fellowship award to Benjamin Mwashote. This financial support is gratefully acknowledged.

CHAPTER 3

ASSESSMENT AND REDUCTION OF ENVIRONMENTALLY INDUCED ARTIFACTS IN SUBMARINE GROUNDWATER DISCHARGE SEEPAGE METER MEASUREMENTS

Publication Status:

Mwashote et al. 2010. Assessment and eradication of environmentally induced artifacts in submarine groundwater discharge seepage meter measurements. Manuscript prepared for submission to: *Estuarine, Coastal and Shelf Science*.

Abstract

Submarine groundwater discharge (SGD) measurements obtained from conventional benthic chamber based seepage meters, placed in areas exposed to waves and currents have been found to be subject to varying degrees of artifacts. These artifacts are mainly associated with Bernoulli-induced flow, the vertically directed flow arising due to water movement across topographic features. In an attempt to address this limitation, we conducted experiments at a site in the northeastern Gulf of Mexico (next to Florida State University Coastal and Marine Laboratory, FSUCML) using automated heat-type seepage meters (seepmeters). The study revealed that SGD seepmeter measurements were influenced by variations in wind speeds (likely a reflection of current flow). Our results indicate that it is possible to significantly reduce these artifacts by burying (or submerging) the seepmeter to nearly the same level as the sediment topography. When such an arrangement is not practical, a viable alternative is to deploy in parallel, an identical seepmeter “blank” insulated from the underlying sediment by a non-porous material such as a child’s plastic play-pool. Measurements obtained in both ways compared well with those obtained from the ^{222}Rn geochemical tracer approach. An inverse correlation was observed between sea level variations and SGD measurements by both seepmeters and the ^{222}Rn geotracer approach. Artifacts in SGD seepmeter

measurements coincided with sharp changes (transitions) in wind directions. While the study revealed that in general wind speeds > 6 m/s were associated with enhanced SGD measurements in seepmeters with buried and unburied benthic chambers, the influence was greater in the unburied meters, and more pronounced for SGD rates < 2 cm/day.

Introduction

The most common submarine groundwater discharge (SGD) measuring approaches include: seepage meters, piezometers, geochemical or geophysical tracers and modeling. Among these methods, seepage meters and geochemical tracer methods are the most widely used (Burnett et al. 2003; Taniguchi et al. 2003a). The bulk of seepage meters used in SGD measurements originate from the Lee-type seepage meter, which is made from the top or bottom section of a 55-gallon steel drum (Lee 1977). It has recently been demonstrated that automated continuous SGD monitoring methods could provide reasonably high resolution SGD measurements (Taniguchi and Iwakawa 2001; Mwashote et al. 2010). Among the array of contemporary automated systems is the continuous heat-type automated seepage meter (seepmeter), which was developed by Taniguchi and Fukuo (1993), and the RAD7 based RAD-AQUA (DurrIDGE Co. Inc.) for radon-in-water measurements (Burnett et al. 2001).

Seepage meters have been used to quantify SGD under a variety of conditions in many nearshore coastal environments and lakes over the years (Lee 1977; Bokuniewicz 1992; Cable et al. 1997). However, these devices have also drawn concerns with regard to the Bernoulli-type flow induced around the seepmeters (Shum 1992; 1993). Such flow was suggested to be an important source of artifacts in a study conducted in the Florida Keys (Shinn et al. 2002). However, several studies also showed strong evidence of a link between tidal and aquifer head variations and seepage measurements, suggesting that the seepmeter response is not only due to artifacts (Chanton et al. 2003; Corbett and Cable 2003). Variables that may influence the observed rate of SGD include hydraulic gradients, sediment permeability, height above the sea floor, ripple length and amplitude, wavelength and water wave period. It has been demonstrated that water penetration into

sediments results from pressure gradients that develop over sediment bedforms (Huettel and Gust 1992; Huettel et al. 1996). In their study conducted in a sandy ripple bed, Huettel et al. (1996) showed that differential pressure can result to vertical pore water velocities as high as 2.5 cm/h (60 cm/day) in sediment mounds of 2.5 cm height when bottom water current velocities approach 10 cm/s. In a more recent study at a site on the east coast of Florida, Cable et al. (2006) observed Bernoulli-induced flow, but this was considered a minor component of the overall flow recorded in the seepage measurements. The present study was designed and conducted in order to assess the influence of environmentally-induced (Bernoulli-related flow) artifacts in SGD seepmeter measurements (SGD_{seep}), and to subsequently test practical ways of reducing and to possibly ultimately eliminate such artifacts so that seepmeters could remain viable tools in SGD measurements.

The purpose of the present study was to address the following:

1. Investigate the effects of burying (submerging) seepmeter benthic chambers into the sediment and use of “blanks” to evaluate artifacts in SGD_{seep} estimations.
2. Assess possible relationships between SGD_{seep} estimations and wind speed as well as wind direction (we hypothesize that landward and oppositely directed winds would have different impacts on SGD_{seep} estimations).
3. Compare long-term SGD_{seep} obtained by direct seepmeter measurements with estimations obtained via the ^{222}Rn geochemical tracer approach (SGD_{rad}).
4. Assess any relationship between SGD_{seep} estimations and sea level (tidal) variations.

Materials and Methods

Study Area

Field measurements were carried out at a study area located in the northeastern coastal Gulf of Mexico, an area known for the presence of seepage and submarine springs (Rutkowski et al. 1999; Burnett et al. 2002). The area (Fig. 3.1) lies within the Woodville

Karst Plain, which extends from about 80 km inland to the coastal zone where the Florida State University Coastal and Marine Laboratory (FSUCML) is located at Turkey Point, Florida. A more detailed description of the study area is given elsewhere (Bugna et al. 1996; Santos et al. 2008, 2009; Li et al. 2009).

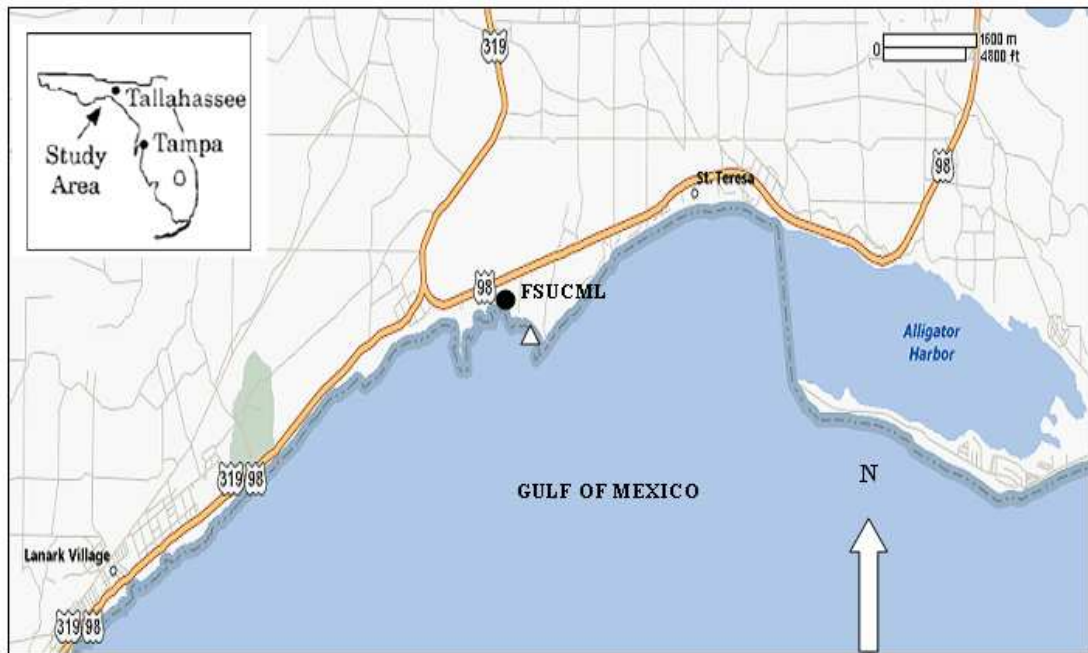


Fig. 3.1: Map showing the study area at FSUCML. The site location (N 29°55', W 84°31') is indicated in the map by an open triangular shape (index map source: <http://www.mapquest.com/beta/maps>).

Field Measurements

In order to assess the effects of various environmentally-induced artifacts on SGD measurements, long-term seepmeter measurements were conducted for periods of up to two weeks. The automated heat-type seepage meters (seepmeters) used in this study utilized benthic chambers of cross section area 2550 cm² modified from the design of Lee (1977). The seepmeters (Fig. 3.2) were allowed to equilibrate for at least 24 h before measurements started. A datalogger (Data Hog 2, Skye Instruments Limited, UK) that was programmed to allow automatic readings to be taken at 2 minute intervals, averaged and stored at 10 minutes intervals, was used for field data collection (Mwashote et al. 2010). Wind speed and direction were measured at a local FSUCML weather station while the seawater level was measured with an ultrasonic water-level meter. Additionally, weather data were obtained online (www.wunderground.com) from a weather station located at Alligator Point, ~10 km from the study site.

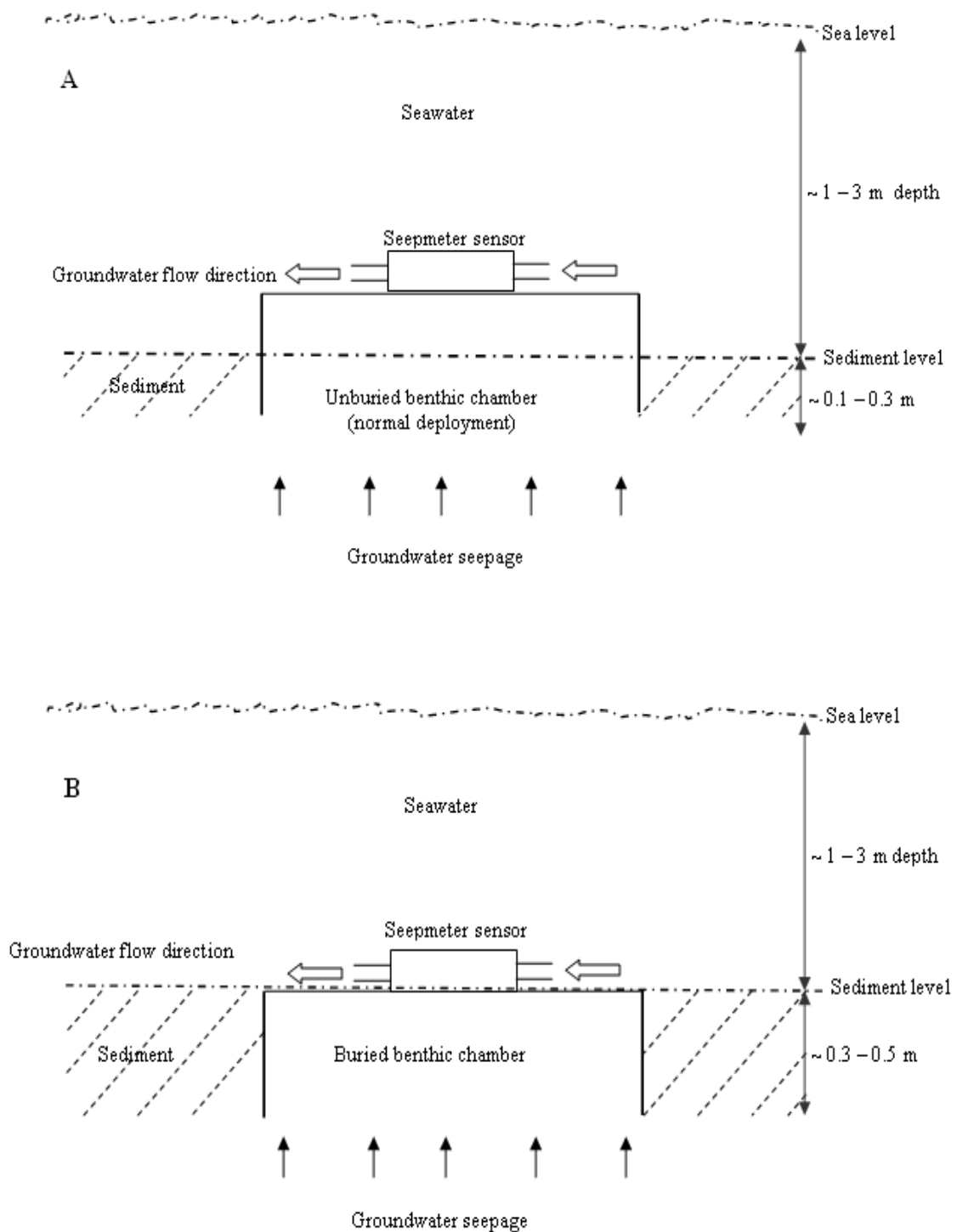


Fig. 3.2: Seepmeter benthic chamber deployment: (A) Unburied benthic chamber (typical normal deployment mode), (B) Buried benthic chamber.

During any particular field deployment, up to five seepmeters were deployed at the study site, facilitated by aid of a 76.2 m (250 ft) long electrical extension cable (for data and power transmission) for each seepmeter, perpendicular to the shore. The furthest distance of deployment of the seepmeters from the shore was 182 m (on boat aided occasions only), while the shortest was 15 m. During typical deployments, the datalogger, battery and all associated accessories were located and operated from the shore. To assess the effect of artifacts related to Bernoulli – induced flow on SGD_{seep} measurements, seepmeters were deployed at the study site, with one of the benthic chambers completely submerged or nearly at the same level as the sediment topography, and the other only partially submerged, with ~ 5 - 20 cm exposed. Parallel seepmeters that acted as “blank” controls were similarly deployed inside non-porous materials (child’s plastic play-pool) at the same site. The “blank” control was deployed by placing a benthic chamber inside a plastic play pool filled with sand and buried in the seabed to the same extent as the submerged chambers. The average separation between the blank and submerged seepmeter chambers was ~ 0.5 – 1 m. Regular monitoring of groundwater level was also maintained at a nearby water well (P1) which was ~ 100 m inland from the shoreline. Additionally during the same period, ^{222}Rn , which is a good geochemical tracer for SGD (SGD_{rad}), was also monitored at the same study site by employing two RAD7’s (DurrIDGE Co. Inc.) according to the procedure described in Burnett and Dulaiova (2003) for short term data. For long term SGD_{rad} data, we used that which was obtained at the same site during the same period via the lab (FSUCML) long-term set up (Santos et al. 2009).

Results and Discussion

Time-series field experiments were conducted to assess the relationships between SGD measurements and three main physical environmental factors: sea level (tidal variations), wind speed, wind direction and groundwater level of a nearby water well (P1). The results of these field deployments are shown and described in Figs. 3.3 – 3.11 and Tables 3.1 and 3.2 in the following sections.

Relationship Between SGD_{seep} Measurements and Sea level, Wind Speed and Direction

For field deployments of 08 – 12 July'07, in which the seepmeter benthic chamber was buried in the sediment, variations in SGD_{seep} were strongly inversely correlated with sea - level (Fig 3.3A). During this deployment period, the tidal variations were spring-diurnal. There was practically no seepage observed in the control benthic chamber that was simultaneously deployed at the same site during this deployment.

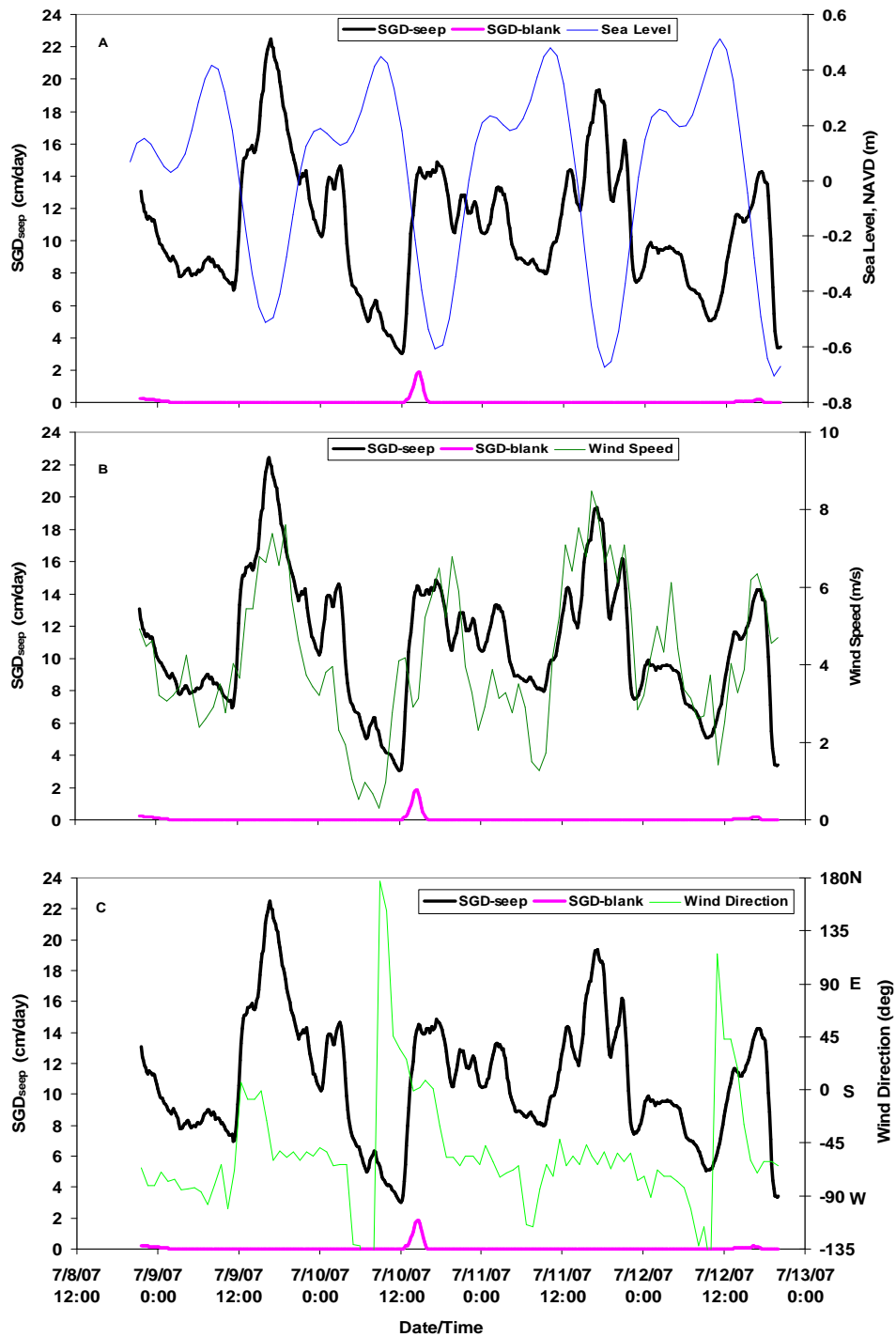


Fig. 3.3: Relationship between SGD_{seep} variations with: (A) Sea level, (B) Wind speed and (C) Wind direction, Θ (where, $\Theta = 180 - \text{actual angle}$, in degrees), for the period: 08 – 12 July '07. Buried chambers (the blank chamber was deployed inside a child's plastic play pool).

The correlation coefficient between SGD_{seep} and sea level was -0.63 ($R^2 = 0.4$; $p < 0.01$). This is a strong inverse relationship. The R^2 statistic suggests that the correlation between SGD_{seep} and sea level explains up to $\sim 40\%$ of the variability observed. There was also a direct correlation between SGD_{seep} and wind speed as shown in Fig. 3.3B. The correlation coefficient between these variables was 0.57 ($R^2 = 0.32$; $p < 0.01$). This relationship indicates that up to 32% of the SGD_{seep} variations could be explained by this correlation. The average wind speed was 4.2 ± 2.3 m/s ($n = 1192$).

Fig. 3.3C shows a weak inverse correlation between SGD_{seep} and the wind direction. The predominant wind direction was mainly due south westerly and the correlation coefficient between the variables was -0.16 ($R^2 = 0.03$; $p < 0.01$). This indicates that only up to 3% of the SGD_{seep} variability could be explained by this relationship. It is to be noted that wind directions (Fig. 3.3C) are indicated in terms of angle, Θ (where, $\Theta = 180 - \text{actual angle}$, in degrees), instead of the actual degrees, since this being an angular scale, would have likely resulted to an ambiguity in interpretation especially for angles $> 180^\circ$ (for instance, $0^\circ = 360^\circ$, both of which represent the N direction).

For the field deployment of 06 – 11 August'07 (Fig. 3.4A), variations were significantly negatively correlated between SGD_{seep} and sea level. The correlation coefficient was -0.4 ($R^2 = 0.16$; $p < 0.01$). The R^2 statistic indicated that up to 16% of the variabilities in SGD_{seep} could be explained by the correlation. In this experiment, the benthic chambers were also completely buried in the sediment and tidal variations displayed a mixed diurnal pattern.

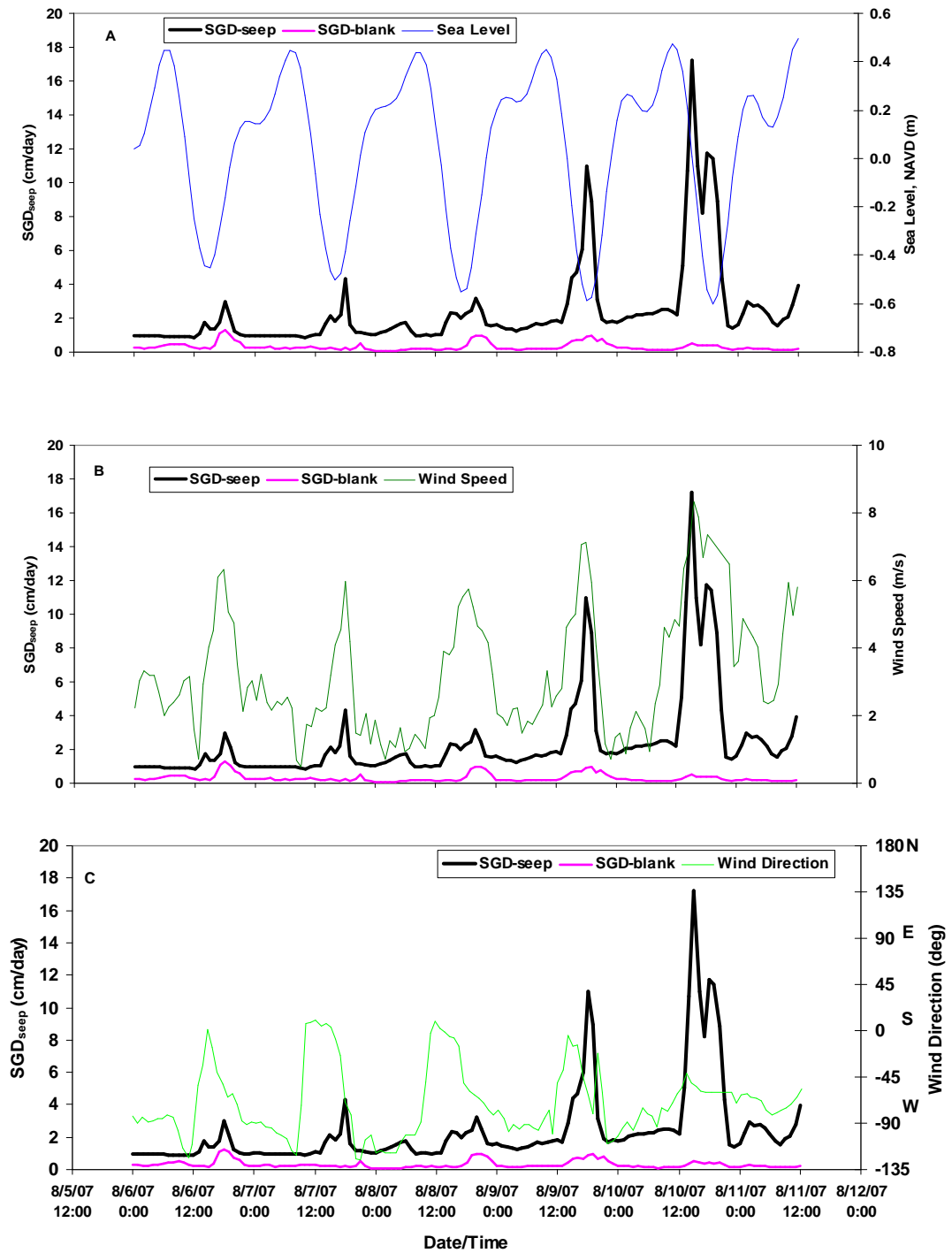


Fig. 3.4: Relationship between SGD_{seep} variations with: (A) Sea level, (B) Wind speed and (C) Wind direction, Θ (where, $\Theta = 180 - \text{actual angle}$, in degrees), for the period: 05 – 11 August'07. Buried chambers (the blank chamber was deployed inside a child's plastic play pool).

A positive correlation between SGD_{seep} and wind speed was evident as seen in Fig. 3.4B. The correlation coefficient between the variables was ~ 0.58 ($R^2 = 0.33$; $p < 0.01$) and up to 33% of the SGD_{seep} variability is explainable through this relationship. The average wind speed during the deployment was 3.2 ± 2.0 m/s ($n = 1558$). There was a weak inverse relationship between SGD_{seep} and wind direction, which predominantly south westerly (Fig. 3.4C). The correlation coefficient was -0.25 ($R^2 = 0.06$; $p < 0.01$). This means that it would be possible to explain up to 6% of the SGD_{seep} can be explained by this correlation.

Fig.3.5A shows results of a typical deployment where the benthic chambers were unburied (normal mode of deployment) in the sediment. This was conducted during the period 29 – 31 May'07. In this deployment, variations were significantly positively correlated between SGD_{seep} and the sea level. The correlation coefficient was 0.75 ($R^2 = 0.56$; $p < 0.01$). The R^2 statistic indicates that up 56% of variabilities in SGD_{seep} could be explained by this correlation. The tidal variations were nearly neap tide with a semi-diurnal pattern.

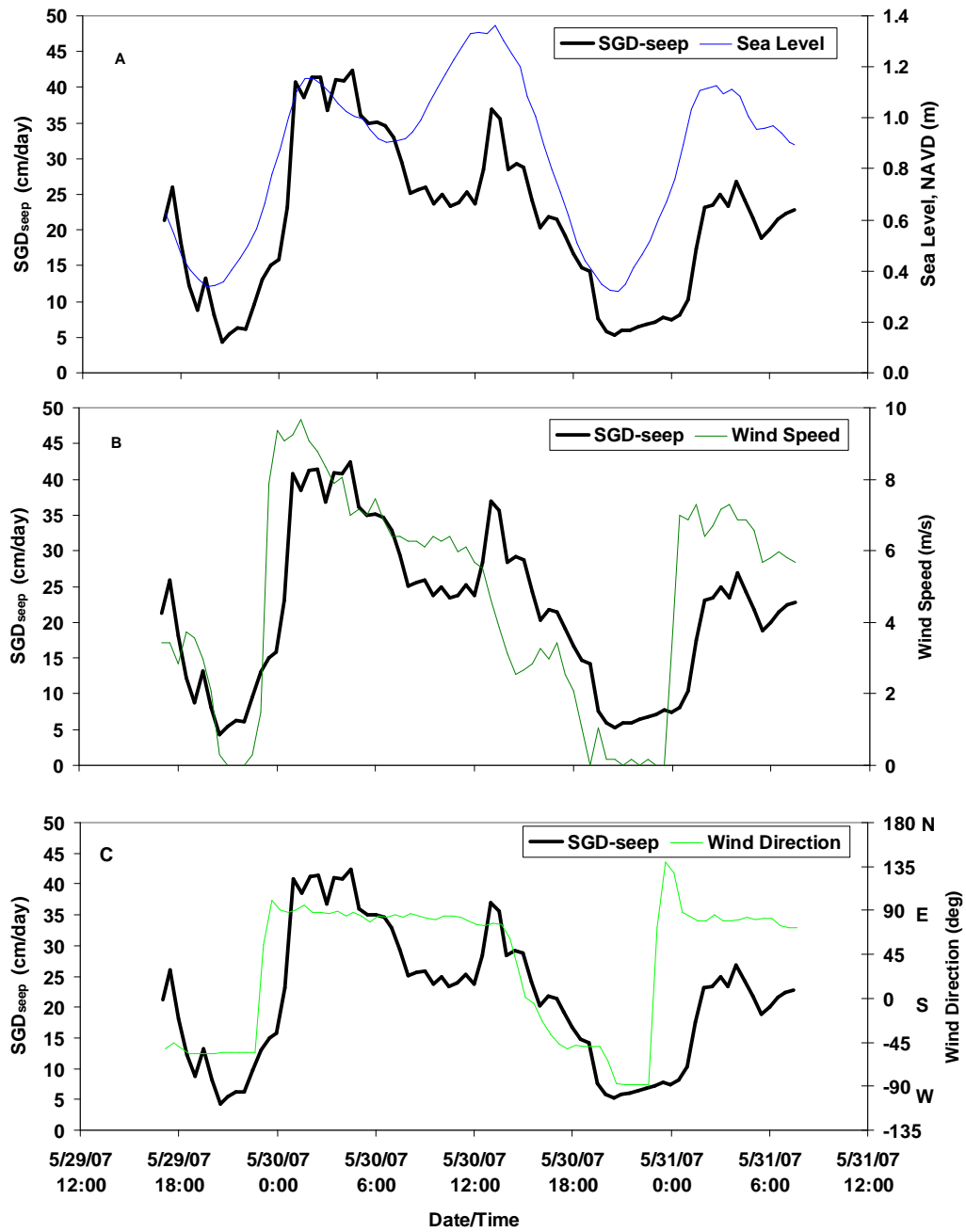


Fig. 3.5: Relationship between SGD_{seep} variations with: (A) Sea level, (B) Wind speed and (C) Wind direction, Θ (where, $\Theta = 180 - \text{actual angle}$, in degrees), for the period: 29 – 31 May'07. Unburied chambers.

There was also a significant positive correlation between SGD_{seep} and wind speed (Fig. 3.5B). The correlation coefficient was 0.75 ($R^2 = 0.57$; $p < 0.01$). The R^2 statistic indicates that this relationship alone could account for up to 57% of the variability in SGD_{seep} . The average wind speed was 4.5 ± 2.7 m/s ($n = 91$). A significant negative correlation between SGD_{seep} and wind direction (Fig 3.5C) was also observed. The correlation coefficient was -0.62 ($R^2 = 0.38$; $p < 0.01$) and the predominant wind directions were alternating between easterly and south westerly. The R^2 statistic indicates that up to 38% of SGD_{seep} variability can be explained by this correlation.

For the period, 29 – 31 May'07 (Fig. 3.6), the highest wind speeds were observed mainly in the evenings, between 18:00 and 0:00 hours (rising from about 18:00 and peaking around 21:00 hours before tapering off thereafter to lowest wind speeds). The lowest wind speeds coincided with the time when the wind direction was from the southerly to easterly direction (Fig. 3.5C). A similar observation was also depicted during the deployment period, 05 – 11 August'07 (Figs. 3.4). During both deployments, lowest wind speeds were < 1.8 m/s, and directed from southerly to easterly direction (i.e. *sea breeze* – winds toward the land). In these deployments, the highest wind speeds (> 6 m/s) occurred when the wind direction transitioned from either southerly (Fig. 3.4), or easterly (Fig. 3.6), to south westerly direction (i. e. *land breeze* – winds toward the sea). It would thus appear from these observations that a *land breeze* tends to favor the highest SGD_{seep} rates while the converse is true during a *sea breeze* (Figs. 3.4, 3.5 and 3.6). In other words, there seems to exist an SGD_{seep} consistent (land-sea breeze) correlation that is closely related to the sinusoidal tidal variation nature.

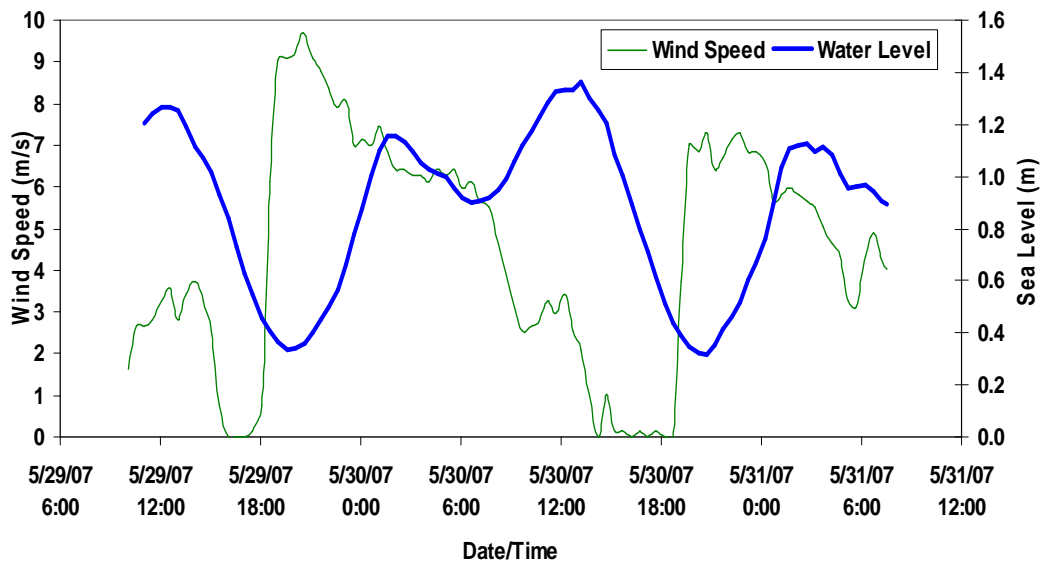


Fig. 3.6: Relationship between Sea Level and Wind speed for the period: 29 – 31 May'07.

Relationship Between SGD_{rad} Measurements and Sea Level, Wind Speed and Direction

There was also a significant negative correlation between SGD_{rad} (^{222}Rn derived SGD) and sea level at the 90% confidence level or higher (Fig 3.7A). This was based on concurrent measurements done during the period 29 – 31 May'07. The correlation coefficient was -0.38 ($R^2 = 0.14$; $p < 0.01$). The R^2 statistic indicates that this relationship could explain up to about 14% of the variabilities in SGD_{rad} . During this period, the tidal variations were nearly neap tide with a semi diurnal pattern.

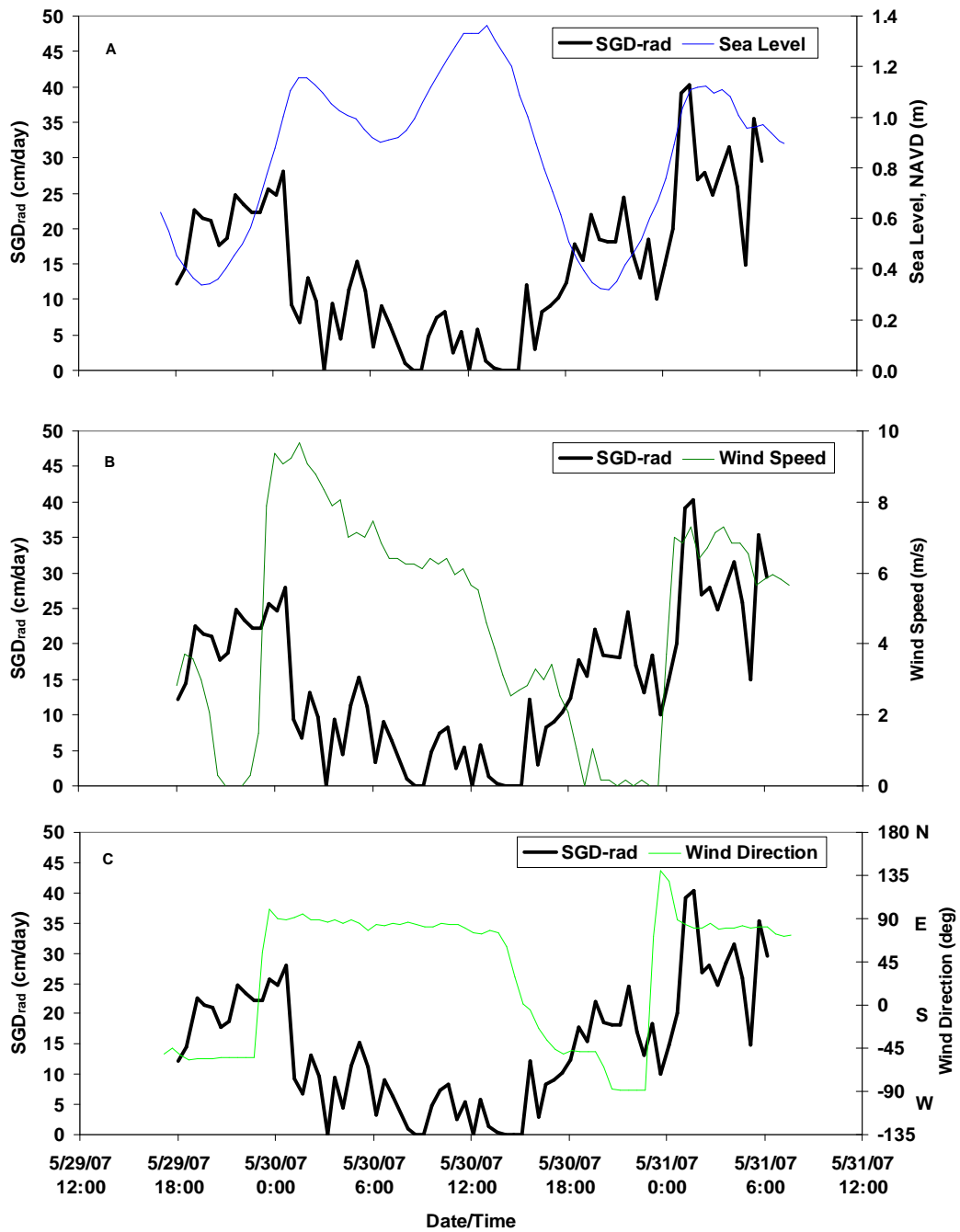


Fig. 3.7: Relationship between SGD_{rad} variations with: (A) Sea level, (B) Wind speed and (C) Wind direction, Θ (where, $\Theta = 180 - \text{actual angle}$, in degrees), for the period: 29 – 31 May'07.

In contrast, there was no significant correlation between SGD_{rad} and wind speed at 90% confidence level or higher (Fig. 3.7B). The correlation coefficient was -0.08 ($R^2 = 0.01$; $p > 0.1$). The average wind speed was 4.5 ± 2.7 m/s ($n = 91$). Similarly, there was no significant correlation between SGD_{rad} and wind direction at 90% confidence level or higher (Fig. 3.7C). The correlation coefficient was 0.16 ($R^2 = 0.03$; $p > 0.1$) and the average predominant wind direction was mainly south easterly.

Effect of Burying (Submerging) the Seepmeter Benthic Chamber in Sediment and Application of Blanks on SGD_{seep} Estimations

While it is evident from the summarized results (Table 3.1) that there exists varying correlations between SGD_{seep} measurements and the different environmental factors (sea level, wind speed and direction), the strongest relationship appears to exist between SGD_{seep} and both sea level and wind speed variations, both of which induce currents that could be responsible for some of the artifacts observed (Bernoulli effect).

Table 3.1: Summary of correlation analysis between SGD measurements and environmental variables.

Figure	Type of deployment	Dependent Variable	Independent Variable	Correlation Coefficient	R ²	Average Wind Speed and Direction	n	p-Value	Type of Correlation
3A	Buried Chamber	SGD _{seep}	Water Level	-0.63	0.4			< 0.01	Significant
3B	Buried Chamber	SGD _{seep}	Wind Speed	0.57	0.32	4.2 ± 2.3 m/s; SW	192	< 0.01	Significant
3C	Buried Chamber	SGD _{seep}	Wind Direction	-0.16	0.03			< 0.01	Significant
4A	Buried Chamber	SGD _{seep}	Water Level	-0.4	0.16			< 0.01	Significant
4B	Buried Chamber	SGD _{seep}	Wind Speed	0.58	0.33	3.2 ± 2 m/s; SW	1558	< 0.01	Significant
4C	Buried Chamber	SGD _{seep}	Wind Direction	-0.25	0.06			< 0.01	Significant
5A	Unburied Chamber	SGD _{seep}	Water Level	0.75	0.56			< 0.01	Significant
5B	Unburied Chamber	SGD _{seep}	Wind Speed	0.76	0.57	4.5 ± 2.7 m/s; E, SW	91	< 0.01	Significant
5C	Unburied Chamber	SGD _{seep}	Wind Direction	-0.62	0.38			< 0.01	Significant
6	Not Applicable	Wind Speed	Water Level	0.31	0.1	4.5 ± 2.7 m/s; E, SW	91	< 0.01	Significant
7A	Not Applicable	SGD _{rad}	Water Level	-0.38	0.14			< 0.01	Significant
7B	Not Applicable	SGD _{rad}	Wind Speed	-0.08	0.01	4.5 ± 2.7 m/s; E, SW	91	> 0.10	Not significant
7C	Not Applicable	SGD _{rad}	Wind Direction	0.16	0.03			> 0.10	Not significant

Our field experiments revealed contrasting relationships in variations between SGD_{seep} and sea level. For the case of normal deployments (unburied benthic chambers), the correlation was found to be positive (direct), while it was negative (inverse) for the buried chambers. Since the latter measurements tended to be in closer agreement with the independent concurrent SGD_{rad} measurements (Table 1), this approach likely provides more consistent measurements with less impact from the Bernoulli – induced flows arising due to topographic roughness. SGD_{seep} measurements tend to be more consistent when the benthic chambers are fully submerged compared to when they are partially submerged, as in the case of normal deployment (Table 1). Thus the action of completely burying benthic chambers in the sediment during SGD_{seep} measurements appears to reduce environmentally induced artifacts in the SGD results. As show in Table 2, such deployments also result in SGD_{seep} measurements that are in better agreement with those obtained by the independent ^{222}Rn approach (SGD_{rad}).

However, it is still debatable whether the significant correlation found between SGD measurements and wind speed and direction was purely as a result of Bernoulli – induced artifacts associated with topographic roughness of the seabed or perhaps this could mean that the latter (wind) actually inherently enhances SGD somehow? Although more work is suggested to decisively resolve the exact magnitude of contribution attributed to each of these two impacts, the summary of results in Table 1 showing significant correlation in most of the experiments, suggest that there was likely a varying level of SGD enhancement derived purely from wind speeds. Higher wind speeds (> 4 m/s) tended to have a higher impact. The fact that the unburied benthic chambers tended to correspond to higher positive correlations with SGD_{seep} and wind speed measurements compared to corresponding measurements derived from buried chambers, suggests a likely greater impact induced from Bernoulli – flow related artifacts on unburied compared to buried deployments.

From analysis of the SGD_{blank}/SGD_{seep} ratio (this criteria is preferred for analysis because the resultant ratio tends to provide a better resolution on the relative impacts deriving from the Bernoulli - flow related artifacts on SGD_{seep} measurements) as an approximate

criteria for assessment of environmental impacts on SGD measurements (Figs. 3.8 and 3.9), it seems clear that there was increased influence on SGD_{seep} measurements during the period of highest sea-level change (rising and ebbing of the tide).

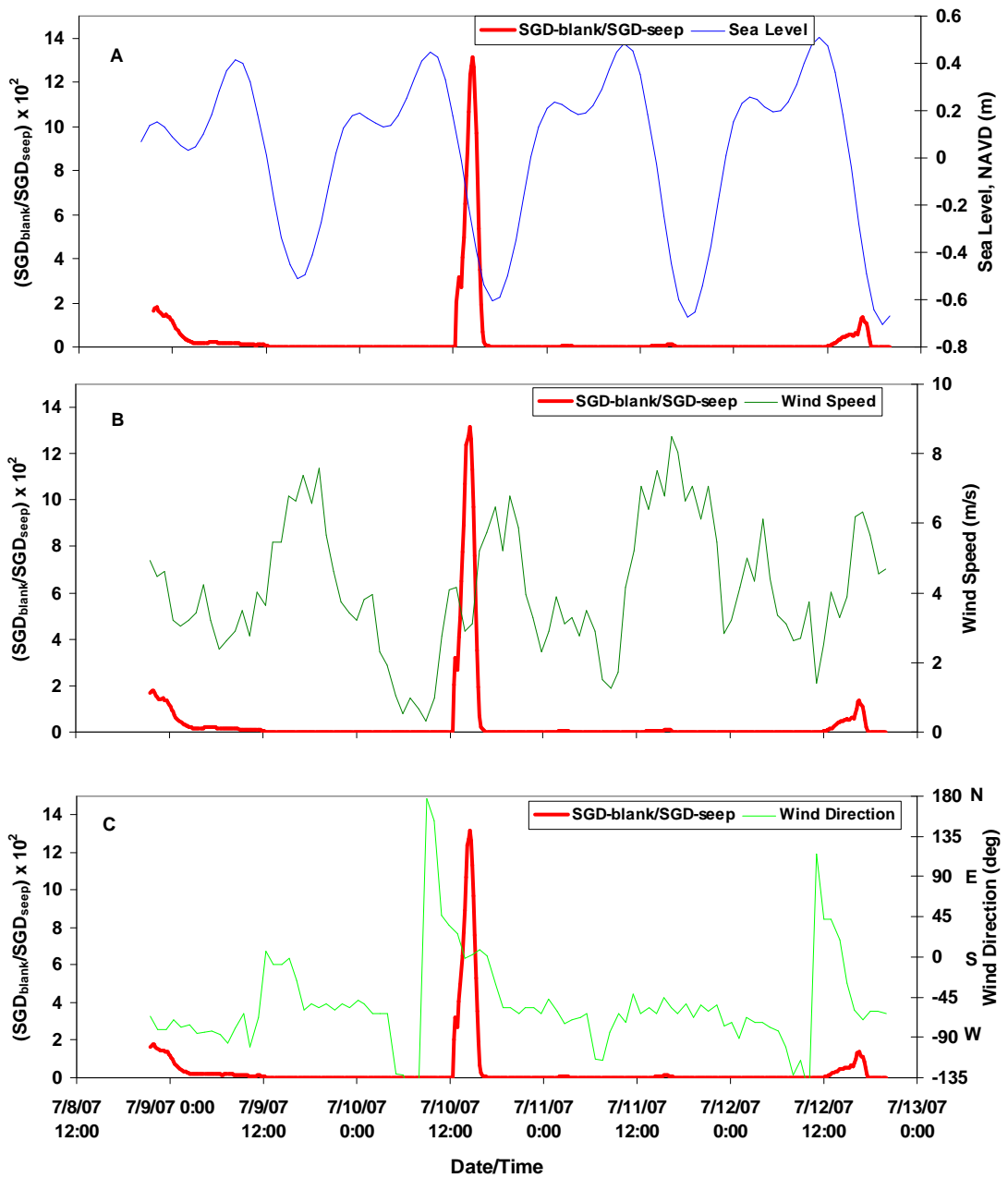


Fig. 3.8: Relationship between SGD_{blank}/SGD_{seep} ratio variations with: (A) Sea level, (B) Wind speed and (C) Wind direction, Θ (where, $\Theta = 180 - \text{actual angle}$, in degrees), for the period: 08 – 12 July'07.

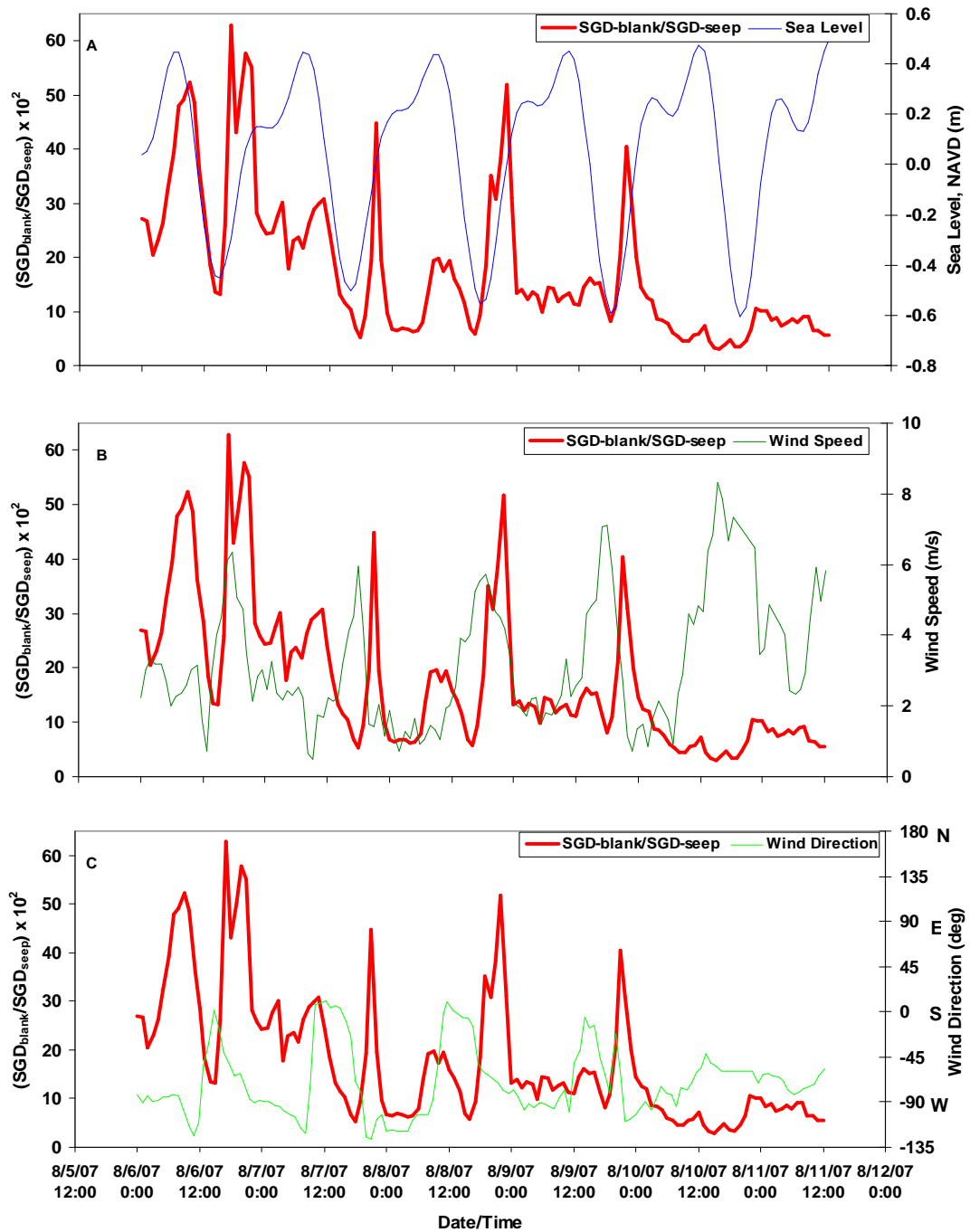


Fig. 3.9: Relationship between SGD_{blank}/SGD_{seep} ratio variations with: (A) Sea level, (B) Wind speed and (C) Wind direction, Θ (where, $\Theta = 180 - \text{actual angle}$, in degrees), for the period: 05 – 11 August'07.

A similar observation was also seen on the $SGD_{\text{blank}}/SGD_{\text{seep}}$ ratio during the peak of wind speeds. For instance as depicted in Fig. 3.4, when winds transitioned from southerly to westerly direction (average speed > 6 m/s), the highest SGD_{seep} values were realized which were also apparently accompanied by the highest seepage artifacts. Unfortunately, low tides also occurred almost exactly at the same time. In general however, the impact of wind speed on SGD_{seep} was more pronounced for those measurements which were < 2 m/s. It is to be noted that even when these artifacts are observed, the maximum $SGD_{\text{blank}}/SGD_{\text{seep}}$ ratio is still < 0.14 (Fig. 3.8), but less occasionally it approached 0.6 (Fig. 3.9). The majority of times however, this ratio was approximately zero (Fig. 3.8).

In general, our observations were closely correlated with the functioning of the Ekman transport concept (Neumann and Pierson 1966), within shallow coastal environments such as the case with our study site. In very shallow water (i.e. $H < 0.2 d_E$), the Ekman flow (where wind and current directions are normally orthogonal to each other) is essentially controlled by wind stress and bottom friction. Under these circumstances, the Coriolis force becomes insignificant and the current aligns with the wind direction nearly completely. The shallower the water, the more does the Ekman transport - which becomes the transport of the total water column under these conditions - pointing in the direction of the wind. In our case this phenomenon was most apparent during the *land breeze* situations (winds directed seaward, south westerly), when SGD_{seep} and associated artifacts (Figs. 3.4 and 3.9) were at their highest.

With these observations alone however, it is difficult to distinguish between the individual impacts of wind speed, wind direction and those due to the sea level variations, since as depicted in Figs. 3.3 and 3.4, their occurrences seemed concurrent. This is also confounded by the fact that analysis between seawater level and wind speed variations (Table 3.1), revealed a significant positive (though weak) relationship between them, with a correlation coefficient of 0.31 ($R^2 = 0.09$; $p < 0.01$). In addition, the average predominant wind direction during much of the deployment period remained fairly constant from the south westerly direction (Table 3.1). Further work is therefore

suggested with regard to resolving the individual impacts of wind direction and wind speed in relation to the overall Bernoulli – induced impacts on SGD_{seep} measurements.

Comparison Between SGD_{seep} and SGD_{rad} Estimates

In addition to the general agreement in trend, there was an overall strong positive long term correlation between SGD_{seep} and SGD_{rad} during the measurements conducted in the period May'06 - February'07 (Fig. 3.10). The correlation coefficient for the averaged monthly measurements for this period was 0.91 ($R^2 = 0.83$; $p < 0.01$). These results revealed a good agreement between the SGD_{seep} and SGD_{rad} , especially for seepmeter measurements in which the benthic seepage chambers were submerged (buried) in sediment (Table 3.2) as opposed to the unburied or partially submerged, or normal deployment (Taniguchi 2001). Although the SGD_{seep} and SGD_{rad} obtained from averaging long-term measurements during the period May'06 through February'07 are not significantly different, the absolute short term SGD_{seep} values tended to be on the higher side (by $\sim 9\%$) compared to those of SGD_{rad} (Figs. 3.5, 3.7 and 3.10, Table 3.2).

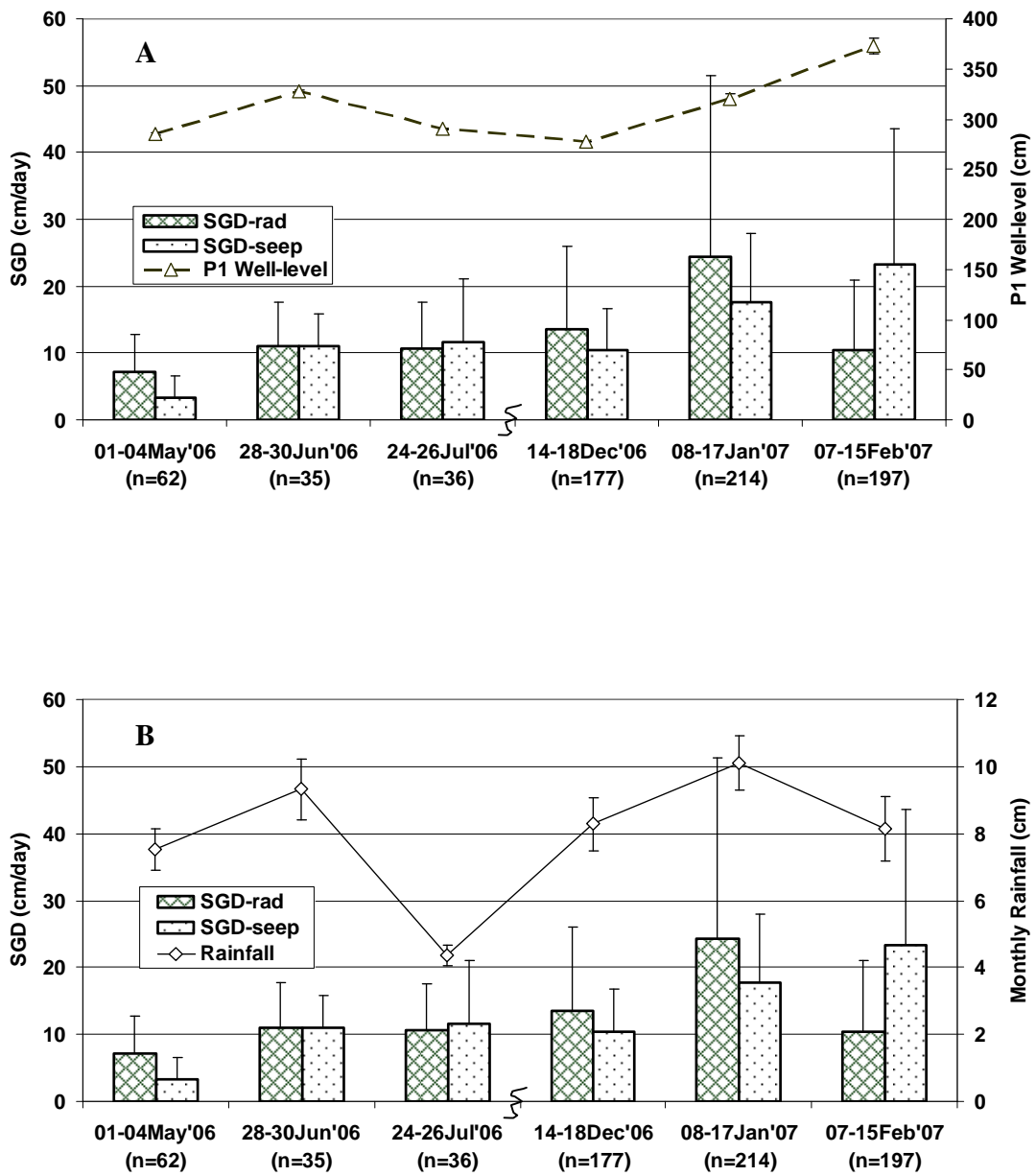


Fig. 3.10: Average long-term relationship between SGD_{seep} and SGD_{rad} with: (A) P1 Well water-level and (B) Monthly Rainfall. Error bars represent 1σ (standard deviation).

Table 3.2: Comparison of SGD measurements obtained from buried and unburied benthic seepmeter chambers and relative difference between SGD_{seep} and SGD_{rad} .

Date	SGD_{seep} (cm/day)	SGD_{rad} (cm/day)	Percent difference $\{(SGD_{seep} - SGD_{rad})/SGD_{rad}\} * 100$	Type of deployment	n
May 29-31, 2007	21.4 ± 11.3	14.7 ± 10.3	46.1	unburied (normal)	47
July 10-12, 2007	10.7 ± 3.2	8.7 ± 8.5	22.8	buried	71

It is to be pointed out that the SGD estimations obtained via the radon (SGD_{rad}) approach are integrated over a larger area compared to the SGD_{seep} results, which are more localized to the site covered by the benthic seepage chamber (Mwashote et al. 2010). The trend of our results were to a great extent in line with recent SGD assessments in the Yellow River, China, that were conducted using similar approaches, where it was found that absolute SGD measurements using the ^{222}Rn approach were in some cases, ~ 70% lower than those determined by automated seepage meters (Peterson et al. 2008).

It was also observed in this and in an earlier study in the area, that rain events can positively impact SGD measurements (Santos et al. 2009), though it was found that ~ 95 % of the SGD was contributed by recycled sea water (Santos et al. 2008). During this study observations of groundwater level time-series measurements taken on a well, P1, which was located inland (~100 m) from the shoreline at the study site, showed positive correlation with variations in SGD (Fig. 3.10). Well level variations in general are often associated with the status of recharge of surficial aquifers within the surrounding area.

The relationship between SGD and P1 well-level variations representing these long term measurements (May'06 – February'07) is evident (Fig. 3.11). The correlations depicted here could approximately be expressed as linear mathematical empirical relationships:

$$P1_{(gwl)} = 4.5 (SGD_{seep}) + 257$$

(for SGD_{seep} , where $P1_{(gwl)}$ = groundwater level for P1, cm; $R^2 = 0.7$)

$$P1_{(gwl)} = 0.3 (SGD_{rad}) + 308$$

(for SGD_{rad} , where $P1_{(gwl)}$ = groundwater level for P1, cm; $R^2 = 0.01$)

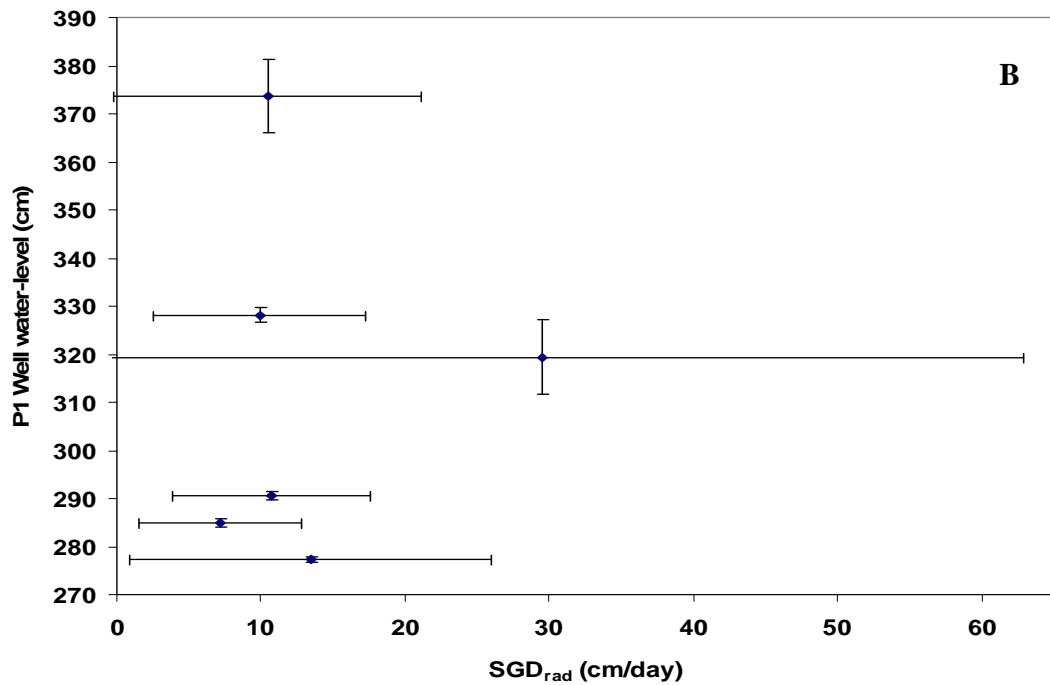
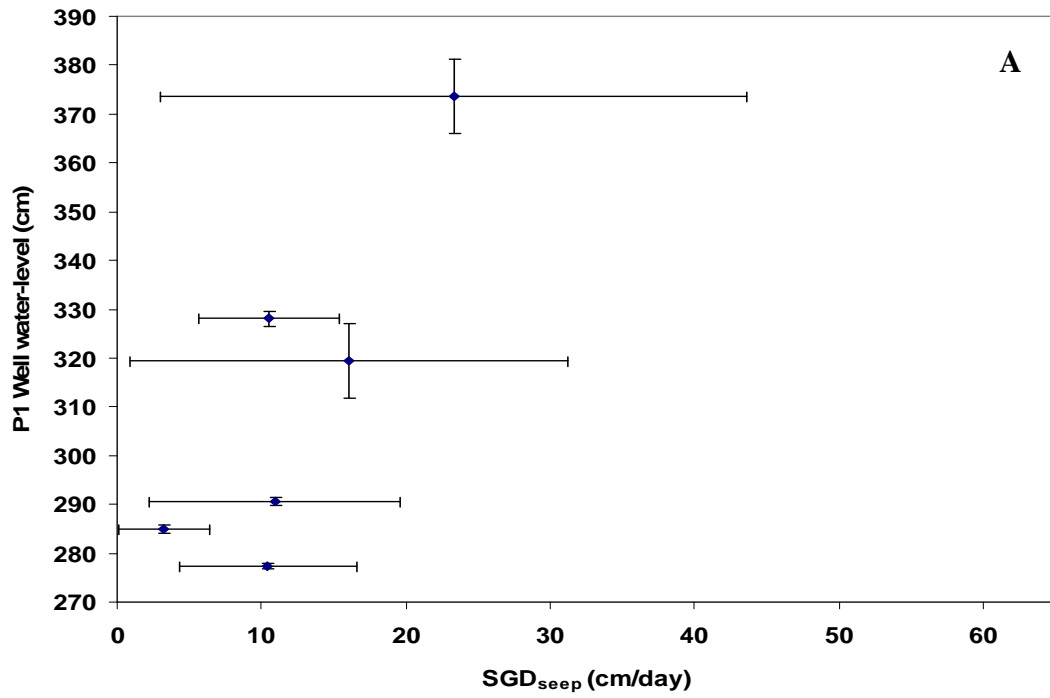


Fig. 3.11: Average correlations between P1 well water-level and: (A) SGD_{seep} and (B) SGD_{rad} measurements. Each data point represents average monthly measurements from May'06 through February'07. Error bar represents 1σ (standard deviation).

Although the correlation appeared to be stronger for $P1_{(gwl)} - SGD_{seep}$ compared to that of $P1_{(gwl)} - SGD_{rad}$, these relationships nonetheless serve to augment the long – term agreement (Fig. 3.10) observed between the two SGD estimation approaches (SGD_{seep} and SGD_{rad}). In general the relationship between SGD measurements and P1 - well groundwater level was more evident for long term measurements compared to short term measurements. Furthermore, the relative sizes of the error bars on the $P1_{(gwl)}$ – axis and the SGD_{seep} – axis reveal that although there exists some correlation between variations in groundwater level and SGD, the proportionately greater size of error bars seen on the SGD_{seep} – axis compared to the $P1_{(gwl)}$ – axis, is a clear reflection of the fact that the overall SGD measured is also significantly influenced by other factors besides the terrestrial groundwater discharge. This is an observation that has also been implied in previous studies in the same area that showed that re-circulated seawater contributes ~ 95 % of the observed SGD (Santos et al. 2008).

An approximate quantitative estimation of the overall average SGD per shoreline length {i.e. $(cm^3/cm^2.day).cm = cm^3/cm.day$ or $10^{-4} m^3/m.day$ } at the study site using these two different approaches for the period May'6 - February'07 were:

$$SGD_{seep}: 105,000 \pm 91,000 \text{ cm}^3/\text{cm.day} \quad (= 10.5 \pm 9.1 \text{ m}^3/\text{m.day})$$

$$SGD_{rad}: 77,000 \pm 49,000 \text{ cm}^3/\text{cm.day} \quad (= 7.7 \pm 4.9 \text{ m}^3/\text{m.day})$$

This general agreement in these SGD quantitative estimations also underscores the fact that the two techniques could either be used independently or in a complimentary manner. Complimentary use of these techniques has often proven more beneficial especially where spatial scales are important considerations (Burnett et al. 2003). The width of the seepage face was assumed to be ~ 200 m (Burnett et al. 2003, Taniguchi et al. 2003a), for the conversions shown above.

Conclusions

While important environmental factors, including sea level, wind speed, hydraulic gradient, wave set up, swells and rainfall, are important considerations in SGD measurements, it is likely that some of these environmental factors may impact different SGD measuring techniques to varying extents. It has previously been observed that some of these conditions can combine to induce pressure gradients that generally lead to Bernoulli-type flow artifacts on the prevailing topographic features found at the seabed such as sediment mounds or in our case, seepmeter benthic chambers (Huettel et al. 1996; Shinn et al. 2002; Cable et al. 2006). From the field results obtained in this study, there is compelling evidence that variations in sea level, wind speed and direction can play a role in influencing the magnitude of SGD_{seep} . In circumventing these potential adverse effects on SGD_{seep} measurements, our results (Figs. 3.3, 3.4) have demonstrated that, submerging (or burying) the seepage meter benthic chambers to the same topographic level as the sediment, effectively reduces the effects of the Bernoulli-induced flow that appears to be enhanced by the sea level variations (tide action) and wind velocity with respect to benthic chambers that were unburied (unsubmerged) in the sediment. Alternatively, parallel similar seepage meters could similarly be deployed inside non-porous materials (such as a child's plastic play-pool) to act as "blanks," and then subsequently accounted for in corrected SGD_{seep} measurements, to provide similar results. As shown in Table 3.1, SGD_{seep} measurements that were conducted in this manner showed a closer agreement compared with those obtained by an independent SGD measuring technique at the same study site (SGD_{rad} or ^{222}Rn geochemical tracer approach), than those where such considerations were not taken into account as revealed by their corresponding correlation analysis. Moreover, this fact is further reinforced by Table 2 results that reveal that the difference between SGD_{seep} and SGD_{rad} measurements are much greater (~twice) for deployments with unburied than with buried benthic seepage chambers.

Acknowledgements

The FSUCML management and staff are sincerely appreciated for their help and logistics during the entire study. Special thanks are to research colleagues Isaac Santos, Natasha Dimova and Rick Peterson whose help at field greatly contributed to the success of this study.

CHAPTER 4

SUBMARINE GROUNDWATER DISCHARGE IN THE SARASOTA BAY SYSTEM: ITS ASSESSMENT AND IMPLICATIONS FOR THE NEARSHORE COASTAL ENVIRONMENT

Publication Status:

Mwashote et al. 2010. Submarine Groundwater Discharge in the Sarasota Bay System: Its Assessment and Implications for the Nearshore Coastal Environment. Manuscript prepared for submission to: *Continental Shelf Research*.

Abstract

A study was conducted from July 2002 through June 2006 in order to assess the significance of submarine groundwater discharge (SGD) to Sarasota Bay (SB), Florida. The assessment approaches used in this study included manual seepage meters, geochemical tracers (radon, ^{222}Rn and methane, CH_4 , and sub-seafloor resistivity measurements.

The estimated SGD advection rates in the SB system were found to range from 0.7 to 24.0 cm/day, except for some isolated hot spot occurrences where higher rates were observed. In general, SGD estimates were relatively higher (5.9 – 24.0 cm/day) in the middle and south regions of the bay compared to the north region (0.7 – 5.9 cm/day). Average dissolved inorganic nutrient concentrations within the SB water column ranged: 0.1 – 11 μM ($\text{NO}_2 + \text{NO}_3$), 0.1 – 9.1 μM (NH_4) and 0.2 – 1.4 μM (PO_4). The average N/P ratio was higher in the north compared to the middle and south regions of the bay. About 40 % of the regional nutrient fluxes occurred in the north and the while ~ 60% were in the middle and south regions combined. The latter two regions also had the highest overall nutrient flux per water volume ratio, thus making them potentially more vulnerable to nutrient loading. On average, we estimate that about 27 % of the total N in

the SB system was derived via SGD. The prevalence of shallow embayed areas in the SB system and the presence of numerous septic tanks in the surrounding settlements enhanced the potential effects of nutrient - rich seepages.

Statistical comparison of the quantitative approaches revealed a good agreement between SGD estimates from manual seepage meters and those derived from the ^{222}Rn model ($p = 0.67$; $\alpha = 0.05$; $n = 18$). CH_4 was found to be useful for qualitative SGD assessments. CH_4 and ^{222}Rn were correlated ($r^2 = 0.31$; $\alpha = 0.05$; $n = 54$). Resistivity profiling was shown to be a viable tool for rapid, large scale surveys that yield useful information on subsurface salinities.

Introduction

Background

Sarasota Bay is a barrier island enclosed lagoon located on the southwest coast of Florida (United States), surrounded by the city of Sarasota. Over the last five decades, due to increased anthropogenic pressure, Sarasota Bay has experienced a slow but steady decline of its ecosystem's general health. It has had problems of water and sediment quality; increased nitrogen and poor clarity; loss of seagrasses, wetlands and coastal habitats; overuse; and adverse effects on marine biota. The Sarasota city population has grown, with more residential, commercial and industrial development, creating pollution (Sarasota Bay Estuary Program, SBEP 2006).

The bay and beaches are the center of a multi-million dollar tourism industry, the main industry in Sarasota. Due to population growth, seagrass and mangrove habitats have been altered to provide for waterfront development. As a consequence of this development, there has been increased loss of marine habitat and pollution. For instance, there are miles of shoreline replaced by seawalls and intense residential and commercial development, including numerous fill projects and dredging. Many areas of the bay were dredged to create navigable waterways and new home sites. This has resulted in increased storm water, wastewater, sediment and chemical contaminants being discharged into the

bay. The large numbers of septic tanks in the area have resulted in elevated N loading, especially in Roberts Bay, Phillipi Creek, Blackburn Bay and Little Sarasota Bay. Septic tanks alone remain a major environmental health issue and significant source of N. Storm water runoff is estimated to contribute 56% of N load with 60% coming from residential areas (FGS 1985; USGS 2007).

Over 1400 different native species of plants and animals and about 500,000 people are resident in Sarasota Bay area (SBEP 2006). Since the 1950's nitrogen loading into the bay has risen three fold and is still increasing with additional development (USGS 2007). The increase in algal growth increasingly blocked light to submerged seagrasses, and biological and chemical activity caused oxygen depletion in the water. Sarasota Bay was named in 1987 by the US Congress as of "national significance," and was designated as part of a National Estuary Program in 1989. This helped stimulate research concerning storm water, waste water and septic systems. The Sarasota Bay Program developed a comprehensive plan (Comprehensive Conservation Management Plan, CCMP) in the early 1990's as an attempt to address these problems. Early efforts for rehabilitation of the Sarasota Bay environment were focused on treating wastewater and storm water, which are the major nitrogen sources. The base flow (groundwater flow into tributaries) was then estimated to contribute 8% of the nitrogen to the bay (SBEP 2006). However, the results reported here will show that this is an underestimate given that SGD was shown to contribute about 12 % of N. Our estimates are based on the regional nutrient concentrations in groundwater, associated with SGD flux determinations made via independent approaches that were described in this study.

Several previous studies have documented the importance of SGD in the supply of nutrients and other dissolved components to many coastal environments (Valiela et al. 1990; Capone and Bautista 1985; Capone and Slater 1990; Oberdorfer et al. 1990). However, actual mechanisms driving the discharge can be quite varied (Bokuniewicz and Pavlik 1990). For instance, Lapoint et al. (1990) found significant inputs of nitrogen and dissolved organic phosphorous discharged to canals and surface waters in the Florida Keys, which may have been an important factor for initiating phytoplankton blooms in

the area. It was also suspected that nitrogen rich groundwater may have been responsible for nourishing algal mats in Bermuda (Lapoint and O'Connell 1989) as well as bays and reefs in Jamaica (D'Elia et al. 1981). SGD is particularly important in these cases because shallow groundwaters are enriched in nitrogen species, often due to contamination from septic tanks (Corbett et al. 1999). Perhaps of even greater significance and historical importance is that groundwater contaminated by bacterial pathogens from sewage and septic systems was responsible for 63% of all water borne illness in the US during the 1970's (Porter 1985). Elsewhere, Paul et al. (1995) directly traced sewage effluent from a septic tank into surface water in less than 12 hours in Key Largo Florida, while Dillon et al. (2000) also documented impacts on surface waters from sewage disposal.

While the potential for contaminated groundwater to have an impact on surface waters is greatest in coastal areas and restricted bodies of water, the impact of groundwater into a coastal system is dependent on several variables. These include the amount and type of nutrient enrichment in the groundwater, circulation, tidal flushing, porosity and permeability of the underlying strata, hydraulic head and the corresponding groundwater flow. Due to variability in many of these parameters, the exact location of discharge into coastal regions may be difficult to determine by only monitoring the standard water quality constituents, such as nutrient concentrations or turbidity, or by the exclusive use of any one particular method.

Significance and Objectives of Study

As efforts to reduce surface water pollution continue and are successful, possible SGD pathways of contamination will also need to be understood. The main purpose of this study was therefore to assess SGD in the Sarasota Bay system and determine if it plays a significant role in the water and nutrient budgets of the bay system with respect to other sources. In this work, three independent approaches were employed including manual seepage meters, natural tracers (^{222}Rn , CH_4) and a relatively new technology: sub-seafloor resistivity measurements. Together, these approaches were used in order to locate, characterize and quantify SGD rates within the bay system.

Study Area: Description of the Sarasota Bay System

The Sarasota Bay system (SB system) extends from the north, Anna Maria Sound, to the south, Venice Inlet. The bay lies between barrier islands called keys that separate the body of water from the Gulf of Mexico. Longboat Key, Lido Key, Siesta Key, and Casey Key are the major keys that delineate the main bay system and its smaller portions. Sarasota Bay has a watershed of 417 km² of which 65% is uplands and 35% is wetlands. The SB system is about 26 km long and 6.1 km wide at the widest point and has a surface area of about 97 km² (SBEP 2006; USGS 2007). The two major portions are Sarasota Bay and Little Sarasota Bay, but there are many smaller creeks, embayments and bayous. Freshwater enters the bay system through small tidal bayous and creeks, whose input includes storm water runoff and SGD. Major tributaries to the bay system are Whitaker Bayou, Hudson Bayou and Phillipi Creek. The highest concentration of septic tanks (approximately 35,000) is found within Phillipi Creek catchment area (Lipp et al. 2001). Whitaker Bayou receives advanced treated wastewater effluent from the city of Sarasota municipal treatment plant (Dillon and Chanton 2005). Numerous other bayous and canals are also found within the bay system. For reference, the study site (Fig. 4.1) was divided into three general bay regions: North, Middle and South.

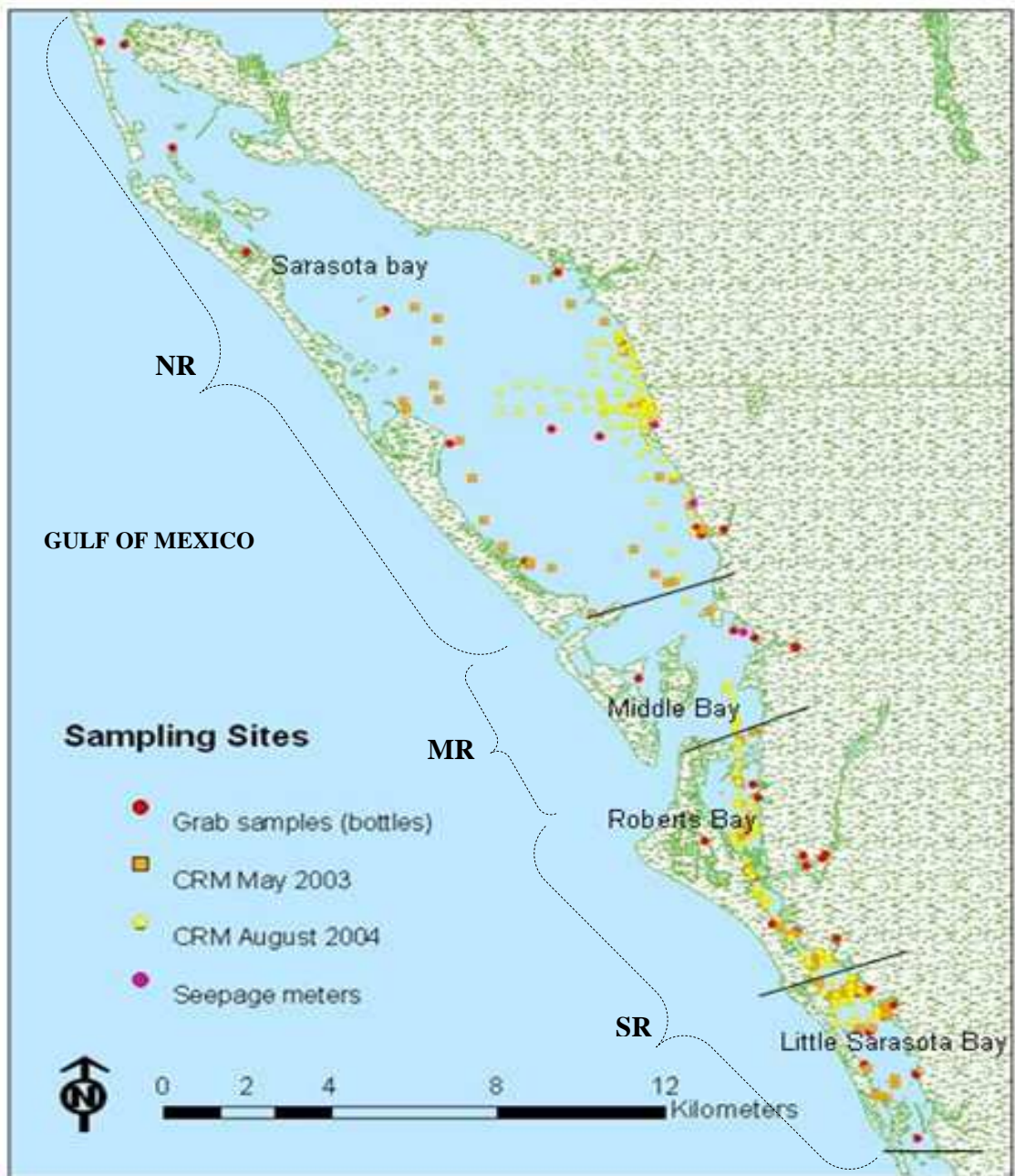


Fig. 4.1: Study area showing sampling sites for radon grab (bottle) samples, continuous radon monitor (CRM) transects and seepmeter SGD measurements within the Sarasota Bay system. For purposes of the study, the area was divided into three regions: North Region (NR, water volume $\approx 80\%$), Middle Region (MR, water volume $\approx 12\%$) and South Region (SR, water volume $\approx 8\%$). This is also the region referred to Sarasota Bay (SB). The assumed 200 m SGD regime area within the SB system is $\sim 7.8 \text{ km}^2$ ($\sim 8\%$ of the total SB area). The North Bay region lies on latitudes $\geq 27.3444^\circ \text{ N}$. Middle Bay (MB) is found within latitudes $27.3047 - 27.3444^\circ \text{ N}$, while the South Bay region lies within latitudes $27.1250 - 27.3047^\circ \text{ N}$.

The South Bay region comprises Roberts Bay (RB) and Little Sarasota Bay (LSB). The bay regions are generally all shallow, particularly the South Bay, less than 2 m, except for within the Intracoastal Waterway (Table 4.1). The North Bay is somewhat deeper, up to 4 m in some areas. Passes are open at the North and Middle Bay (NB and MB). The South Bay has only one pass (within RB). Phillipi Creek is a tidal creek within the South Bay (within RB). The land adjacent to Phillipi Creek had a high septic tank population at one time (mostly currently replaced) that was blamed in part, for the degradation experienced within RB. The mean annual rainfall of the area is about 140 cm, primarily from mid-June to mid-October (Fig. 4.2). Only about 30-35% contributes to surface water runoff, 5% is recharged into the groundwater and 65-70% is lost through evapotranspiration (USGS 2007). Most of the rain water enters the bay system as storm water runoff via creeks and bayous. Inlets provide for water exchange to Gulf of Mexico at Anna Maria Sound, Longboat Pass, New Pass, Big Pass and Venice Inlet. The land around the bays is mostly flat and poorly drained, with swamps, marshes and ponds throughout the area. The water table is near the land surface in most areas nearby, and some areas are characterized by artesian flow (mainly in the North region). Extensive natural drainage systems have been channelized. The surficial aquifer generally flows west and south. Below the sandy/shelly area is sandy limestone with a carbonate mud matrix, with varying amounts of clay, phosphatic sediments, dolomites and limestone (FGS 1985).

Table 4.1: Estimates of physical characteristics of the Sarasota Bay system (SBEP 2006; FGS open file report 10 Geology of Sarasota Co. 1985).

Region within SB System	Total passes present	Average length (km)	Average width (km)	Average depth (m)	Area (km²)	Estimated residence* time (days)
North	2	19	5	2.5	75.1	5 – 12
Middle	2	4	3	2.5	11.1	5 – 12
South	1	6	2	1.5	10.5	3 – 7

* = Estimates were made using a modified simple tidal prism model approach described in Dyer (1973); Dyer and Taylor (1973).

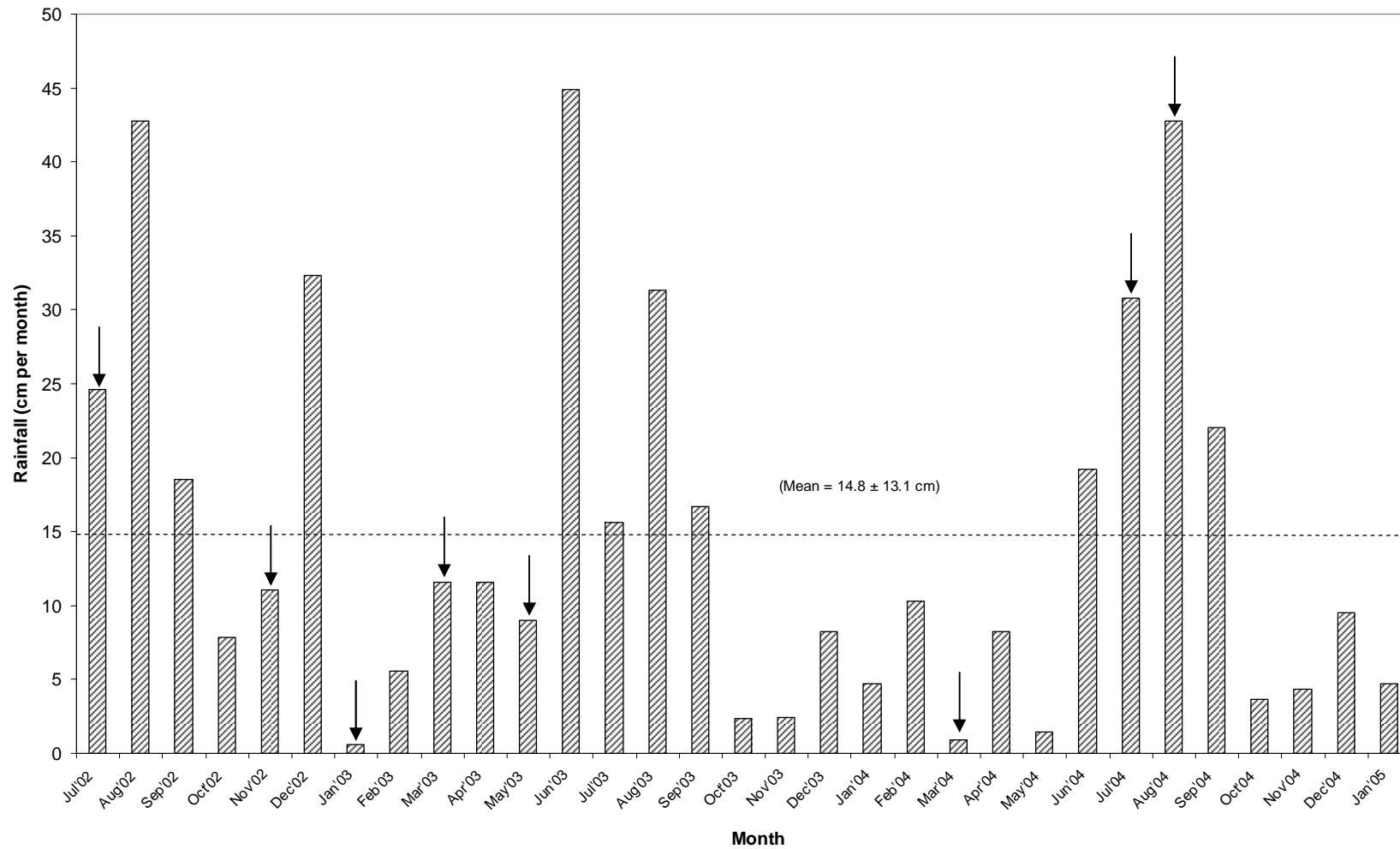


Fig. 4.2: Monthly rainfall variation around the Sarasota Bay region, July '02 – January '05 (Note that places with arrows indicate sampling periods). Rainfall data source: *Southwest Florida Water Management District 2005*.

The predominant sediment type around New College area (within NR) is of undifferentiated quaternary fossiliferous composition while at the RB site (found within SR) it is mainly of the Arcadia Formation. Sediments at the NC site consist of clay, silt, sand, phosphate and carbonate in varying admixtures (Petuch 1986) and the lithologies of the Arcadia Formation may consist of clayey, sandy/silt, phosphatic carbonates, phosphatic sands, variably sandy/silt, phosphatic clays and clean sand (Scott et al. 1988; Brewster-Wingard 1997). A regionally persistent clay bed within the Arcadia Formation occurs in the southern region (Barr et al. 1996).

Materials and Methods

General Approach

Previous research in the SB system identified areas of potential groundwater contamination in the southern bay (FGS 1985; SBEP 2006). Samples for radon and methane were collected from these areas in addition to other areas within the system. Radon samples were analyzed within 4 days (about one half-life) while methane samples were held in ice or refrigerated and analyzed within 2 weeks. Manual seepage meters were also deployed within the SB system in order to directly determine seepage rates, and resistivity surveys were conducted to assess areas within the SB system with freshwater in the shallow subsurface.

Radon Measurements

The method for measuring ^{222}Rn in grab samples of seawater was first developed by Broecker (1965) and modified by Key et al. (1979) and Mathieu et al. (1988). More recently a continuous radon monitor (CRM) approach was developed (Burnett et al. 2001; Dulaiova et al. 2005). Both bottle sampling and the CRM approach were used in this study.

^{222}Rn - Bottle Technique

Radon samples were collected at several sampling sites periodically in (helium) evacuated 6-liter high density polyethylene bottles on various occasions (a minimum of

bimonthly interval) from July 2002 through to June 2006. There were 125 individual samples and approximately 20% of these were duplicates. ^{222}Rn samples were collected about 0.3 m above the bottom using a peristaltic pump and Tygon tubing fitted into helium filled 6-liter bottles. The tubing was flushed twice with ambient water before filling the bottles about 2/3 full and clamping off the intake and vent hoses.

During laboratory analysis, an extraction-transfer line was used to strip radon gas from the samples by passing helium through the water samples at a rate of 200 mL per minute for 90 minutes. The gas stream flowed through a drying tube filled with drierite and ascarite to remove H_2O and CO_2 , respectively, and radon was condensed on a liquid nitrogen cold trap, while helium was vented into the atmosphere. The appropriate valves were closed and the trapped radon was heated and allowed to flow into an evacuated alpha scintillation cell together with helium to bring the pressure up to one atmosphere. The cell was placed in a photomultiplier alpha scintillation counter after at least 3 hours ingrowth time to count ^{222}Rn and its two alpha-emitting daughters, ^{218}Po and ^{214}Po . The water samples were then stored for at least 20 days for radon ingrowth and then the process was repeated twice to measure ^{226}Ra . At the conclusion of the analysis, the volume of the water in the containers was accurately measured and then safely disposed. In order to provide sufficient resolution to measure small changes, $\pm 10\%$ of the measured concentration was used as the data quality objective for radon measurements. Standard equations for estimating precision based on counting statistics were used and standards were run on a regular basis.

For a radioactive species such as radon, the quantitative estimation is made by measuring the number of counts (n) obtained in a detector over time (t). If the time is small compared to the half-life of the source, then it can be shown that the probability distribution of the counts obtained in repeated equal counting times is given by a Poisson distribution. Furthermore, when n is large (≥ 30), the Poisson distribution is well approximated by a normal (Gaussian) distribution (Longworth 1998). When one measurement is performed, the best estimate of the true number of counts is n and the estimated standard deviation, s , for a single measurement is $s = \sqrt{n}$. In addition to the

“counting errors” described above, ^{222}Rn calibration uncertainties should also be considered as well as the uncertainty of the detector background count rate. The efficiency of the detectors was determined by the analysis of NIST-traceable ^{226}Ra solution standards which have known amounts of ^{222}Rn (^{226}Ra is the radioactive parent of ^{222}Rn). Multiple runs of NIST standards were used to evaluate the standard deviation by the common expression:

$$s = \sqrt{\frac{\sum_{i=1}^n (x_i - \bar{x})^2}{n - 1}} \dots\dots\dots(4.i)$$

This was combined with the stated NIST uncertainty of the standard to set an overall calibration uncertainty. The background uncertainty was obtained by counting the alpha scintillation cells filled with helium. Such background measurements were made on each cell before use for actual samples. Finally, all known sources of uncertainty were combined using standard formulations for propagating errors (Longworth 1998).

Sediment Equilibration Experiments

Sediment samples were collected at 27 sites to estimate radon in pore waters. A grab sampler (Petite Ponar) was used to collect sediment samples which were placed into polythene sampling bags. The site number, date and time were recorded on the sample bag until analyzed. These samples were used for “sediment equilibration” experiments to assess porewater ^{222}Rn values and in deriving diffusive ^{222}Rn flux estimations (Martens and Klump 1980; Cable et al. 1996). Sediment subsamples of approximately 70 g were weighed and placed in a 250-mL Erlenmeyer flask with 120 mL of radium free DI water. A stopper with two clamped tubes was placed in the neck and the stopper was sealed with marine sealant. The flasks were placed on a shaker table in a water bath for at least 30 days. Radon was then measured using the extraction procedure described above. Degassing time was set at 60 minutes.

²²²Rn and ²²⁶Ra Calculations

Total ²²²Rn activities in water samples were calculated by the following equation:

$$A_{222} = \frac{R}{3(E)(L)} \times \frac{1}{e^{-\lambda t_1}} \times \frac{\lambda t_2}{1 - e^{-\lambda t_2}} \dots\dots\dots(4.ii)$$

Where:

- A₂₂₂ = activity of total ²²²Rn (dpm/L),
- R = the net sample count rate per minute (cpm),
- E = the total efficiency of the system (including stripping, trapping, transferring, and cell counting efficiencies expressed as a fraction). The factor of three accounts for the two alpha-emitting daughters as well as ²²²Rn,
- L = sample volume (liters),
- λ = the radioactive decay constant for ²²²Rn (1.235 x 10⁻⁴ /min),
- t₁ = time from the beginning of sample degassing to beginning of counting (min),
- t₂ = counting time (min).

This procedure provided the total amount of ²²²Rn activity at the time of analysis. In order to calculate "excess" radon, a correction must be applied for the amount of radon in the sample which is supported by ²²⁶Ra. After an appropriate ingrowth period, the activity of ²²²Rn is measured again in a similar manner. In this case two de-emanations are necessary (the first of which can be the radon analysis) and the time between them will define the ingrowth of ²²²Rn from the parent ²²⁶Ra. Repeated analyses of ²²⁶Ra samples were performed to assure consistent results. The calculation of the radium activity is similar to that used for ²²²Rn except that a correction was added for the radon ingrowth period as shown in the following equation:

$$A_{226} = \frac{R}{3(E)(L)} \times \frac{1}{(1 - e^{-\lambda t_1})(e^{-\lambda t_2})} \times \frac{\lambda t_3}{1 - e^{-\lambda t_3}} \dots\dots\dots(4.iii)$$

Where:

A_{226} = activity of ^{226}Ra (dpm/L),

t_1 = radon ingrowth time (the time from the end of the initial degassing of the sample to the start of sample de-emanation, min),

t_2 = time from end of sample flushing to time counting is initiated (min),

t_3 = counting time (min).

All other variables in the ^{226}Ra equation are the same as those discussed for the initial ^{222}Rn calculation. After both total ^{222}Rn at the time of sample analysis and ^{226}Ra are determined, any "excess" ^{222}Rn present in the sample ($^{222}\text{Rn}_{\text{ex}} = ^{222}\text{Rn}_t - ^{226}\text{Ra}$) may be corrected back to the time of sample collection by use of a standard decay equation, $A_t = A_0 e^{-\lambda t}$ where t in this case represents the time interval in between sample collection and analysis, i. e.:

$$^{222}\text{Rn}_0 = ^{222}\text{Rn}_t / e^{-\lambda t} \dots\dots\dots(4.iv)$$

Continuous ^{222}Rn - Mode (CRM) Surveys

Data were also collected using a continuous radon monitor (CRM) for two survey transects during May 2004 and August 2004 and two time-series at a fixed sites: New College – Caples (NC) and Roberts Bay (RB), 08-12 January 2003 (Fig. 4.1). For the case of CRM assessments, the CRM system (Rad 7 radon monitor from DurrIDGE Inc.) analyzes ^{222}Rn from a constant stream of water passing through an air-water exchanger that distributes radon from a running flow of water to a closed air loop. The air stream is fed to a commercial radon-in-air monitor which determines the concentration of ^{222}Rn by collection and measurement of the alpha-emitting daughters, ^{214}Po and ^{218}Po . Since the distribution of radon at equilibrium between the air and water phases is governed by a well-known temperature dependence, the radon concentration in the water is easily calculated.

SGD Estimates from ^{222}Rn

When the CRM was used in a time series mode, generally the concentration results (and thus inventory) were analyzed over short time periods, for instance each hour or two.

With integration times this short, loss of radon by decay and inputs via diffusion can usually be ignored. The flux of radon out of the water column by atmospheric evasion was calculated using well-known relationships of radon emanation to wind speed, temperature, and concentration gradients (MacIntyre et al. 1995). Adjustments to inventories as a consequence of tidal variations were easily performed with measurements or estimates of the tidal stage and radon concentrations of incoming and outgoing waters. Radon inventories were generally normalized to mean tidal height so this effect was discounted.

In order to calculate SGD rates, the measured radon concentrations were converted to fluxes of excess (unsupported) ^{222}Rn into the system (assumed to be dominated by groundwater) and corrected for various losses (Cable et al. 1996; Burnett and Dulaiova 2003). Fluxes were estimated by examining the change in inventories (^{222}Rn concentration \times depth). The model thus addresses: (1) correction for supported ^{222}Rn ; (2) atmospheric loss of radon at the air-sea interface; (3) dilution and loss of radon from the system via tidal and other mixing processes; and (4) estimates the input of radon via SGD.

In order to convert to water fluxes (ω , cm/day), the estimated total ^{222}Rn fluxes (dpm/cm².day), F_{total} , is divided by the concentration of excess ^{222}Rn ($\text{ex } ^{222}\text{Rn}_{\text{pw}}$, dpm/cm³) in the fluids entering the system according to the equation (Burnett and Dulaiova 2003):

$$\omega \text{ (cm/day)} = F_{\text{total}} / \text{ex } ^{222}\text{Rn}_{\text{pw}} \dots\dots\dots(4.v)$$

Fig. 4.3 depicts a basic mass balance “box” type model which describes the various inputs and losses. The model is similar to those used in previous radon studies (e. g., Corbett et al. 1999) in that it describes various source and sink terms for radon in the system.

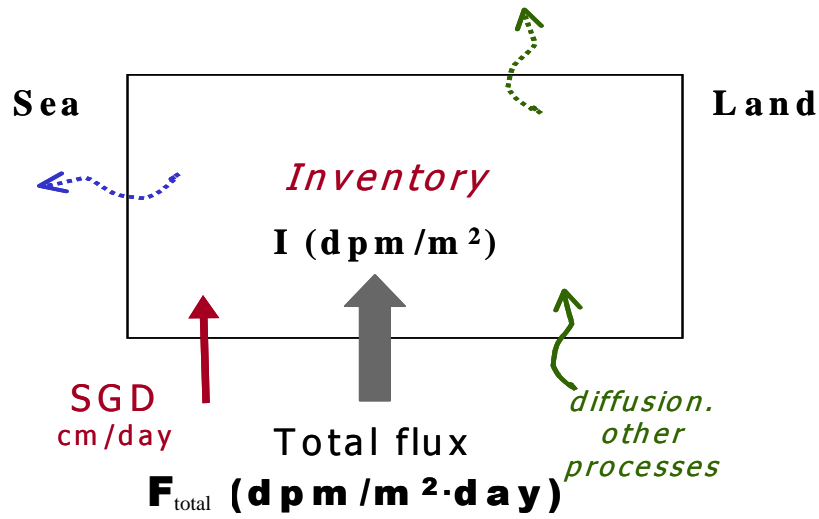


Fig. 4.3: Conceptual box model for ^{222}Rn model (Burnett and Dulaiova 2003).

Estimation of ^{222}Rn from Diffusion

Diffusive fluxes (F_{diff}) from porewater profiles were estimated according to two approaches. With Fick's First Law adapted from Berner (1980):

$$F_{\text{diff}} = -\phi D_s (dC/dZ), \dots\dots\dots(4.vi)$$

and also from the depth independent estimation model in Martens (1980):

$$F_{\text{diff}} = (\lambda D_s)^{1/2} (C_{\text{eq}} - C_o) \dots\dots\dots(4.vii)$$

Where,

ϕ = sediment porosity

D_s = effective wet sediment diffusion coefficient

dC/dZ = gradient of ^{222}Rn concentration at the sediment-water interface

λ = decay constant for ^{222}Rn

C_{eq} = ^{222}Rn in wet sediment at equilibrium with radium in the sediment
(measured via sediment equilibration)

$C_o = {}^{222}\text{Rn}$ in the overlying water at sediment-water interface multiplied by the sediment porosity to obtain a value corresponding to the ${}^{222}\text{Rn}$ concentration in wet sediment

For the estimation of D_s , we used the approximation from Peng et al. (1974):

$$-\log D_o = (980/T) + 1.59 \dots\dots\dots(4.viii)$$

Where,

D_o = molecular diffusion of radon through water

T = temperature (in Kelvin, K)

Sediment tortuosity is then corrected for in order to obtain the effective diffusion coefficient, $D_s \approx \phi D_o$ (Ullman and Aller 1982).

Methane Measurements

Methane samples were collected in dissolved oxygen bottles and stored on ice until analysis. The tubing from the peristaltic pump was placed into the bottom of the bottle and the water was allowed to gently overflow for approximately 3 bottle volumes before sealing.

Methane samples were then analyzed in the laboratory by the headspace equilibration technique (McAuliffe 1971; Chanton et al. 1989). Samples were transferred from the DO bottle to a 60 mL disposable syringe equipped with a 3-way stopcock. The syringe was rinsed with nitrogen three times before use, and stored disassembled between usages. Water is pulled into the syringe through small diameter Tygon tubing which fits snugly over the end of the stopcock. Entry of air into the syringe was avoided. After 25 mL of the sample has been transferred to the syringe, an equal volume of N_2 was pulled into the syringe as a headspace. The stopcock was closed and the syringe containing the sample and the headspace were shaken vigorously for 2 minutes. The headspace was injected into the FID GC through a manual gas sampling valve. This injection occurred across a 2

inch precolumn packed with drierite. Peak height was quantified on a Hewlett Packard integrator. Sample concentration was checked against working standards tied to standards obtained from Scott Specialty Gas of Plumsteadville, PA.

Headspace concentrations in ppmv (parts per million by volume, = $\mu\text{L/L}$) were determined by reference to known standards. Headspace CH_4 concentrations are converted to dissolved concentrations in μM as shown below.

$$(\mu\text{L/L}) / (R((\text{Latm})/(\text{mol K})) * T (\text{K})) \dots\dots\dots(4.ix)$$

where R is the gas constant from the ideal gas law, ($PV = nRT$), and T is temperature in Kelvin, K.

Seepage Meter Measurements

Groundwater seepage rates into surface water bodies are often made using manual seepage meters. Manual seepage meters are open-ended chambers placed over the bay floor with a vent tube to which a plastic sample bag is attached to collect groundwater seeping from the bay floor (Fig. 4.4).

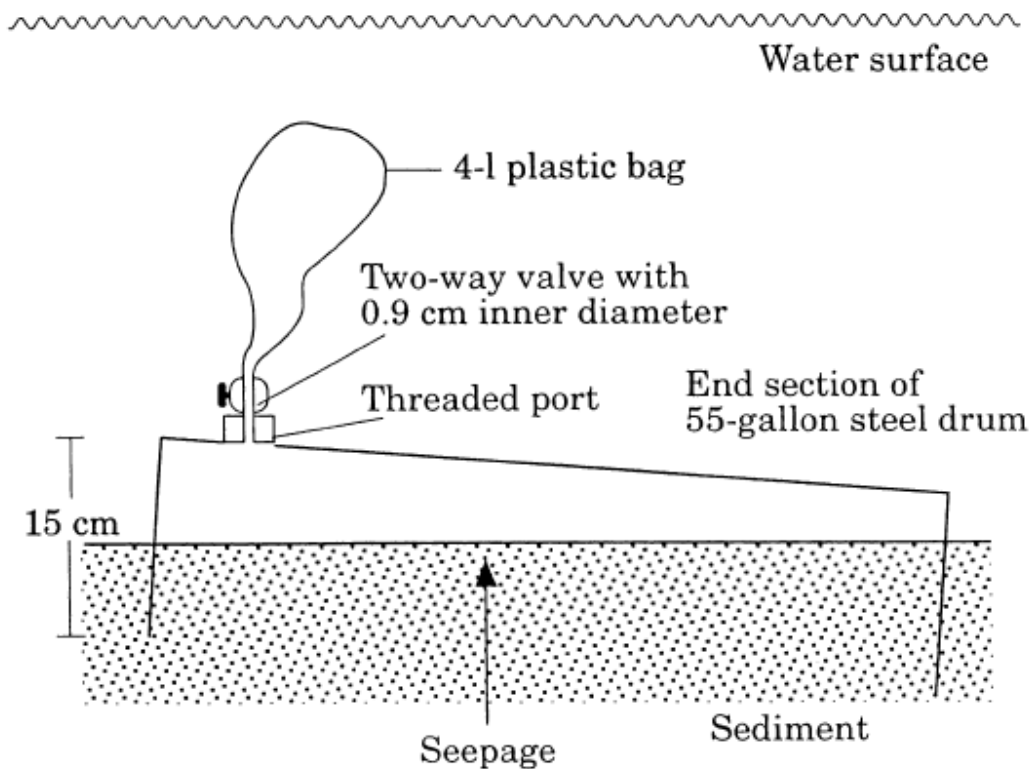


Fig. 4.4: Lee-type, manual seepmeter (Lee 1977; Taniguchi et al. 2003a). When water seeps into the chamber it displaces water that is forced into a plastic bag attached to a tube in the top of the drum. The change in volume over a measured time interval provides the seepage rate.

This device was first developed by Israelsen and Reeve (1944) to measure water loss from irrigation canals. Later, Lee (1977) designed a seepage meter consisting of one end of a 55-gallon (208 L) steel drum, fitted with a sample port and plastic collection bag. In this study we deployed several manual seepage meters at three sites between May and July 2004. Deployment sites were selected because they were in areas of suspected seepage and could be accessed from shore (Fig. 4.5).



(A)

(B)

Fig. 4.5: Field manual seepage meter and “bottle” (^{222}Rn) sampling (grab sampling using a peristaltic pump), within the Sarasota Bay system during: (A) Low tide and (B) High tide.

During the manual seepage meter deployments in the field, plastic bags were pre-filled with 1 L ambient seawater before deploying them on the drum chambers which had been left for an initial ~ 4h to achieve equilibration at the deployed site. This serves as a precautionary measure aimed at addressing measurement artifacts that can readily arise from frictional resistance and head loss along the internal boundary of meter, attachment tube, reservoir bags as well as short-term influx of water after the plastic bags have been attached to the seepage meter (Shaw and Prepas 1989, 1990a,b; Shinn et al. 2002). The SGD flow rate, in cm/day, was computed by dividing the change in volume (cm^3) of water collected in the seepage bag by the cross-section area (cm^2) of the benthic chamber and dividing the result of this by the time taken (hours converted into days), for the volume of water to collect. Thus, net measured water volumes (in cm^3), collected in the bag after every ~ 1 h on a known area (2550 cm^2), yielded the seepage rate ($\text{cm}^3/\text{cm}^2 \cdot \text{day} = \text{cm}/\text{day}$).

Resistivity Survey

Resistivity surveying is an electrical method of geophysical prospecting which depends on variations in the conductivity, or resistivity, of rock layers. The apparent resistivity of the ground is determined by measuring the potential difference across two electrodes while introducing current into the ground through two other electrodes (TIQ 2006). Streaming and fixed cable marine resistivity offer a potential as a reconnaissance surveying method for detecting subsurface zones of freshwater (Swarzenski et al. 2007).

Resistivity data for regional comparisons with radon data were collected in May 2003 and February 2004 using the AGI SuperSting of Advanced Geosciences, Inc. The system continually records and stores data using a multi-channel resistivity receiver as well as collection of position coordinates from a GPS receiver. The 100-m streaming resistivity cables used contain a current electrode pair and nine potential electrodes set up to be used in a custom AGI 100 m dipole-dipole array with a 10 m spacing (Greenwood et al. 2006). The streamers were towed across the water's surface at a speed of ~3-5 knots.

To obtain correct global positioning, a WAAS differential GPS was available throughout the survey area from a NMEA 0183 2.0 stream of the Lowrance 480M GPS/sonar. The transducer was set to 200 kHz and had a depth of resolution of ± 5 cm. The entire set of small-scale surveys was conducted over a period of approximately 9 hours. To detect the variations in terrain conductivity produced by variations in pore water salinity, a Geonics EM-31 instrument floating at the water surface in a vessel with minimal metal parts was used. Since this instrument could not be calibrated except in very resistive settings with uniform ground saturation conditions, a floating Schlumberger resistivity array was constructed for this purpose. To determine an average integrated value for the shallow (uppermost 1-2 meters) seafloor conductivity from EM-31 apparent conductivity readings, a Schlumberger resistivity sounding run was done at a calibration site in shallow (<1 m water depth) water. The data were then inverted for a two layer model. The terrain conductivity inferred from inversion of the EM-31 was then adjusted to match the value derived from the resistivity sounding. The adjustment, or correction factor, was subsequently applied in EM-31 readings. A repeat calibration was then conducted at the end of the survey.

Elsewhere, similar streaming and fixed cable marine resistivity studies have been used in recent years, with varying degrees of success, to identify zones of submarine groundwater discharge. Such studies include those of Manheim et al. (2004), Stieglitz (2005); Povinec et al. (2006), Swarzenski et al. (2007) and Taniguchi et al. (2007).

Nutrient Measurements

Nutrient samples of bay water and groundwater were filtered through glass fiber filters (0.70 μm) and kept at 4°C in the field, before transporting to the laboratory at the Florida Department of Environmental Protection (FDEP) for analysis within the shortest possible time. For storage that required waiting periods beyond two days, they were stored in a deep freezer (at temperatures < 10 °C). In the laboratory, samples were analyzed for dissolved inorganic nutrients (nitrate + nitrite, phosphate, and ammonium) within a period of less than two weeks. Sodium phenolate was added as a preservative to ammonium samples before refrigeration. Analyses were conducted using a Lachat auto-

analyzer according to manufacturer's guidelines and standard methods described in Parsons et al. (1984) and Grasshoff et al. (1999). Measurements of DOC were made using a Shimadzu TOC-V series total carbon analyzer according to the method of Benner and Strom (1993).

SB System Flushing (Residence) Time Estimations

The approximate flushing (residence) times of the different regions in the SB water system were estimated by using a modified simple tidal prism model (Dyer 1973; Dyer and Taylor 1973). In the model, the residence time, *I*, was estimated by taking into consideration the flooding and ebbing cycles during both the neap and spring tides in the SB region. The model represents the bay region as a box with low tide (or flood tide) volume *V* and intertidal (or average) volume *P*. The empirical equation for calculating residence time, *I*, measured in days, is:

$$I = P / (P - V / T) \dots\dots\dots(4.x)$$

where *T* is tidal cycle period in days. The simple tidal prism model assumes that the bay water is well mixed. Estimates were made for both semi-diurnal and diurnal tidal range scenarios, as the SB system experiences both. Residence times estimated in this manner are the minimum estimates possible.

Results

Radon Determinations

Grab Samples

During every sampling session within the SB system (Fig. 4.1), grab samples were collected in as many regions as possible in a north to south direction. The radon measurements were all made during the interval July'02 – July'04. The distributions of the ²²²Rn concentrations within the three regions of the SB system through this period are shown in Fig. 4.6. These measurements reveal that the ²²²Rn levels relatively were very high for surface waters (> 20 dpm/L) and were generally highest in the south region.

There was no significant difference between concentration levels that were observed in the north the middle areas (t-test: $t = -0.15$; $p = 0.88$; $n = 145$). It is also interesting to observe that concurrent CH_4 measurements also depicted a similar variation trend as shown in the average SB ^{222}Rn concentrations (Figs. 4.6 and 4.7; Table 4.2).

Continuous ^{222}Rn Mode (CRM) Surveys

The two CRM surveys that were conducted on 27-28 May'03 and 18-19 August'04 revealed a trend consistent with the grab samples in the distribution of ^{222}Rn within the SB system. Although these CRM surveys were conducted at different times, their trend remained markedly consistent along the north – south direction within the SB system, as revealed in the scatter plots (Fig. 4.8). The two 2-day surveys each confirmed the average variation trend that was observed throughout the nearly two-year grab sampling period (Fig. 4.6, Table 4.2). There was however, more scatter for the ^{222}Rn concentrations that were observed during May'03 compared to the results in August'04. It is also to be noted that the former measurements were conducted during a period of relatively less rainfall than the latter (Fig. 4.2).

Methane (CH_4)

The temporal and spatial variations in CH_4 concentrations were observed to closely follow that of ^{222}Rn . For instance, a linear relationship between CH_4 and ^{222}Rn concentrations in all the regions of the SB regional system was observed for all concurrent samples assessed within the SB system (Fig. 4.7).

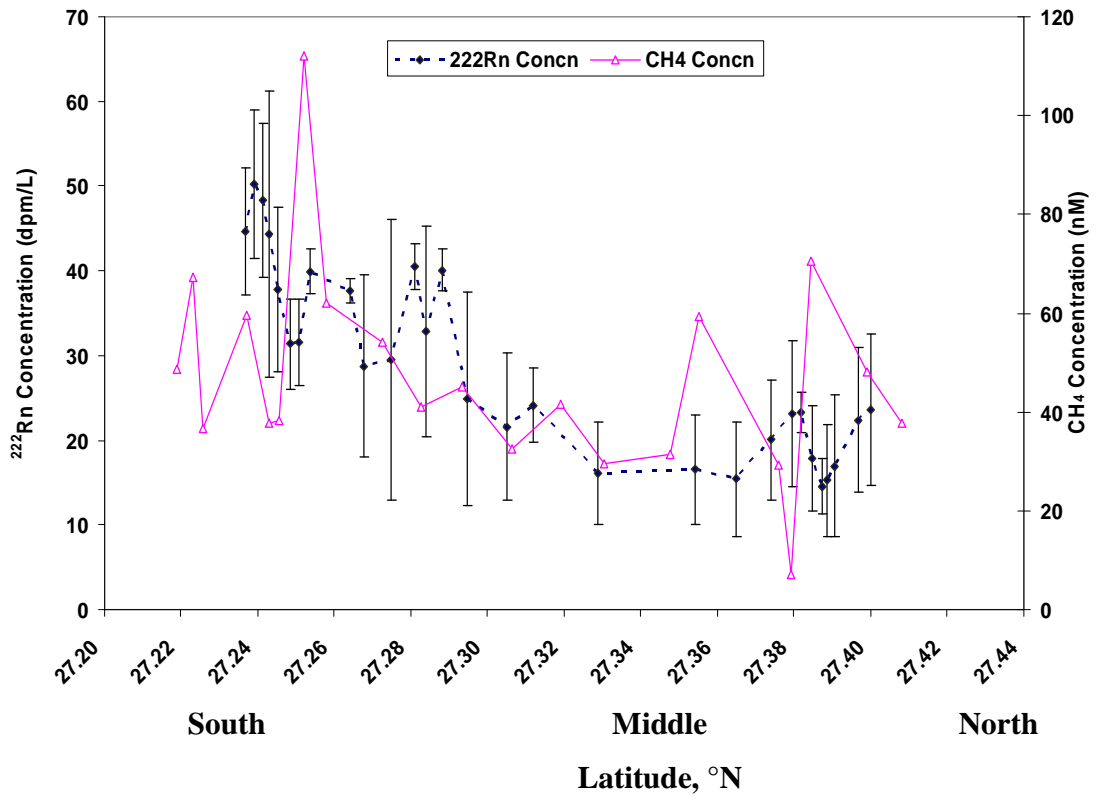


Fig. 4.6: Summary of ^{222}Rn and CH_4 concentration distributions in the Sarasota Bay system during the period July'02 to July' 04. Each plotted point is derived from averaging five different points, representing five different time periods (or samples); $n = 5$.

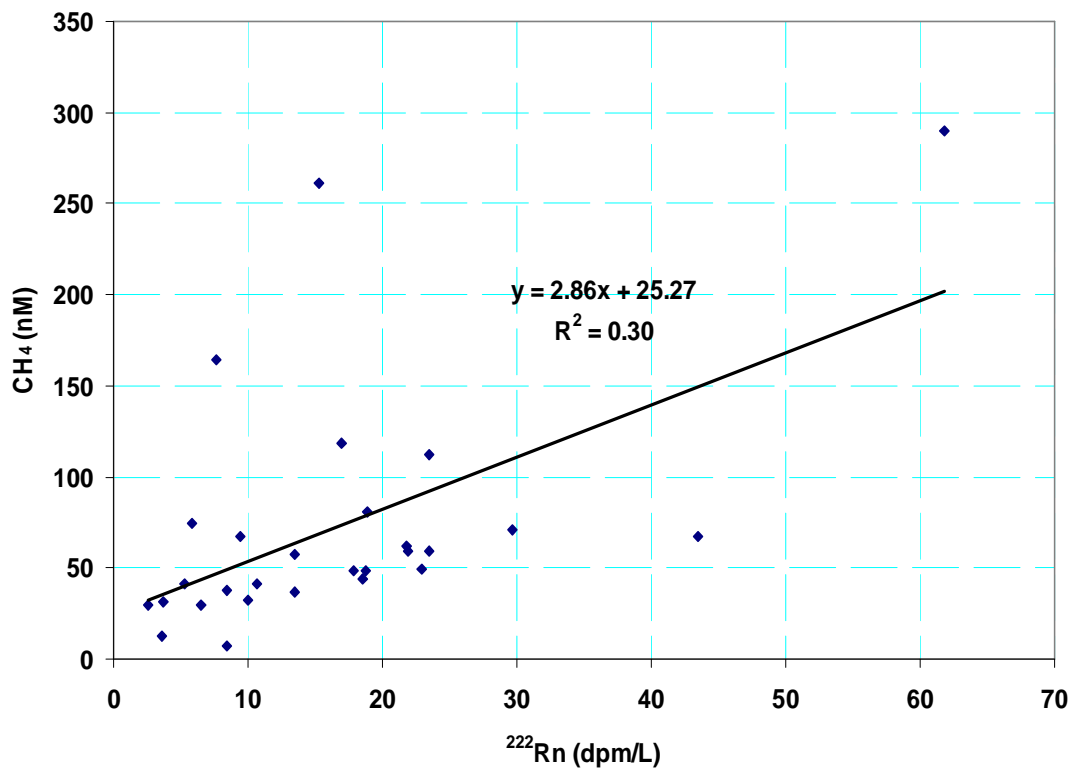


Fig. 4.7: Relationship between ^{222}Rn and CH_4 concentrations in the Sarasota Bay system, July'02, November'02 and March'03.

Table 4.2: Average seawater ^{222}Rn and CH_4 concentrations in the Sarasota Bay system during the period July'02 to July'04 for bottle samples; 18-19 August'03 for CRM survey.

Region within SB System	Average CH_4 (nM) n = 19	Average ^{222}Rn concentration (dpm/L) n = 214	
		Bottle	Survey
North	56.9 (41.5)	15.7 (14.1)	20.2 (2.1)
Middle	34.6 (6.3)	12.4 (11.3)	24.7 (2.5)
South	50.6 (12.7)	25.6 (16.0)	42.3 (4.2)

Figures shown in parentheses indicate standard deviations (1σ).

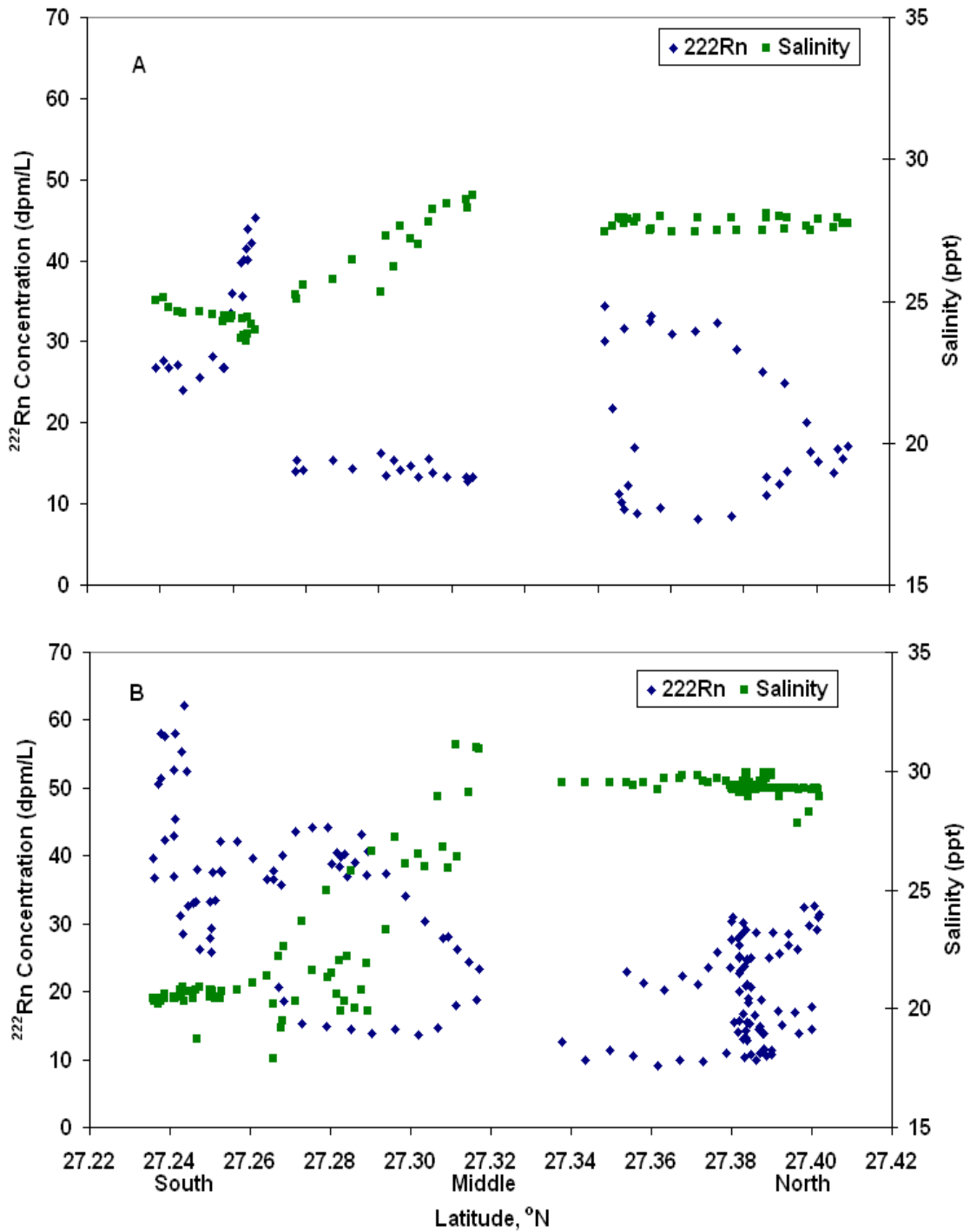


Fig. 4.8: Scatter plots for ^{222}Rn (CRM) survey transects conducted within the Sarasota Bay system showing salinity variations for two different periods (A) 27 – 28 May'03 and (B) 18-19 August 2004. In both periods, the plots clearly depict lowest salinities, coinciding with the highest ^{222}Rn concentration levels in the South Region relative to the other regions.

Continuous ^{222}Rn Mode (CRM) Fixed Station Estimates

The time-series continuous radon measurements were conducted at two fixed stations within the SB system: (1) New College, NC (within the North Bay); and (2) Roberts Bay, RB (within the Middle Bay). These measurements were conducted during the same period of time (Fig. 4.9). The variations at NC and RB showed similar trends throughout the measurement period with high concentrations in the same range as the southern region of the bay shown earlier (Figs. 4.6, 4.8). The internal consistency of these results is somewhat remarkable since these two sites were separated by approximately 14 km. The relative mean of ^{222}Rn concentration at RB (39.4 ± 7.3 dpm/L) was essentially the same as that at NC (38.9 ± 7.2 dpm/L). The close trend similarities between these two regional sites may suggest a common ^{222}Rn source for the two regions.

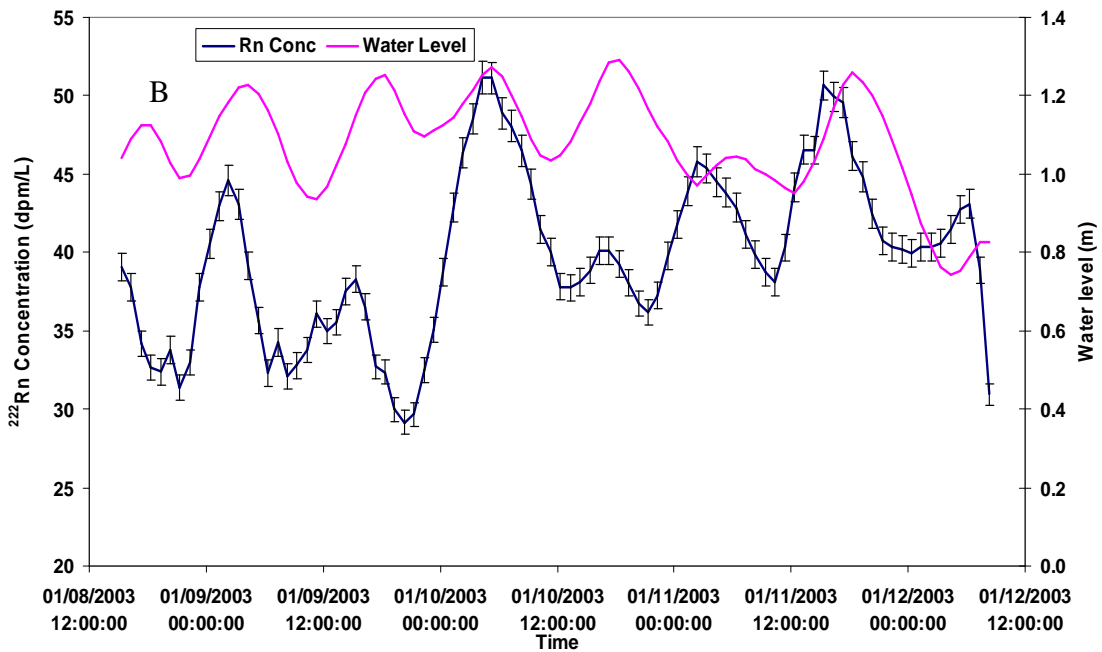
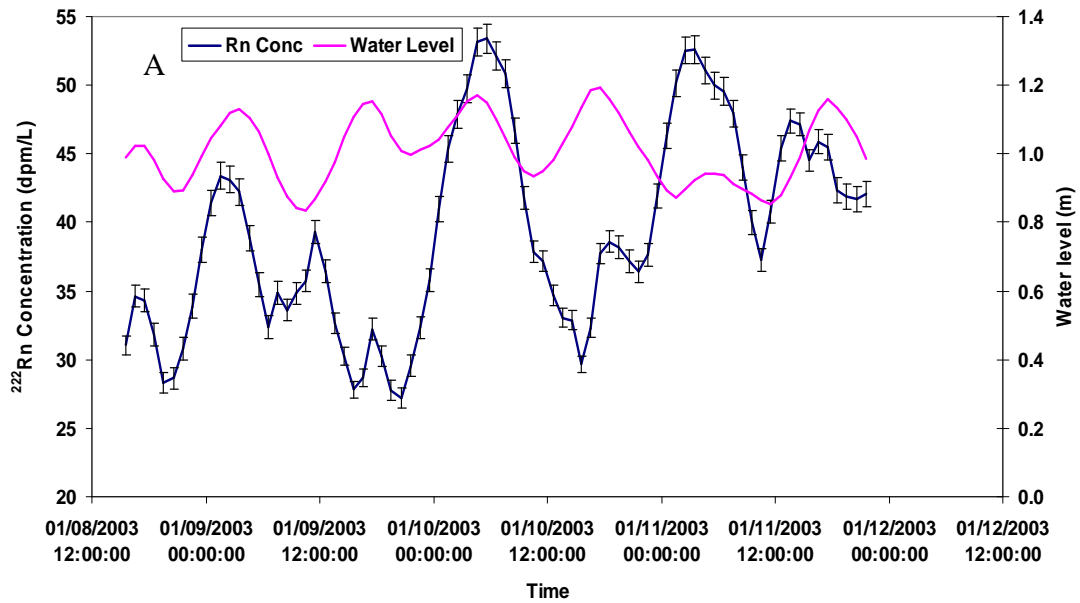


Fig. 4.9: Variations over time of seawater ^{222}Rn concentrations (dpm/L) and water level at two fixed stations: (A) Roberts Bay, RB - Middle Bay (Mean concentration = 39.4 ± 7.3 dpm/L) and (B) at the New College, NC - North Bay (Mean concentration = 38.9 ± 7.2 dpm/L), within the Sarasota Bay system during a time series monitoring, 8-12 January 2003.

²²²Rn End Member Estimates and Diffusive Fluxes

In an attempt to establish the most reasonable end member for groundwater ²²²Rn concentrations, a number of sediment equilibration experiments were conducted on nearshore sediments that were collected from within the SB system. The choice of locations for collection of sediment samples were mainly two fold - easy access and the fact that the areas were within the vicinity of coastal sites that were suspected to have considerable seepage, mainly due to karstic, highly – transmissive carbonate zone within the area (Fretwell and Stewart 1981; USGS 2007). In addition to pore water ²²²Rn, estimated diffusive fluxes can be compared with the derived SGD advective fluxes determined from the ²²²Rn model and seepage meter measurements. These experiments produced estimated pore water values ranging from 170 to 800 dpm/L, with a mean value of 390 ± 180 dpm/L (Table 4.3; n = 27).

Table 4.3: Results of sediment equilibration experiments from the Sarasota Bay system, May03 – March'04.

Latitude (°N)	Longitude (°W)	Site Name	Wet sediment ²²² Rn Conc (C _o) dpm/L	Pore water ²²² Rn Conc (C _{eq}) dpm/L	Estimated Diffusive ²²² Rn Flux (=F _{diff}), dpm/m ² /d	Diffusive ²²² Rn Flux (SGD equivalent, cm/d)	Region within SB system
27.409	82.575	Bowlees Creek (Whitfld Est)	72	193	168	0.043	North
27.386	82.567	New College	224	419	269	0.07	
27.384	82.585	Mid Sar Bay	67	197	179	0.046	
27.383	82.565	New College	154	184	42	0.011	Middle
27.358	82.557	Whitaker Bayou (Ind Bch)	230	643	571	0.148	
27.357	82.605	Longboat Key	52	183	180	0.047	
27.355	82.547	Whit Bayou	185	330	199	0.052	
27.353	82.553	Whit Mouth	141	475	460	0.119	
27.329	82.542	Anchorage	184	269	118	0.03	
27.325	82.531	Hudson Bayou	275	635	498	0.129	
27.311	82.546	Siesta Key Brgde (Bascule)	175	465	400	0.103	
27.3	82.548	Roberts Bay	132	169	52	0.013	
27.293	82.547	Bascule Bridge (south)	165	379	295	0.076	
27.289	82.556	Siesta Key Canal	98	251	210	0.054	South
27.285	82.545	Roberts Bay	156	384	315	0.081	
27.277	82.55	Philippi Creek (across)	129	248	164	0.042	
27.276	82.529	PC small bridge	242	290	66	0.017	
27.276	82.525	Phil Cr	285	803	715	0.185	
27.263	82.542	Stickney Bridge (north)	168	252	116	0.03	
27.253	82.532	Stickney Bridge	230	685	627	0.162	
27.249	82.518	Canal	156	430	377	0.097	
27.239	82.518	Marina	285	762	659	0.17	
27.239	82.51	Hidd Harb (Mouth)	191	415	309	0.08	
27.236	82.516	Little SB	173	358	255	0.066	
27.228	82.516	Siesta Key	219	358	191	0.049	
27.228	82.505	Vamo	169	316	203	0.052	
27.213	82.505	Bird Keys, Vamo	110	342	319	0.082	
MEANS			173	386	295	0.076	
STDEV			63	180	188	0.049	

In addition to the near-surface sediment equilibration experiments, regional estimations for groundwater ^{222}Rn end member concentrations and diffusive fluxes were also estimated via pore water sampling. These samples were collected with a piezometer and the results displayed as ^{222}Rn concentration versus depth profiles (Fig. 4.10). These profiles generally show concentrations near the surface close to those estimated from the sediment equilibration experiments (mean $\sim 390 \pm 180$ dpm/L).

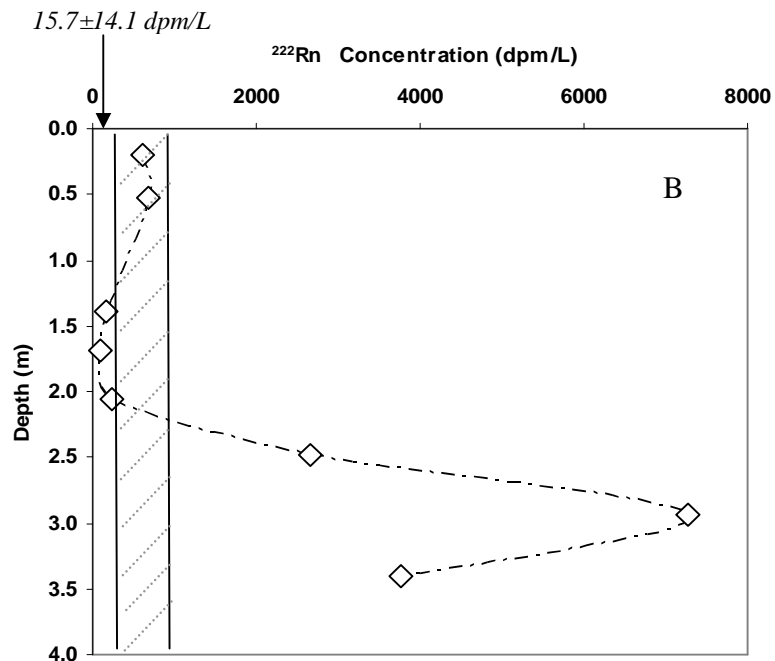
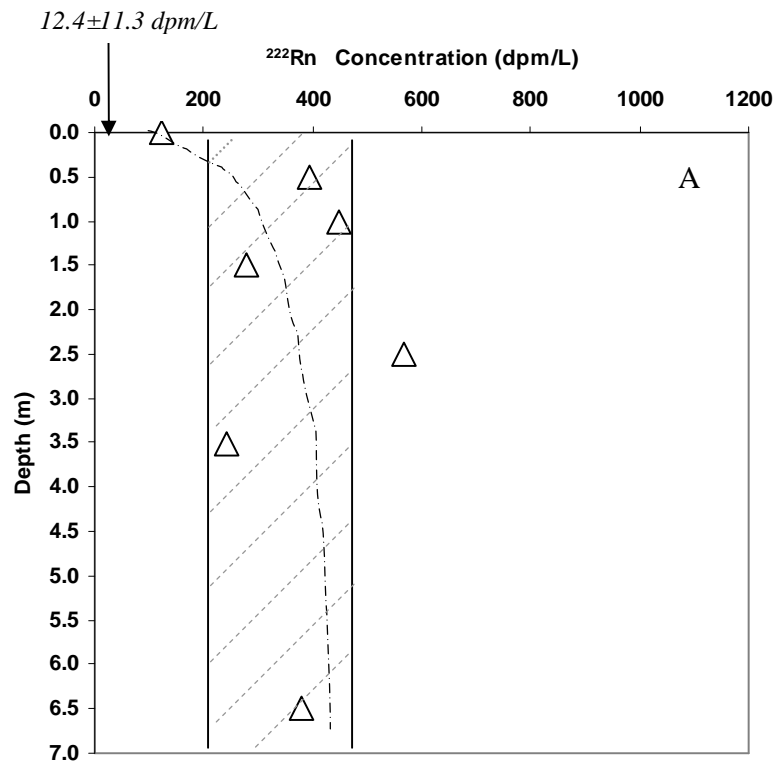


Fig. 4.10: Depth ^{222}Rn concentration profiles (based on piezometer sampling) from the Sarasota Bay System: (A) North Bay region (NC site) and (B) Mid Bay region (RB site). Values shown by arrows are mean bottom water ^{222}Rn concentrations. The shaded band indicate the margin for the equivalent equilibrium concentration zone (390 ± 180 dpm/L).

Resistivity Surveys

In general, the results acquired through streaming resistivity survey mapping of the SB system (Figs. 4.11 - 4.14), revealed a number of areas with resistivity values that suggest more freshwater located near the surface in the south as compared to the north. Although the measured resistivity correlations were subtle and less obvious, the ^{222}Rn concentration observations also indicated higher SGD in the south portion of the SB system (Figs. 4.6 and 4.8). When using the streaming resistivity survey technique, terrain and sediment composition can be a crucial factor while interpreting the results (Manheim et al. 2004).

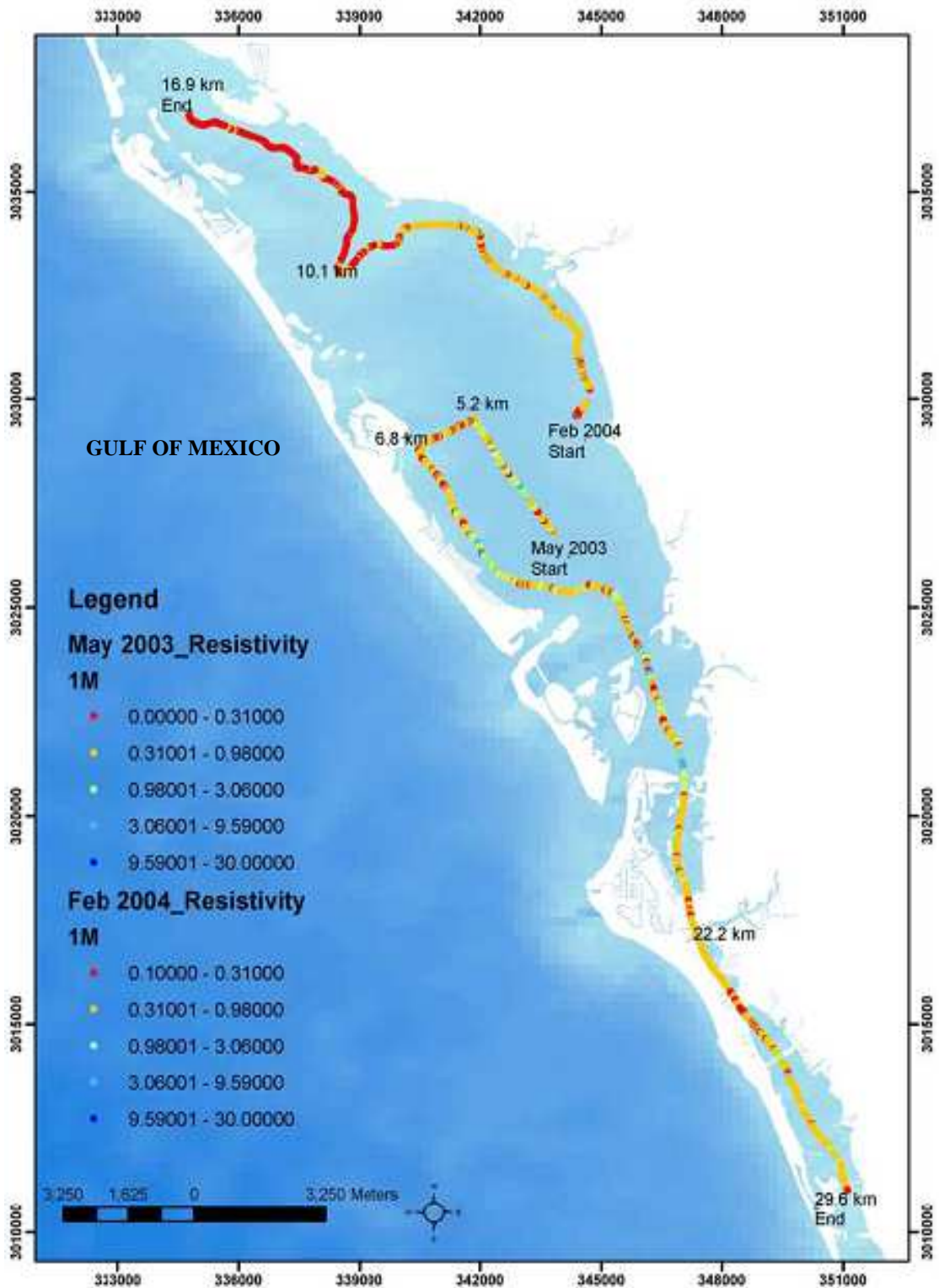


Fig. 4.11: Map showing location of resistivity surveys and dates of acquisition. Inverted resistivity values within the water column (one meter below water surface).

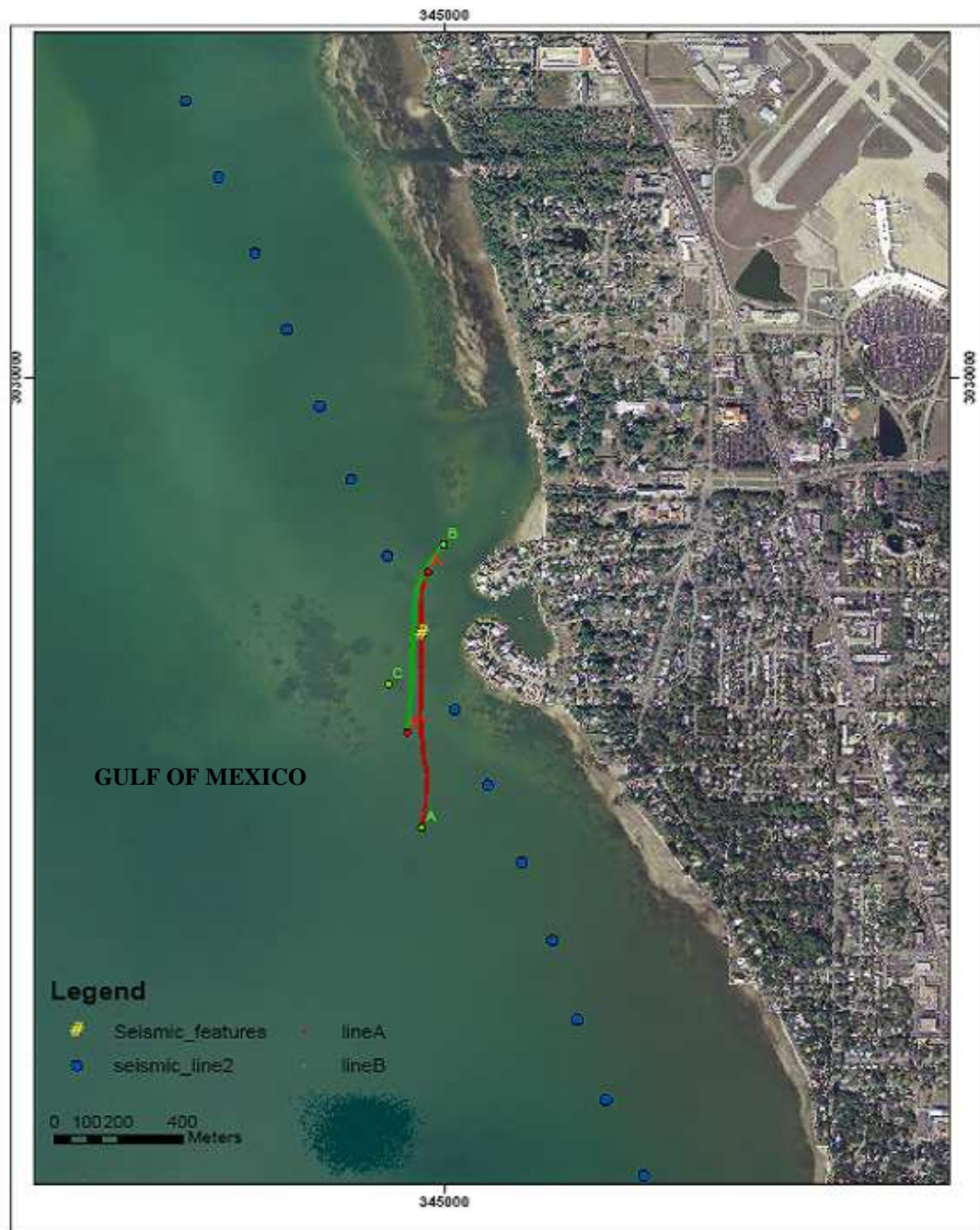


Fig. 4.12a: Location of resistivity Lines A and B. Blue dots show path of seismic profile acquisition (May'03).



Fig. 4.12b: Locations of resistivity lines F, G, and H run at location of seismic line within the Sarasota Bay system (May'03).

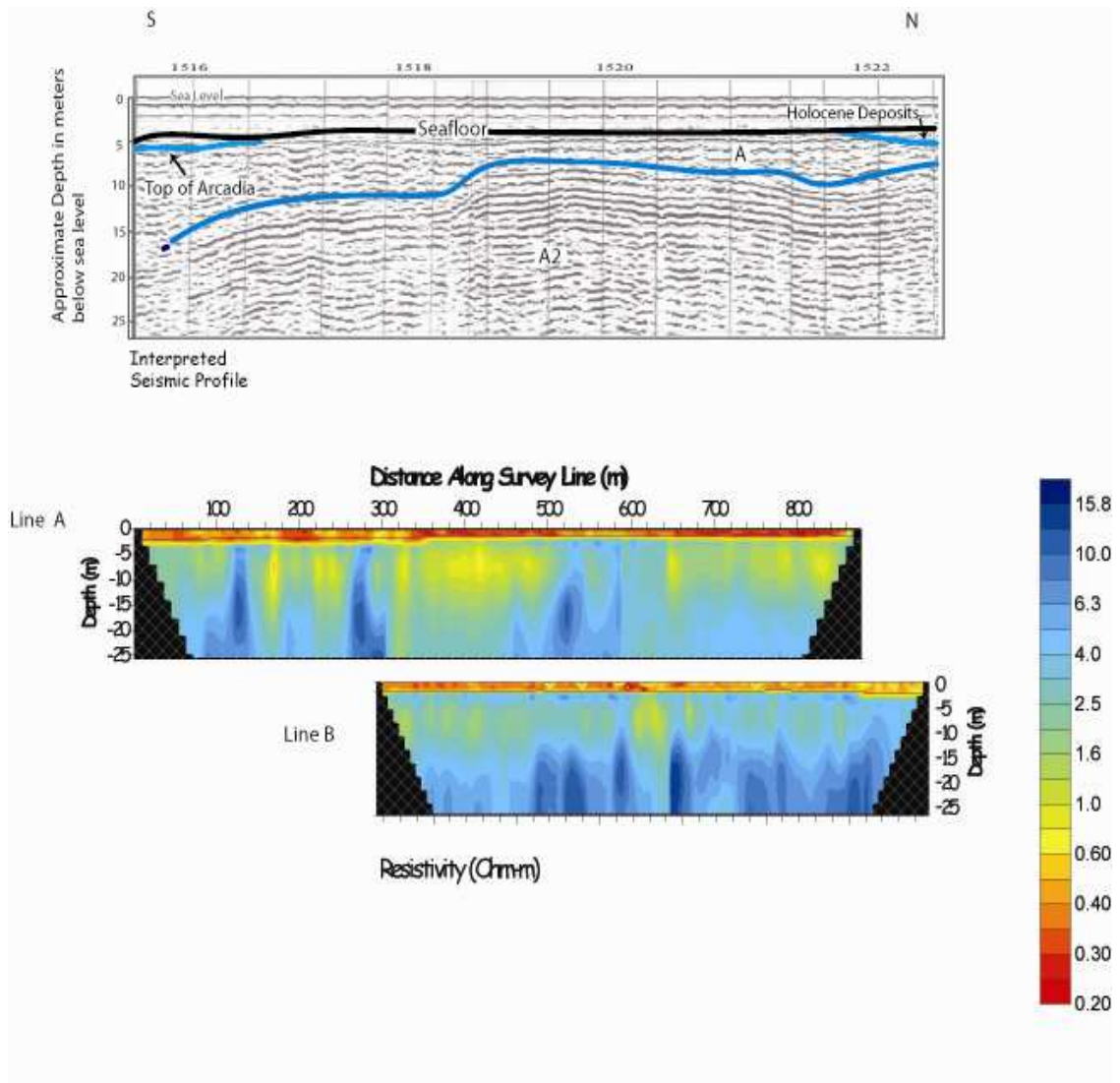


Fig. 4.13: Sample line segments for resistivity survey taken from the northern Sarasota Bay system near New College.

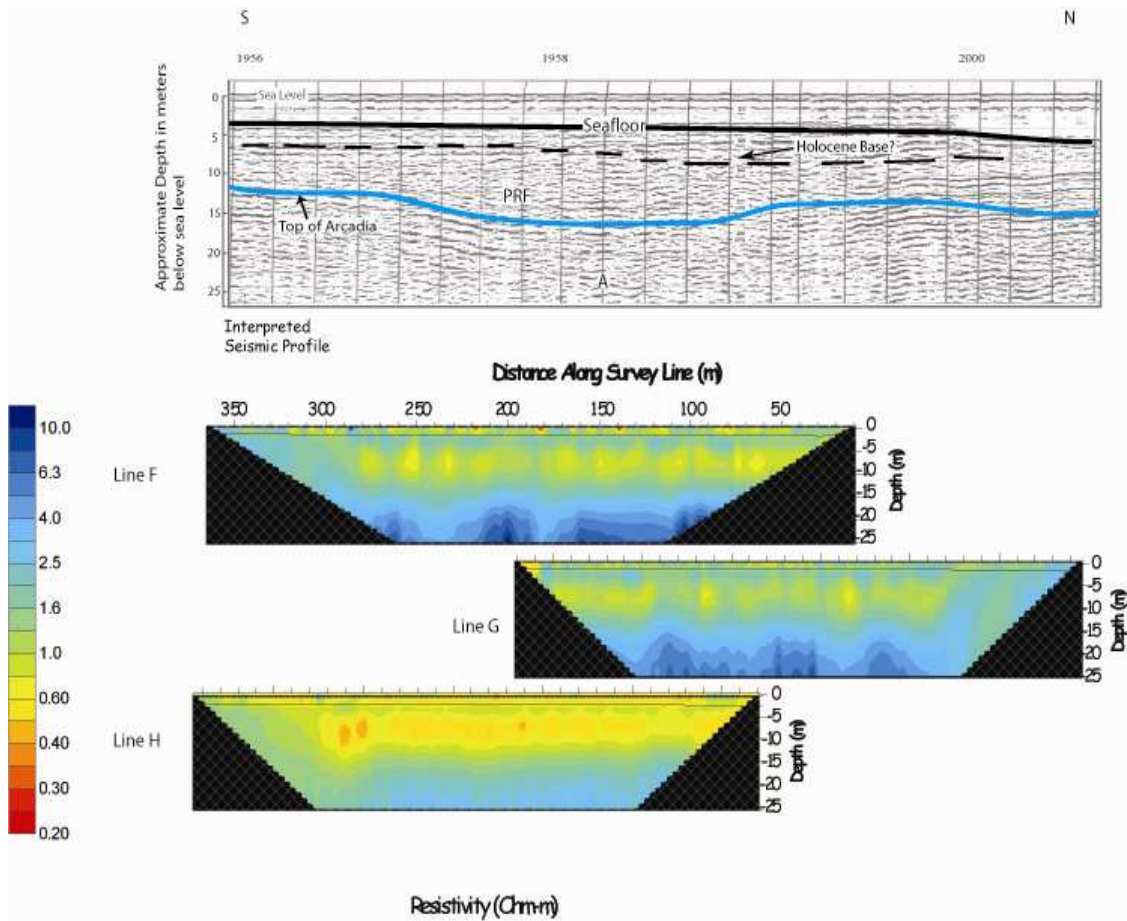


Fig. 4.14: Line sections (as indicated in Fig. 4.12) in the southern bay (Little Sarasota Bay) showing resistivities that decrease around ten meters depth. The 3 different resistivity surveys were run over the location of the seismic surveys at essentially the same time.

Seepage Meter Measurements

Direct SGD measurements obtained through manual seepage meters are shown together with the corresponding ^{222}Rn -SGD advection determinations (Table 4.4). Although the absolute SGD values between the two approaches did not coincide, they were not widely different from each other. Of the three sites considered, the highest seepage meter SGD rates were found at Caples (middle region) while the lowest were observed at Island Park, which is also found within the middle region. The north region (NC) showed medium SGD rates. Since seepage meter determinations are directly dependent on the local seepages at the site, reliable results can only be obtained through several repeat measurements of an area.

Table 4.4: Quantitative estimations of SGD and nutrient fluxes within the different regions of the Sarasota Bay system.

Region in the SB System	Total Surface Area (x 10 ⁶ m ²)	Estimated Total Volume (x 10 ⁶ m ³)	Estimated SGD Rates (cm/day ≡ x 10 ⁻² m/day)			Combined Average SGD (x 10 ⁻² m/day)	SGD Nutrient Fluxes in the SB system (mmol/m ² .day)			
			Bottle (²²² Rn) n = 214	Survey (²²² Rn) n = 214	Seepmeters (Manual) n = 18		NO ₂ +NO ₃	PO ₄	NH ₄	N/P
North Bay	75.1	150.2	5.8 (0.8)	5.6 (0.7)	16.7 (8.5)	5.7 (0.8)	7.9	0.4	0.4	21
Middle Bay	11.1	22.2	4.5 (0.6)	7.8 (1.0)	3.3 (2.3)	6.2 (0.8)	5.4	2.5	2.3	3
South Bay	10.5	15.8	6.5 (0.9)	10.8 (1.4)	-	8.7 (1.2)	0.1	0.6	2.0	4

Figures shown in parentheses indicate standard deviations (1σ) and n is the number of representative SGD rate measurements in each region used in the estimations.

Nutrient Concentrations

Nutrient measurements of bay waters were conducted in January and March'04, in order to get a general sense of concentration levels within the SB system. The results are shown in Tables 4.5 and 4.6.

Table 4.5: Seawater nutrient concentration levels in the Sarasota Bay system. Sampling conducted on 04 January and 04 March '04 for all the SB system regions (North, Middle and South).

Region	DOC (mg/L)	NO ₂ +NO ₃ (µM)	PO ₄ (µM)	NH ₄ (µM)	N/P
North Bay (n = 4)	2.17	1.46	0.23	0.56	9
	9.97	11.2	0.72	0.10	16
	4.81	4.06	0.44	6.11	23
	4.43	0.35	0.18	0.29	4
Mean (Stdev)	5.35 3.30	4.26 4.86	0.39 0.25	1.77 2.91	15

Middle Bay (n = 4)	12.4	0.75	0.90	1.59	3
	5.76	0.17	0.29	0.95	4
	5.81	0.33	0.81	9.14	12
	4.57	1.36	1.08	7.99	9
Mean (Stdev)	7.13 3.54	0.65 0.53	0.77 0.34	4.92 4.25	7

South (n = 10)	6.43	0.13	0.27	0.67	3
	6.81	0.19	0.37	0.94	3
	6.79	0.21	0.34	0.94	4
	2.93	0.24	0.39	1.06	2
	2.92	0.27	0.37	3.87	11
	2.23	0.34	0.41	1.63	5
	13	0.71	1.22	0.00	0
	8.70	2.01	1.05	5.63	7
	7.63	1.96	1.15	9.06	10
	12.5	1.25	1.35	0.00	0
Mean (Stdev)	6.99 3.74	0.73 0.74	0.69 0.44	2.34 2.97	5

Table 4.6: Average groundwater nutrient concentrations in wells found within the vicinity of the SB system.

Region	NO₂ + NO₃ (μM)	Total Dissolved P (μM)	NH₄ (μM)	N/P
North	138 \pm 215 (n = 3)	6.9 \pm 9.1 (n = 9)	7.8 \pm 6.2 (n = 9)	21
Middle	44.2 \pm 85 (n = 4)	28.3 \pm 41 (n = 5)	28.4 \pm 27.1 (n = 7)	3
South	1.2 \pm 0.7 (n = 6)	7.1 \pm 8.5 (n = 17)	23.4 \pm 12.1 (n = 30)	4

Groundwater raw nutrient data source: Watershed Monitoring Section of the Florida Department of Environmental Protection, FDEP.

Discussion

SGD, Water Volumes and Residence Times

The magnitude of SGD in the SB system was evident from the independent measurements that were carried out (Tables 4.4 and 4.7). The average regional SGD estimates were obtained by averaging the individual estimated regional SGD rates (in m/day, cm/day = 10^{-2} m/day) derived from the two ^{222}Rn model approaches (bottle and CRM). The residence times of the waters of the SB system, estimated via a modified tidal wedge approach (Dyer 1973) ranged from 3 to 11 days. As shown in Table 4.1, the north and middle regions of the SB system had similar residence times which were slightly higher than for the south region of the bay. Extended residence times may result in enhanced primary productivity of the system if elevated nutrient levels develop. This might have been the case in areas within the south and middle regions of the SB system, partly due to the existence of numerous septic tank systems in the surrounding area. Indeed previous studies within the SB bay system, revealed considerable transport of contaminated waters into the bay with effluent from shallow septic systems (Lipp and Griffin 2004). More recently, Peeler et al. (2006) showed a correlation of elevated nitrate and caffeine levels being linked to population centers and their associated waste water treatment plants.

Table 4.7: SGD - advection and diffusive flux estimations using different approximation approaches within the Sarasota Bay system.

SB System Region	Temperature (°C)	Porosity	Equilibration	Depth (m)	²²² Rn	D _o (m ² /day)	D _s (m ² /day)	²²² Rn flux (=J)	Bay Area (x 10 ⁴ m ²)	SGD estimates
			sediment ²²² Rn concn (x 10 ² dpm/L)		depth profile (x 10 ² dpm/L)			Diffusion (dpm/m ² /day)		(^{a,b,‡} = Flux/ex ²²² Rn _{pw} ; + = manual seepmeters) (cm/day)
North (NC site)	31.2	0.684	3.86	0	1.89	1.54E-05	1.06E-05	273	75.1	0.071^a
				0.2	6.03			15		0.004^b 16.7[‡] 6.8[‡]
Middle (RB site)	19.9			0	1.25	1.16E-05	7.93E-06	314	5.5	0.081^a
				0.5	3.95			3		0.001^b

^aJ = D_s*λ^{1/2}(C_{eq}-C_o), diffusive flux

^bJ = -φ*D_s*dC/dZ, diffusive flux

[‡] Radon model advection (SGD) estimates, overall average for SB system (~ 2 - 3 orders of magnitude higher than diffusive SGD flux)

⁺Manual seepmeter measurements, average for the NC site (~ 2 - 3 orders of magnitude higher than diffusive SGD flux)

The north region showed lower nutrient concentrations perhaps because of a relatively larger seawater volume compared to the other regions. In relation to the other regions of the SB system (Table 4.6), the north region accounts for about 80% of the total volume of seawater present, while the middle and south regions only account for about 12% and 8% respectively.

²²²Rn Model and Seepage Meter SGD Estimates

The bulk of SGD estimations in the SB system were carried out using the “grab sampling” (bottle) method (Fig. 4.5). The measurements covered included various periods between July’02 and August’04. The overall estimated groundwater advection (SGD) in the three main regions within the SB system, during the study period ranged from 0.7 to 24 cm/day. In the north region of the SB system the range was from 0.7 to 5.9 cm/day, while in the middle and south portions of the bay the range was from 5.9 to 24 cm/day.

On average, SGD estimates in the SB system that were made by the ²²²Rn bottle technique were relatively lower compared to those made using seepage meters and the continuous mode ²²²Rn techniques (Table 4.6). This was not unexpected however because in the former method (based on grab sampling), the radon mixing losses in the estimations are neglected since these are instantaneous samples, while this aspect is accounted for in the case of CRM estimates made by a non-steady state mass balance approach. The average salinity within the SB system during the investigation period was 26.0 ± 4.2 ppt.

The relatively unusually high ²²²Rn concentration levels (> 20 dpm/L) measured through the entire SB system (Fig. 4.6) could imply one of the three possibilities, either; the SB waters have high SGD prevalence, or the presence of minerals associated with ²²²Rn (i.e. ²²⁶Rn) in the underlying rocks, or the SGD into the bay contain very high concentrations of ²²²Rn per volume discharged. However, looking at other independent evidence such as the high CH₄ concentrations whose variation trend closely follows that of ²²²Rn (Fig.

4.6), and the generally low salinities within the SB system (Fig. 4.8), it is more probable that the high ^{222}Rn are associated with the prevalence SGD rather than the other two possible factors. This is further augmented by the manual seepage meter SGD values which averaged about 10 ± 5.4 cm/day (Table 4.4) for NR and MR combined, where the seepage meters were deployed.

The two CRM surveys that were conducted in May'03 and August'04 revealed a relatively consistent trend in the distribution of the radon concentration estimates, within the entire SB system (Fig. 4.8). It was evident from the observed trends that relatively high SGD rates were likely present in the south region and the lowest levels in the middle region of the bay (Fig. 4.8). While the observed trend of SGD estimates is likely attributable to the local hydraulic gradients, and to a great extent on the surrounding regional catchment areas, it is also important to consider the prevailing sediment properties and structure within the different regions. Hydrological conductivity of sediments and the topography of an area are integral factors that could directly determine the net SGD rates (Hornberger et al. 1998).

The trends in groundwater advection estimates performed using the CRM survey and those that were done by the bottle method at the different sampled sites within the SB system were largely in agreement in magnitude.

The continuous SGD measurements at two fixed stations within the SB system, at NC and RB sites were synchronized and conducted within the same period of time (Fig. 4.15).

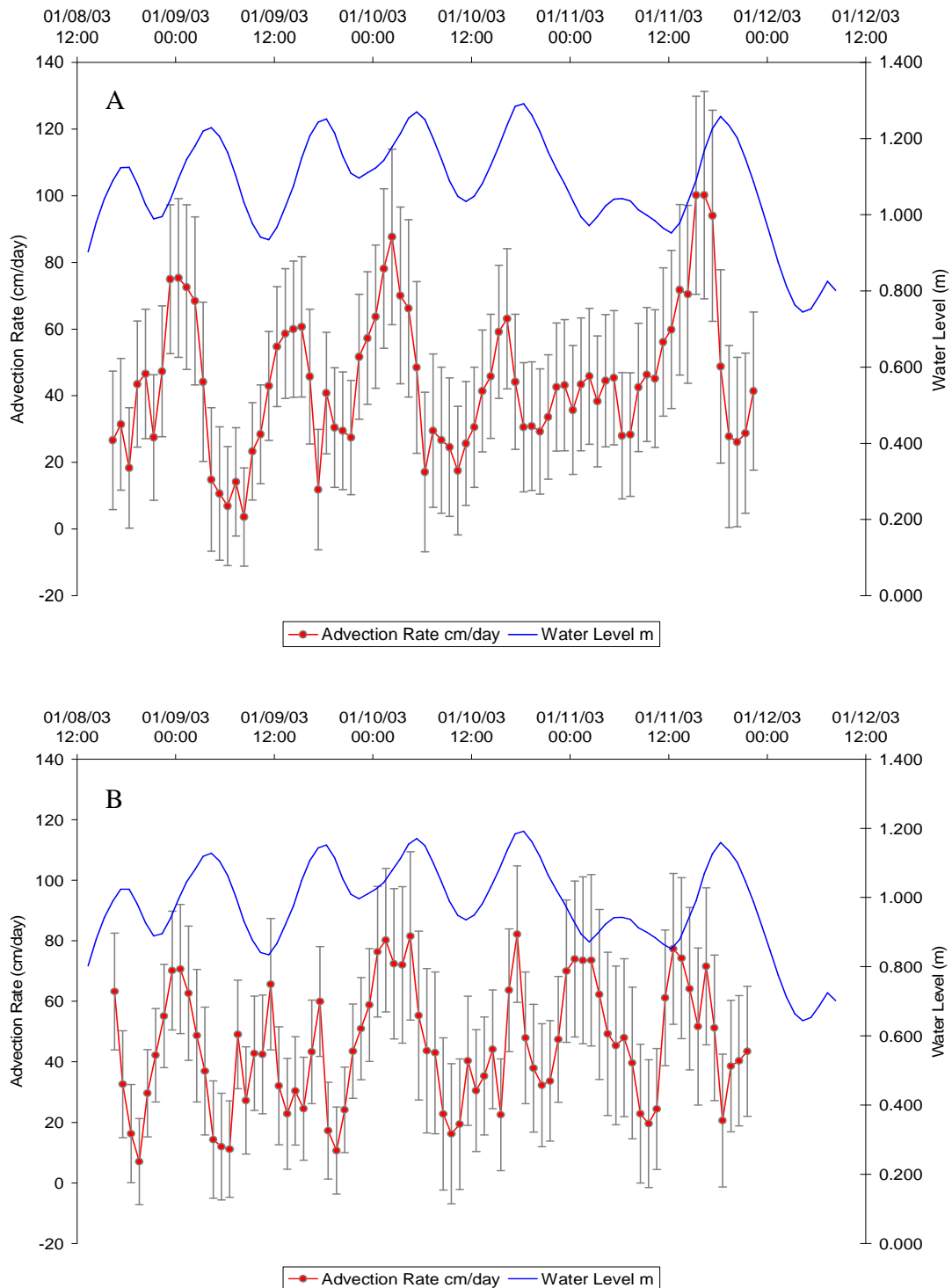


Fig. 4.15: Variations over time of estimated advection rate (cm/day) with water level at fixed sites: (A) at the New College, NC – North Bay (Mean advection = 43 ± 20 cm/day) and (B) at Roberts Bay, RB - Middle Bay (mean advection = 46 ± 21 cm/day), within the Sarasota Bay system during a time series monitoring, 8-12 January 2003. Groundwater end member used was 390 ± 180 dpm/L.

These two time-series sites were “hot spots” identified in the survey, so their SGD estimates were relatively high as expected. In spite of the fact that these two sites were about 14 km apart their radon concentrations and SGD estimates were very similar (Figs. 4.16 and 4.17). A statistical analysis revealed no significance difference between the measurements ($p = 0.62$; $\alpha = 0.05$; $n = 78$), and the relative estimated SGD mean at RB (46 ± 21 cm/day) was essentially the same as at NC (43 ± 20 cm/day). The representative pore water end-member radon concentration used in the CRM advection model estimations was 390 ± 180 dpm/L. This was the average value derived from several sediment equilibration experiments that were conducted on nearshore sediment cores collected throughout the SB system (Table 4.3). It should be noted that the “ \pm ” associated with these estimated fluxes refer to real standard deviations (1σ) and are not uncertainty values.

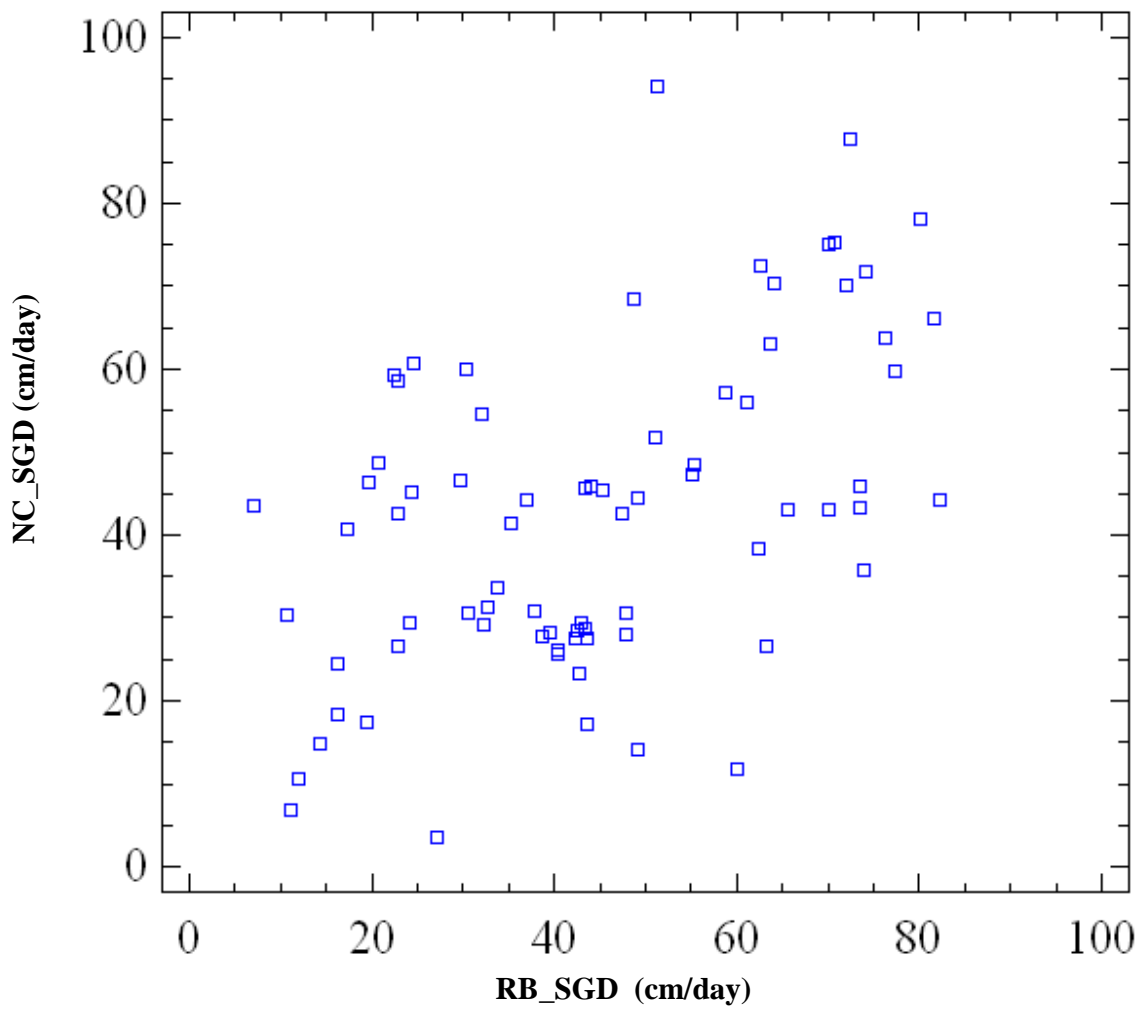


Fig. 4.16: A scatter plot of synchronized ^{222}Rn -SGD (cm/day) estimates (CRM) at the two time series sites, NC (North) and RB (Middle) within the Sarasota Bay system, 8-12 January 2003.

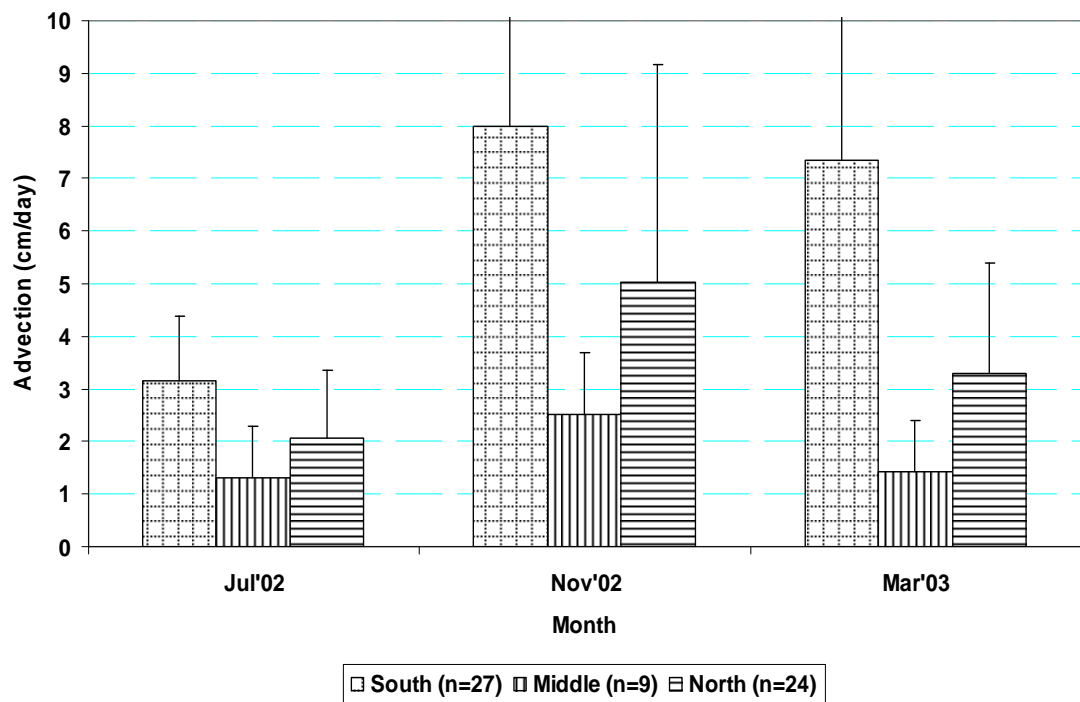


Fig. 4.17: Average advection (^{222}Rn model) within different regions of the Sarasota Bay system, July'02, November'02 and March'03.

The similarities between these two fixed CRM regional sites (Fig. 4.15) may indicate a common SGD supply source for the two regions, perhaps a regional aquifer that discharges in both regions. In both plots, the general sinusoidal SGD variation pattern at the two sites closely related to the way the tidal wave varied. In each case, the highest SGD peak occurred a few hours after the lowest tide water level was reached. A similar phase difference has also been observed elsewhere. For instance, in their correlation analyses between SGD and sea level in Osaka Bay, Japan, Taniguchi and Iwakawa (2004) found that SGD changes were delayed by 4 hours after sea level changes.

There were differences in SGD estimates via CRM and seepage meters within the same bay regions (average difference of ~ 33%). It should be noted that the SGD measurements at NC and RB sites were made at distances close to the shoreline within areas that were generally known to have substantial submarine seepage (these substantial diffuse SGD were evident through measurements taken using manual seepage meters within the area). It is therefore likely that the relatively higher overall CRM SGD estimations in the two time series sites compared to the observed seepage meter values were probably due to the karstic, high-transmissive nature of the carbonate zone predominant in areas around where NC and RB sampling sites were located (Fretwell and Stewart 1981; USGS 2007).

The SGD values derived from estimated diffusive fluxes obtained from equilibration experiments on sediment cores of the SB system were negligible compared to SGD advection estimations (Tables 4.3, 4.7). The estimated ^{222}Rn diffusive fluxes were at least two orders of magnitude lower compared to calculated fluxes estimates derived from the ^{222}Rn model within the same sites (Table 4.7). It is interesting to observe a marked difference in ^{222}Rn concentrations in piezometer samples from NC and RB sites (Fig. 4.10). While the surface ^{222}Rn concentrations from both areas were similar, there was a sharp difference observed in terms of their depth concentration profiles. The NC sediment ^{222}Rn concentrations profile increased gradually and remained fairly constant beyond the 2 m depth level at a value of ~ 390 dpm/L, which is essentially the same as the pore water end - member based on the sediment equilibration experiments. Unlike the

NC profile however, the RB site ^{222}Rn pore water concentration profile revealed an irregular variation with depth (Fig. 4.10). While the average ^{222}Rn concentrations above 2.5 m depth level were < 250 dpm/L, a prominent peak was found at around 3 m of about 7000 dpm/L. This peak is likely indicative of the presence of a uranium enriched phosphatic sediment or freshwater lens at this depth since the ^{222}Rn concentration levels tapered off to lower concentrations at deeper levels, showing that the elevated levels were mainly localized at the 2.5 – 3.5 m depth range. The low salinity range (1.7 – 4.8 ppt) observed within this depth and the higher values at shallower sediment depths (11.7 – 23.9 ppt) confirm the presence of a freshwater lens.

In contrast to ^{222}Rn , CH_4 is rarely used as a quantitative SGD tracer. However, the potential usefulness of CH_4 as a groundwater tracer is quite evident in the results shown in Fig. 4.7. A direct graphical correlation analysis of the CH_4 and ^{222}Rn data revealed a fairly strong relationship ($r^2 = 0.31$; $\alpha = 0.05$; $n = 54$) between the two data sets. In spite of CH_4 not being a conservative SGD tracer, its marked qualitative potential in SGD estimations is owed to the fact that the relative concentrations of CH_4 associated with advecting groundwater compared to those in ambient seawater ($\text{CH}_{4\text{gw}}/\text{CH}_{4\text{sw}}$) is typically higher by some orders of magnitude. In the present study, this ratio was ~ 16 (i.e. one order of magnitude higher). In a previous study, Bugna et al. (1996), measured both CH_4 and ^{222}Rn concentrations of up to three orders of magnitude (concentrations of up to about 3300 and 2100 times higher respectively) in groundwater from an offshore spring compared to the respective ambient seawater concentrations.

Seepage meters on the other hand are site specific and dependent on the specific local sediment environment where the benthic chamber is deployed. Reliability of the seepage meter SGD estimations is normally based upon a representative number of deployments made within a given location. Although some individual SGD estimations obtained by direct manual seepage meter measurements at some sites within the SB system appeared to differ from those derived from the ^{222}Rn approach (Fig. 4.16), when pooled, the overall data agreed more closely and no statistical difference was found among them (t-test: $p = 0.12$; $\alpha = 0.05$; $n = 18$). In their review, Burnett et al. (2006) found good agreement in

patterns and overlapping calculated advection rates on independent estimations by seepage meters and the radon model, during an intercomparison SGD study which was conducted at the same location (West Neck Bay - Shelter Island, New York).

Relationship Between ^{222}Rn and CH_4

The significant elevation of radon and methane in groundwater compared to the surrounding ambient water makes them particularly useful tracers of groundwater to the nearshore coastal waters. Nonetheless, it is important to note that methane is also produced and consumed in a number of microbially mediated reactions and thus its direct application in SGD assessments require a more careful analysis (Bugna et al. 1996). In spite of this fact however, there is evidence that methane has been successfully utilized as a tracer of hydrothermal vent activity in the water column nearby an Oregon marginal ridge (Kulm 1988). Although CH_4 is non-conservative, it may still be a useful tracer because of the relatively large concentration difference that exists between seawater and groundwater, which in some cases has been found to be up to three orders of magnitude (Bugna et al. 1996). A number of methane studies such as that of Burke et al. (1983), have provided further supporting evidence to the effect that microbial activity associated with suspended particles is likely to be responsible for excess CH_4 . This is further augmented by the fact that freshwater (SGD) is more favorable to CH_4 production than the seawater environment (Angelis 1993). Generally, sulfate reduction (HS^- production) precedes methanogenesis (methane production) because sulfate-reducing bacteria outcompetes methanogens for substrates (Capone and Kiene 1988). Given that methanogenesis is more important in freshwater than it is in seawater, the abundant presence of CH_4 a nearshore coastal environment will most likely be indicative of freshwater (SGD) advection. While CH_4 may be a good SGD indicator, its non conservative nature precludes it from being used as a quantitative assessment tool for SGD. In this respect, ^{222}Rn is better suited for such use since it is both an inert gas and like CH_4 also available at relatively high concentrations in groundwater environments compared to surface water. Nevertheless, CH_4 is an important qualitative tool for SGD assessments.

Resistivity Survey

Streaming resistivity surveys offers potential as a reconnaissance surveying method for detecting zones of fresher groundwater (Figs. 4.11, 4.12). Calibration points at < 1.5m depth in Sarasota Bay showed a reasonable correlation between pore water resistivity and *terrain resistivity* as compared to measurements conducted at other depths (Terrain, or land relief or topography, is the third or vertical dimension of land surface. *Terrain resistivity* is therefore the vertical resistivity value of the resistivity measurements).

While calibration points at < 1.5 m depth in the SB system showed a consistent correlation between pore water resistivity and terrain resistivity, on the local (hundreds of meters) scale, lateral variations in resistivities derived from inversions of resistivity data were not found to be reproducible. Nearly coincident lines collected 30 minutes apart in time showed different local signatures. This apparent local lateral variability in the resistivity profiles is inferred to be a result of inversion of noisy streaming resistivity data. Streaming resistivity data in shallow water can be very noisy and suffers from inversion artifacts associated with errors in seafloor depths, electrodes getting pulled out of the water, and 3D effects, among others.

On the regional (kilometers to tens of kilometers) scale the relationship between marine resistivity and tracer-based SGD estimates did not generally follow the expected pattern of higher resistivities associated with higher SGD flux (Fig. 4.11). There appeared to be only subtle differences between resistivity structure in the northern and southern regions of the bay. These small differences show an inverse relationship regionally between advection rates and resistivity values in the north and south portions of the bay. The north region of the SB system was dominated by lower flow rates ranging between 0.71 and 5.9 cm/day and higher resistivity values between 3.1 and 30.0 Ω -m. The south region displays generally higher flow rates ranging from 5.9 to 24.0 cm/day with lower resistivity values between 0.31 and 3.1 Ω -m. This inverse relationship is the opposite of what would normally be expected if fresh SGD were the dominant cause of resistivity variability throughout the area. Seafloor resistivities instead may be influenced by stratigraphy, particularly the presence of a clay layer at ~10-15 m depth in the south

region. In the south region, the general trend from the seafloor downward is of decreasing resistivity at the depths associated with the clay layer, and increasing resistivity below clay depths. In the north region, where limestone is close to the bay floor, resistivity values are slightly higher, and the decrease in resistivity around ten meters depth is less pronounced.

To determine whether consistent relationships exist between pore water conductivities and terrain conductivities as measured with streaming resistivity exist near SB system, pore water samples were collected along with surface water resistivity surveys at 3 sites. When water 1D-resistivity inversions were performed at each of these sites and resistivity over the depth interval sampled compared with pore water resistivity, a relatively consistent formation factor was found. This suggests that surface-based resistivity measurements could be used as an indicator of shallow pore water resistivity.

A number of plausible explanations for the observed lower resistivity found at 15 m (Fig. 4.13) compared to resistivities at 10 or 5 m depth are possible. One explanation is that the area is no longer just a discharge area but also a recharge area and because of this two way head gradient, saline surface waters may penetrate to greater depths through conduits found in the limestone and move into the underlying aquifers. The other possible explanation is that over pumping from the underlying Floridan aquifer for irrigation and other purposes had altered the extent and thickness of the freshwater lens and thereby reduced the amount of readily available freshwater. It is also worth noting that there were some temporal differences between the 2003 and 2004 resistivity surveys although both data sets were collected during the dry season (December - May). The May survey occurred at the very end of the dry season, so aquifer levels would be at their lowest and the region would have gone for the longest periods with little to no rainfall, which would produce less available freshwater and thus lead to lower resistivity values. In comparison, the February survey was conducted earlier in the season when aquifer levels were higher than those found in May, since the former was a wetter month than the latter. The additional freshwater input during this time period may be another explanation for the higher overall resistivities found in the north region during the 2004 survey.

Nutrient Fluxes in the SB System

There were no trends in the variation of seawater nutrients that were measured in January and March'04 within the different regions of the SB system (Table 4.4), partially due to limited nutrient data that was available. However, except for $\text{NO}_2 + \text{NO}_3$, there were generally somewhat higher nutrient levels observed within the middle and south regions (albeit not being statistically different), as compared to the north region. Since the nutrient data were only from occasional grab samples, it is difficult to expect these data to reveal a representative nutrient distribution trend for the entire SB system. It is possible that the apparent higher nutrient levels observed within the middle and south regions is due to factors related to the general ocean water circulation, rather than to their actual source. Factors such as residence time, mean depth, number of passes and sediment characteristics, could all be contributing to the regional nutrient distribution. It is also expected that groundwater seepage into the SB system influences the nutrient concentrations since the groundwater nutrient concentrations tend to be high (Table 4.5). Such an effect might be especially important in areas that have longer residence times where the expected occurrence of rapid tidal dilution effect to the open Gulf of Mexico (GOM) is impeded. This is more likely to happen within the middle and south regions rather than in the north as there is a much larger volume of water involved (~ 80% of SB system water is found within the north region alone). Because of the apparent complex interactions of these factors, non-linear relationships are likely to result between SGD nutrient supplies and the subsequent concentrations. Our observations are consistent with an earlier work within the SB system by Tomasko et al. (1996), who noted that the water quality parameters did not clearly reflect differences in watershed nutrient inputs. The relative elevation of nutrient levels within the SB regions where relatively substantial SGD was observed (such as in the south region), is in agreement with earlier studies that have associated SGD with dissolved nutrient supply within coastal environments (USGS 2007; Valiela et al. 1990; Capone and Slater 1990).

Groundwater nutrient concentrations for each of the three regions (Table 4.5) were assumed to approximate the SGD or pore water concentration levels in each region.

Groundwater nutrient concentrations in wells for areas surrounding SB system were obtained from the Florida Department of Environmental Protection (FDEP) database (Appendices A.1, A.2, and A.3). Nutrient fluxes for each region were estimated by multiplying the regional estimated SGD rates with the respective average groundwater nutrient concentrations in that region (i. e., Flux = SGD rate x nutrient concentration \equiv m/day x mmol/m³ = mmol/m².day).

On the basis of the regional groundwater nutrient estimates (Table 4.5), except for NO₂ + NO₃, the estimated SGD nutrient fluxes depict elevated values for the north and south regions in all the measured nutrients (Table 4.6), relative to the middle region. Assuming a constant width of the seepage face per shore length within each region of the SB system, then about 40% of the dissolved inorganic regional nutrient fluxes occur in the north while ~ 60% occur in the middle and south regions combined (though normally higher seepage is expected at the nearshore area, even SGD distribution was assumed within each region in making these estimates).

From these estimates it seems clear that the earlier model (WASP4) generated estimate of ~10 % for nitrogenous nutrients being attributed to groundwater may be an underestimate (USGS 2007). As revealed in the present study, SGD is a significant source of nutrients in SB system, and assuming that the SGD seepage regime covers the 200 m coastal zone from the shoreline seaward, then about 27% of total N is associated with SGD in the entire SB system (with base flow included as part of SGD). The estimate is based on the median end member groundwater (N) concentration value within the region. This value is comparable to atmospheric and rainfall inputs which were also estimated at about 27% of total N in the region. 46% of the total N was attributed to surface runoff. In this estimation it was assumed that the general SGD seepage regime lies within 200 m from the shoreline, as has been found in previous studies elsewhere within the region (Burnett et al. 2006). Using the map scale provided for the SB system, the overall area attributed to SGD worked out to approximately 8% of the total area of the SB system. In addition, the middle and south regions have the highest overall nutrient flux per volume ratio compared to the north region, thus making them more susceptible to nutrient loading

effects. Regional SGD nutrient fluxes may depend upon the relative sizes of the catchment basins. Of the three regions in the SB system, the south region has the largest catchment basin area compared the other two regions (Fig. 4.1; USGS 2007).

The regional SGD (groundwater flux) N/P ratio was 21 in the north, 3 in the middle and 4 in the south regions respectively (Table 4.6). Except for the north region, it was evident that all the others had N/P ratios that were less than the theoretical Redfield ratio of 16 (Redfield et al. 1963). The relatively elevated levels of DOC (Table 4.4) within the middle and south regions is consistent with higher SGD in these areas since DOC has often been strongly associated with groundwater, and its inherent terrestrial nutrient loads as well as low pH levels (Goldharber et al. 1977; Santos et al. 2008). In general, there are several possible explanations for the low N/P ratios observed in both the seawater and groundwater of the SB system. Among the probable reasons for the observed low N/P ratio include the fact that, in our estimations we only considered the dissolved inorganic nitrogen (DIN) fraction, while assuming that the other labile nitrogen fractions such as the dissolved organic nitrogen (DON) were negligible. Other reasons that could be attributed to this observation may include the behavior of PO_4 in groundwater. For instance, while reactive phosphorus in groundwater is mostly present as inorganic dissolved PO_4 , it is generally rapidly removed through sorption to ferroxides or co-precipitated with Al and Ca in mineral phases through its flow path (hence raising the N/P ratio), though this removal becomes significantly inefficient in anoxic environments (Zanini et al. 1998). A case in point is a study in Buttermilk Bay, Massachusetts, where the N/P ratio was observed to rapidly increase from 17 at the outlet of a septic system to 40 one meter downstream (Slomp and Van Cappellen 2004). The converse of this may be explained by taking into consideration the relative amount of P present or supplied, with respect to that of N within a region.

A previous study of Sarasota Bay by Dillon and Chanton (2005; 2008) had shown that storm water PO_4 can be a significant source to the underlying groundwater aquifers. They showed that PO_4 concentrations which ranged from 3.5 to 13.8 $\mu\text{mol/L}$, were significantly higher than concentrations in rainwater. While low N/P ratios are rather

unusual for oxic groundwaters where dissolved PO_4 is normally expected to be negligible and the coastal groundwater N/P ratios are typically higher than 16, this is not totally surprising especially if the sorption capacity of an aquifer is overwhelmed due to excessive terrestrial P inputs (Slomp and Van Cappellen 2004). Indeed, values as low as 3 have also been reported in the North Inlet, South Carolina, where P-fluxes were found to average on the higher level, $\sim 900 \mu\text{mol}/\text{m}^2\cdot\text{day}$ (Krest et al. 2000). In a similar study, Suzumura et al. (2000) reported high levels of dissolved PO_4 in groundwater in Tokyo Bay, Japan, where values in excess of $101 \mu\text{M}$ were measured.

The average nutrient fluxes obtained in this study ranged from 2.1 to $8.3 \text{ mmol}/\text{m}^2\cdot\text{day}$ for DIN (combined NH_4 and $\text{NO}_2 + \text{NO}_3$), and 0.4 to $2.5 \text{ mmol}/\text{m}^2\cdot\text{day}$ for total dissolved P (Table 4.6). These values were on average higher than those reported recently in a more pristine site in the northeastern Gulf of Mexico (Santos et al. 2008). The generally high nutrient fluxes observed are partially to be attributed to the reported high density of septic tank systems commonly used in the increasingly populated coastal settlements found in the surrounding area of the SB system (SBEP 2006; USGS 2007). Overall, our nutrient flux values were comparable to other studies done in different coastal environments (Table 4.8).

Table 4.8: Comparison of nutrient flux rates and N/P ratios between this study and other studies.

Study Site	Total Dissolved P	DIN (= NH₄ + NO₂+ NO₃)	N/P	Source
	(mmol/m².day)	(mmol/m².day)		
Tampa, Florida	0.1	0.9	7	Swarzenski et al. 2007
Turkey Point, Florida (FSUCML)	0.4 ± 0.3	8.2 ± 1.2	6 - 813	Santos et al. 2008
Florida Bay, Florida	< 0.03	0.4 – 1.5	-	Corbett et al. 1999
Waquoit Bay, Massachusetts	-	0.55	-	Charette et al. 2001
Nauset Marsh Estuary, Massachusetts	-	24 - 72	> 16	Portnoy et al. 1998
Pettaquamscutt Estuary, Rhode Island	0.03	0.41	14	Kelly and Moron 2002
Kaloko, Hawaii	-	116	-	Paytan et al. 2006
North inlet, South Carolina	0.9	2.4	3	Krest et al. 2000
Sarasota Bay, Florida (SB system)	0.4 – 2.5	2.1 - 8.3	3 - 21	Present Study

The close agreement of the observed SGD trends using both seepage meters and ^{222}Rn has been reported in earlier studies. Burnett et al. (2008), for example, found a similar SGD pattern with seepage meters as well as ^{222}Rn concentrations in Flamengo Bay, Ubatuba, Brazil. Some other studies in various nearshore environments have also found similar observations (i.e. Sholkovitz et al. 2003; Burnett et al. 2006). It is thus suggested that these independent SGD estimation techniques complement rather than substitute for each other. Therefore a better understanding of SGD in an area is more probable when more than one of these approaches are applied in a complementary manner.

Conclusions

In our assessments, ^{222}Rn was shown to be an effective tracer for submarine groundwater discharge. SGD flow rates calculated from the radon box model are consistent in magnitude with those obtained using manual seepage meters. Due to its relatively high concentration in freshwater compared to seawater, methane (CH_4) is potentially useful for qualitative SGD determinations. There is some regional variability in SGD rates within the different regions of the Sarasota Bay system. SGD rates were shown to be relatively higher in the middle and south regions compared to the north region of the system. Although much of it is likely re-circulated SGD, the numerous possibly leaky septic tank systems found within the middle and south relatively highly populated coastal settlements, play an important role in the observed SGD dissolved inputs to the Sarasota Bay system. This was revealed through the regional sea water nutrient concentration levels, nutrient fluxes and N/P ratios. However, the generally large variations in water column nutrient data may be attributed to the relatively limited data that was available in this study.

The estimated advection rates in the Sarasota Bay system were found to range from 0.7 to 24.0 cm/day, except for isolated hot spot occurrences where higher rates were observed. In general SGD estimates were relatively higher in the middle and south regions (5.9 – 24.0 cm/day) compared to the north region (0.7 – 5.9 cm/day). Although nutrient

concentrations did not reveal any obvious trend, the average nutrient flux N/P ratio was higher in the north compared to the middle and south regions.

The importance of SGD in the Sarasota Bay system was evident in that, about 40% of the dissolved inorganic nutrient fluxes via SGD were measured in the north while the remaining ~ 60% occurred in the middle and south regions combined. Overall therefore, about 27% of the total dissolved N is associated with SGD in the entire SB system. In addition, the middle and south regions had the highest overall regional nutrient flux per water volume ratio, compared to the north, thus making them potentially vulnerable for the occurrence of eutrophic conditions.

Acknowledgements

I wish to express my sincere thanks to a number of people without whose help, this project would not have been possible. Margaret Murray, Sarah Kruse and Arnell Harrison were outstanding collaborators who significantly contributed to the success of this work. Kelly Peeler, Christina Stringer, Rick Peterson, Henrieta Dulaiova, Claire Langford and Axel Schmidt assisted on this project both at the field and in the laboratory. The watershed monitoring section of the Florida Department of Environmental Protection (FDEP) database is much appreciated for allowing use of their groundwater nutrient data. This project was jointly funded through a Florida Sea Grant/EPA Grant and an IFP-Ford Foundation PhD Fellowship. This financial support is gratefully acknowledged.

CONCLUSION

The continuous heat-type automated seepage meter can provide reliable, long-term SGD rate measurements that agree both in trend and magnitude with other independent SGD techniques, including the manual seepage meter, radon as a geochemical tracer, and an electromagnetic seepage meter.

Our studies showed that connecting a 76.2 m extension cable to the seepmeter has negligible effects on its SGD measuring capability, as long as calibrations are made with the extension cable connected. Similarly, the apparent effect of low temperature can also be effectively accounted for by conducting calibrations at the anticipated temperatures.

Salinity was found to have no significant effect on the continuous heat-type automated seepage meter measurements as the calibration results from fresh water and sea water agreed to within the 95% confidence level.

The Bernoulli-type flow artifacts on SGD - seepmeter measurements can be significantly reduced by submerging (or burying) the seepage meter benthic chambers to the same topographic level as the sediment.

The study revealed that the percentage difference between SGD_{seep} and SGD_{rad} measurements are much greater (~twice) for deployments with unburied compared to those with buried benthic seepage chambers.

Results of the Sarasota Bay case study revealed regional variability in SGD rates within the different regions of the bay system. SGD rates were shown to be relatively higher in the middle and south regions compared to the north region of the system. This resulted to varying regional sea water nutrient concentration levels, nutrient fluxes and N/P ratios.

About 40% of the dissolved inorganic nutrient fluxes via SGD were measured in the north while the remaining ~ 60% occurred in the middle and south regions of the Sarasota Bay system, combined.

Overall, about 27% of total N is associated with SGD in the entire Sarasota Bay system.

APPENDIX A

Table A.1: Groundwater NO₂ + NO₃ concentrations (μM) in wells in vicinity of SB system.

Region	Latitude (°N)	Longitude (°E)	Station Name	NO ₂ + NO ₃ Concentration (mg/L)	NO ₂ + NO ₃ Concentration (μM)	Well Depth (m)	NO ₂ + NO ₃ Average Concentration (μM)
North	27.4551	81.4710	SW3-UA-2069	5.4	385	17.7	138 ± 215 (n = 3)
	27.3748	81.4949	SW3-CA-2032	0.39	27.8	52.1	
	27.3511	81.3605	SW3-UA-2038	0.01	0.6	14.3	
Middle	27.3235	81.4716	SW3-CA-2039	0.04	3.1	62	44.2 ± 84.8 (n = 4)
	27.2918	82.3641	SW3-UA-2078	2.4	171	7.9	
	27.2744	82.3812	SW3-UA-2066	0.01	0.4	7.0	
	27.2715	81.5458	SW3-CA-2052	0.03	1.9	107	
South	27.2123	81.4803	SW3-UA-2032	0.01	0.8	13.4	1.2 ± 0.7 (n = 4)
	27.1759	81.4929	SW3-CA-2059	0.01	0.6	402	
	27.1002	82.2029	SW3-UA-2058	0.03	2.1	18.9	
	26.5645	81.4828	SW3-UA-2052	0.02	1.3	25.9	

Groundwater raw nutrient data source: Watershed Monitoring Section of the Florida Department of Environmental Protection, FDEP.

Table A.2: Groundwater PO₄ concentrations (μM) in wells in vicinity of SB system.

Region	Latitude (°N)	Longitude (°E)	Station Name	PO ₄ Concentration (mg/L)	PO ₄ Concentration (μM)	Well Depth (m)	PO ₄ Average Concentration (μM)
North	27.5918	81.4306	SW3-UA-2049	0.01	0.3	18.6	6.9 ± 9.1 (n = 9)
	27.5511	81.3538	SW3-CA-2012	0.01	0.3	100.6	
	27.5511	81.3538	SW3-UA-2045	0.74	23.9	18.3	
	27.5413	81.3721	SW3-CA-2068	0.49	15.8	193.2	
	27.4552	81.4710	SW3-CA-2044	0.02	0.6	230.7	
	27.4551	81.4710	SW3-UA-2069	0.01	0.4	17.7	
	27.3852	82.0315	SW3-CA-2008	0.01	0.3	347.5	
	27.3748	81.4949	SW3-CA-2032	0.14	4.5	52.1	
	27.3511	81.3605	SW3-UA-2038	0.48	15.5	14.3	
Middle	27.2950	81.3052	SW3-UA-2031	3.1	100	6.1	28 ± 41 (n = 5)
	27.2928	81.4741	SW3-UA-2072	0.61	19.7	3.0	
	27.2918	82.3641	SW3-UA-2078	0.1	3.2	7.9	
	27.2744	82.3812	SW3-UA-2066	0.51	16.5	7.0	
	27.2545	81.3523	SW3-CA-2067	0.06	1.9	35.4	
South	27.2123	82.2435	SW3-UA-2051	0.01	0.2	7.6	
	27.2123	81.4803	SW3-UA-2032	0.11	3.6	13.4	
	27.1544	82.2616	SW3-UA-2042	0.02	0.5	5.5	
	27.1233	81.3922	SW3-UA-2024	0.75	24.2	16.8	
	27.1139	82.2845	SW3-UA-2014	0.26	8.4	9.8	
	27.1135	82.0748	SW3-CA-2005	0.01	0.2	257.6	
	27.1117	81.4625	SW3-UA-2008	0.26	8.4	8.2	

Table A.2 – continued

Region	Latitude (°N)	Longitude (°E)	Station Name	PO ₄ Concentration (mg/L)	PO ₄ Concentration (μM)	Well Depth (m)	PO ₄ Average Concentration (μM)
South	27.1022	82.1516	SW3-UA-2023	0.1	3.2	10.7	7.1 ± 8.5 (n = 17)
	27.1002	82.2029	SW3-UA-2058	0.1	3.2	18.9	
	27.0500	81.5716	SW3-CA-2003	0.003	0.1	57.6	
	27.0435	82.0856	SW3-UA-2043	0.16	5.2	8.4	
	27.0419	81.3659	SW3-CA-2030	0.01	0.2	127.1	
	27.0419	81.3659	SW3-UA-2100	0.65	21.0	7.3	
	27.0152	82.0001	SW3-UA-2004	0.59	19.1	9.1	
	26.5645	81.4828	SW3-UA-2052	0.62	20.0	25.9	
	26.5645	81.4828	SW3-CA-2019	0.004	0.1	183.5	
	26.5645	81.4828	SW3-CA-2075	0.1	3.1	71.0	

Groundwater raw nutrient data source: Watershed Monitoring Section of the Florida Department of Environmental Protection, FDEP.

Table A.3: Groundwater NH₄ concentrations (μM) in wells in vicinity of SB system.

Region	Latitude (°N)	Longitude (°E)	Station Name	NH ₄ Concentration (mg/L)	NH ₄ Concentration (μM)	Well Depth (m)	NH ₄ Average Concentration (μM)
North	28.0417	81.5720	SW3-UA-2089	0.27	19.3	10.7	7.8 ± 6.2 (n = 9)
	27.5511	81.3538	SW3-CA-2012	0.17	12.1	101	
	27.5511	81.3538	SW3-UA-2045	0.02	1.6	18.3	
	27.5505	81.5241	SW3-UA-2065	0.01	0.8	16.1	
	27.5413	81.3721	SW3-CA-2068	0.15	10.7	193	
	27.4552	81.4710	SW3-CA-2044	0.15	10.7	231	
	27.3852	82.0315	SW3-CA-2008	0.13	9.3	348	
	27.3748	81.4949	SW3-CA-2032	0.05	3.6	52.1	
	27.3511	81.3605	SW3-UA-2038	0.03	2.1	14.3	
Middle	27.3235	81.4716	SW3-CA-2039	0.02	1.1	62.2	28.4 ± 27.1 (n = 7)
	27.2950	81.3052	SW3-UA-2031	1.1	78.5	6.1	
	27.2928	81.4741	SW3-UA-2072	0.38	27.1	3.0	
	27.2918	82.3641	SW3-UA-2078	0.58	41.4	7.9	
	27.2715	81.5458	SW3-CA-2052	0.5	35.7	108	
	27.2545	81.3523	SW3-CA-2067	0.02	1.6	35.4	
	27.2511	82.3457	SW3-CA-2018	0.19	13.6	104	
South	27.2405	82.1616	SW3-CA-2049	0.26	18.6	146	
	27.2250	82.1751	SW3-CA-2002	0.43	30.7	32.6	
	27.2123	82.2435	SW3-UA-2051	0.91	65.0	7.6	
	27.2123	81.4803	SW3-UA-2032	0.08	5.4	13.4	
	27.1759	81.4929	SW3-CA-2059	0.24	17.1	402	
	27.1707	82.0227	SW3-CA-2043	0.04	2.9	296	
	27.1616	82.2403	SW3-CA-2057	0.28	20.0	136	

Table A.3 - continued

Region	Latitude (°N)	Longitude (°E)	Station Name	NH ₄ Concentration (mg/L)	NH ₄ Concentration (μM)	Well Depth (m)	NH ₄ Average Concentration (μM)
	27.1544	82.2616	SW3-UA-2042	0.25	17.8	5.5	
	27.1233	81.3922	SW3-UA-2024	0.08	5.6	16.8	
	27.1139	82.2845	SW3-UA-2014	0.46	32.8	9.8	
	27.1135	82.0748	SW3-CA-2005	0.28	20.0	258	
	27.1028	81.5835	SW3-CA-2063	0.32	22.8	204	
	27.1022	82.1516	SW3-UA-2023	0.45	32.1	10.7	23.4 ± 12.1
South	27.1002	82.2029	SW3-CA-2077	0.24	17.1	128	
	27.0921	82.2342	SW3-CA-2025	0.14	10.0	36.6	(n = 30)
	27.0558	82.2410	SW3-CA-2042	0.29	20.7	33.5	
	27.0500	81.5716	SW3-CA-2003	0.39	27.8	57.6	
	27.0435	82.0856	SW3-UA-2043	0.5	35.7	8.4	
	27.0435	82.0856	SW3-CA-2066	0.35	25.0	50.3	
	27.0419	81.3659	SW3-CA-2030	0.38	27.1	127	
	27.0419	81.3659	SW3-UA-2100	0.43	30.7	7.3	
	27.0340	81.5302	SW3-CA-2035	0.32	22.8	140	
	27.0228	81.4433	SW3-CA-2058	0.36	25.7	419	
	27.0152	82.0001	SW3-UA-2004	0.14	10.0	9.1	
	27.0146	82.0413	SW3-CA-2010	0.44	31.4	107	
	26.5645	81.4828	SW3-UA-2052	0.47	33.5	25.9	
	26.5645	81.4828	SW3-CA-2019	0.41	29.3	184	
	26.5645	81.4828	SW3-CA-2075	0.47	33.5	71.0	
	26.5639	82.1305	SW3-CA-2054	0.25	17.8	189	
	26.5630	81.5816	SW3-CA-2051	0.16	11.4	79.2	

Groundwater raw *nutrient data source: Watershed Monitoring Section of the Florida Department of Environmental Protection, FDEP. Special note* - In the appendices A1-A3 above, the apparent disparity in the number, n, of replicates in some of regional data is due to the fact that the quality control criteria used excluded some of the data from being used in the estimations. It is also observed that there is a wide nutrient concentration range in some of the wells. Data collected from Jan'06 to Jun'06.

APPENDIX B

DEVELOPMENT OF THE CONTINUITY DEVICE, VoST, AND ITS APPLICATION IN THE QUANTIFICATION OF SUBMARINE GROUNDWATER DISCHARGE

Publication status:

Further research is still continuing for development of device.

Abstract

The challenge posed by the need to accurately quantify submarine groundwater discharge (SGD), has led to the currently continuing efforts by scientists for search of suitable tools or approaches that could be reliably used for this purpose. We report for the first time, an inexpensive but efficient novel device which is still under research for further development. The operation of this device, VoST, is based on the law of conservation of mass and the application of continuity principle. It uses the basic conservative water properties: volume, salinity and temperature, from where it also derives its acronym. Preliminary SGD assessments between VoST (Figs. B.1, B.2) and other SGD approaches such as, seepmeters and geotracers (^{222}Rn model), have been found to be in agreement.

Derivation of Steady State Volume-Salinity-Temperature (VoST) – SGD Model Equation

Principle and Assumptions

The steady state Volume-Salinity-Temperature (VoST) – SGD model equation is derived on the following scientific basis:

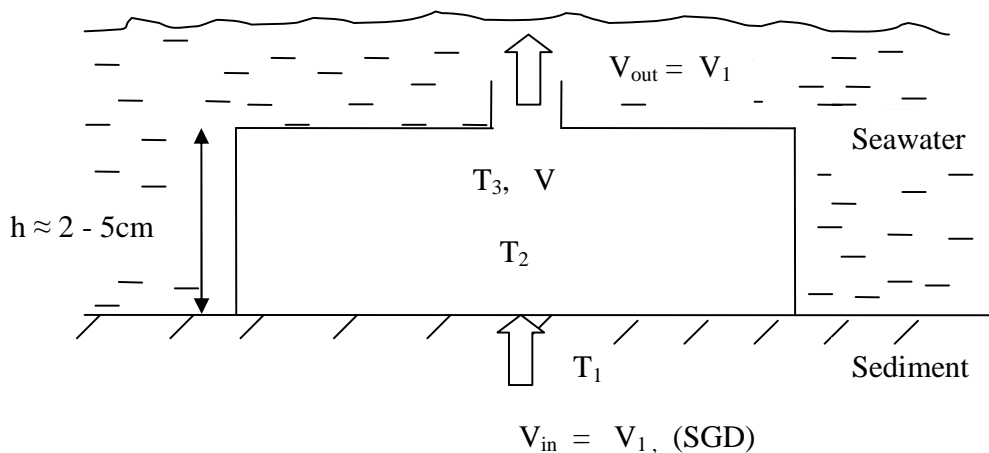
1. The laws of continuity (Hornberger et al. 1998) or conservation of mass (or volume in this case), and energy (heat) apply since a benthic chamber is considered to be a (semi) closed system:

(i.e., $Q_1 = Q_2 = Q_3 = Q = qA = \text{constant}$, and $\rho_1 C_1 V_1 T_1 + \rho_2 C_2 (V - V_1) T_2 = \rho_3 C_3 V T_3$)

2. SGD flux at the sediment-water interface is assumed to be constant (at least during the period of assessment or measurement) from an infinite reservoir (aquifer),
3. The lateral gain or loss of heat of the experimental chamber is negligible,
4. All the SGD flux from the bottom of the benthic chamber is compensated for by loss through the outlet at the top of the chamber, and
5. Water inside the benthic chamber is well mixed and the overall heat and salinity fluctuation within the benthic chamber is solely driven by the SGD flux, i.e., the heat and salinity of the incoming water (groundwater) is different from the overlying water.

** Note: This model holds true for any other conservative property other than temperature (such as salinity).*

Derivation



From the experimental benthic chamber (diameter = 15cm) illustrated above:

$$V_{in} = V_{out} = V_1 \dots \dots \dots (B.i)$$

In this set up, if the laws of continuity and conservation of heat energy (and salinity) are fulfilled and the benthic chamber is considered to be a semi-closed constant flow system,

receiving a constant SGD flux through the underlying sediment, emanating from an infinite reservoir (or aquifer), then we shall have:

$$\rho_1 C_1 V_1 T_1 + \rho_2 C_2 (V - V_1) T_2 = \rho_3 C_3 V T_3 \dots\dots\dots(B.ii)$$

If we assume $\rho_1 \approx \rho_2 \approx \rho_3$ and $C_1 \approx C_2 \approx C_3$ then (B.i) becomes:

$$V_1 T_1 + (V - V_1) T_2 = T_3 V \dots\dots\dots(B.iii)$$

But, $V_1 = Q \Delta t \dots\dots\dots(B.iv)$

Substituting (B.iii) in (B.ii):

$$\Rightarrow (Q \Delta t) T_1 + (V - Q \Delta t) T_2 = T_3 V$$

$$\Rightarrow (Q \Delta t) T_1 + V T_2 - (Q \Delta t) T_2 = T_3 V$$

$$\Rightarrow Q \Delta t (T_1 - T_2) = (T_3 - T_2) V$$

$$\Rightarrow Q = \left[\frac{T_3 - T_2}{\Delta t} \right] \left[\frac{V}{T_1 - T_2} \right] \quad (\text{cm}^3/\text{day, time in days}) \dots\dots\dots(B.v)$$

Or,
$$q = \left[\frac{T_3 - T_2}{\Delta t} \right] \left[\frac{1}{T_1 - T_2} \right] \frac{V}{A} \quad (\text{cm/day}) \dots\dots\dots(B.vi)$$

Since $\left[\frac{T_3 - T_2}{\Delta t} \right] = \text{slope, of the temperature vs time plot (for the linear section),}$

equation (B.vi) can also be written as:

$$q = \text{slope} * V/A * 1/(T_1 - T_2) \quad (\text{cm/day}) \dots\dots\dots(B.vii)$$

Glossary

A = cross section area of the benthic chamber (cm^2)

C_1 = heat capacity of the discharging groundwater (SGD), ($\text{J}/^\circ\text{C}$)

C_2 = initial heat capacity of water inside the benthic chamber ($\text{J}/^\circ\text{C}$)

C_3 = final heat capacity of water inside the benthic chamber ($\text{J}/^\circ\text{C}$)

h = height of the benthic chamber above the sediment level (cm)

Q_1 = volume flux of the discharging groundwater through the sediment (cm^3/day)

Q_2 = volume flux of the discharging groundwater through the benthic chamber (cm^3/day)

q = specific water discharge of groundwater through the sediment (cm/day)

ρ_1 = density of the influxing groundwater (g/cm^3)

ρ_2 = density of the initial water inside the benthic chamber (g/cm^3)

ρ_3 = density of the final water inside the benthic chamber (g/cm^3)

T_1 = initial temperature of the influxing groundwater at the bottom of the benthic chamber ($^\circ\text{C}$)

T_2 = initial temperature of water inside the benthic chamber ($^\circ\text{C}$)

T_3 = final temperature of water inside the benthic chamber ($^\circ\text{C}$)

V = volume of water inside the benthic chamber (cm^3)

V_1 = volume of the influxing groundwater into the benthic chamber during an interval of time, Δt (this volume quantity is the same for V_{in} and V_{out})

SGD = Submarine Groundwater Discharge.

Recommendations for Further Developmental Research on VoST

Preliminary experiments have shown that VoST is a viable SGD device that can potentially provide an inexpensive efficient and simple method for estimation of SGD.

For best results to be realized when using the VoST – continuity SGD device, preliminary experiments have shown that the following conditions are to be observed as closely as possible: Use of high quality sensors that will provide high resolution temperature (or salinity) measurements, depending on which conservative property of SGD is used for the model.

When temperature is used as the conservative SGD property for the model, the benthic chamber used need to be of the highest possible insulative (non-heat conducting) material to ensure negligible gain or loss of heat with respect to the surrounding.

For optimum results with the model, the maximum deployed benthic chamber height above the water-sediment interface should be ≤ 5 cm, and its cross section area and outlet at the top need to be of optimum size (not too large). This effectively minimizes any potential interference that might arise within the chamber from possible external turbulence due to the usually low SGD rates.

When temperature is used as the conservative SGD property for the model, only the linear section (of the temperature vs. time plot) is to be used. The minimum time interval (Δt) chosen should be such as to allow for the seepage water (groundwater) to have completely traveled the distance between the two sensors. Further work is still underway on the VoST – continuity device to improve its overall capability.

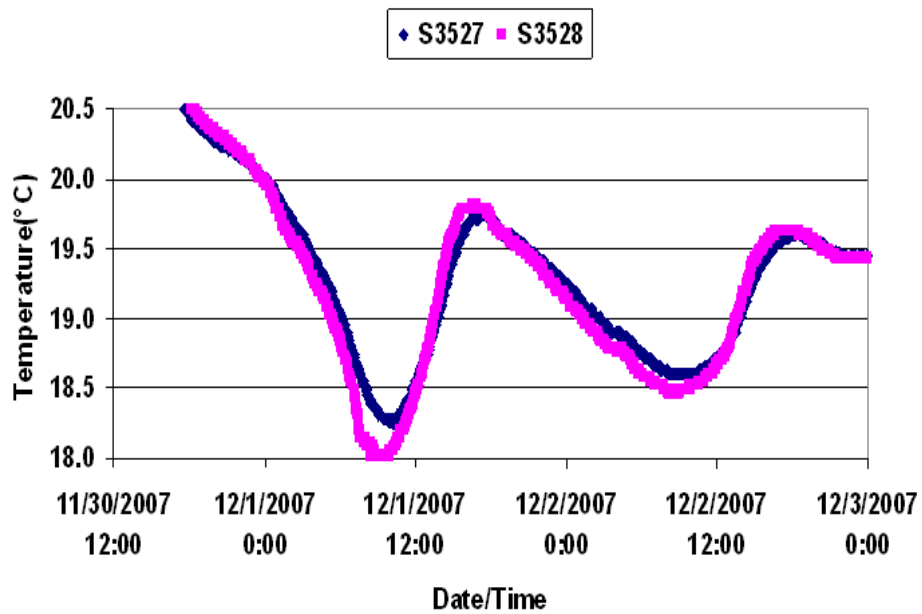


Fig. B.1: Field temperature measurements using VoST device: Temperature sensors installed inside benthic chamber without bottom barrier.

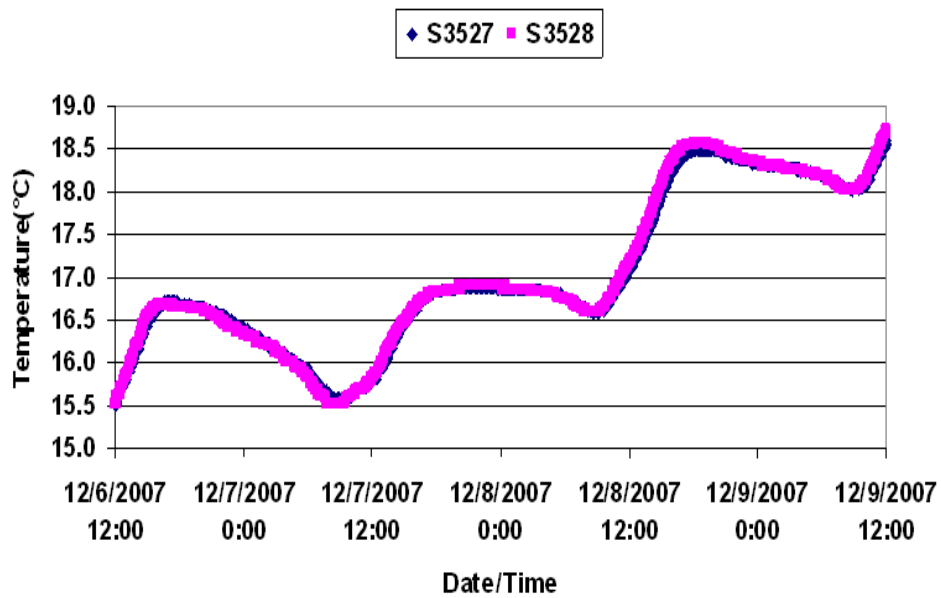


Fig. B.2: Field temperature measurements using VoST device: Temperature sensors installed inside benthic chamber with bottom barrier.

In the estimation of SGD rate using VoST at FSUCML study site, according to the “derivation” diagram above: the temperature measured by sensor S3527 = T_1 , T_2 and for sensor S3528 = T_3 .

(Calculated average SGD rate from the plot = 19.6 ± 7.3 cm/day. This compares well with average values obtained by independent approaches at the same site (Table 2.2)).

REFERENCES

- Angelis, M. A., and Scranton, M. J. 1993. Fate of methane in the Hudson River and estuary. *Global Biogeochemical Cycles* 7: 509 - 523.
- Australian Bureau of Meteorology. 2001. Australian Bureau of Meteorology. <www.bom.gov.au>.
- Barr, F. J., Paffenholz, J. and Rabson, W. 1996. The dual – sensor ocean – bottom cable method: Comparative geophysical attributes, quantitative geophone coupling analysis and other recent advances. SEG/DENVER'96. Technical Program Volume I.
- Benner, R. H. and Strom, M. A. 1993. A critical evaluation of the analytical blank associated with DOC measurements by high temperature catalytic oxidation. *Marine Chemistry* 41: 153 - 160.
- Berner, R. A. 1980. Early diagenesis. A theoretical approach. Princeton.
- Bokuniewicz, H. J. 1992. Analytical descriptions of subaqueous groundwater seepage. *Estuaries* 15: 458 – 464.
- Bokuniewicz, H., and Pavlik, B. 1990. Groundwater seepage along a barrier island. *Biogeochemistry* 10: 257 - 276.
- Brewster-Wingard, G. L. 1997. Reinterpretation of the Peninsular Florida Oligocene: An integrated stratigraphic approach. *Sedimentary Geology* 108(1 - 4): 207 - 228.
- Broecker, W. 1965. The application of natural radon to problems in ocean circulation, in: *Symp. On Diffusion in Oceans and Freshwaters*. T. Ichiye, ed., pp. 116 - 145. Lamont-Doherty Geological Observatory, Palisades, NY.
- Bugna, G. C., Chanton, J. P. Cable, J. E., Burnett, W. C. and Cable, P. H. 1996. The importance of groundwater discharge to the methane budgets of nearshore and continental shelf waters of the northeastern Gulf of Mexico. *Geochimica et Cosmochimica Acta* 60: 4735 - 4746.
- Burke, J. C., Casso, S. A. and Hamblin, R. E. 1983. Tripod modification of sphincter core: Construction operation core extrusion and sampling efficiency. Woodswhole Oceanographic Institute, MA (USA). Q2.622 Methods and Instruments.
- Burnett, W. C. 1999. Offshore springs and seeps are focus of working group. *EOS* 80, 13 - 15.
- Burnett, W. C., Aggarwal, P.K., Aureli, A., Bokuniewicz, H., Cable, J.E., Charette, M.A., Kontar, E., Krupa, S., Kulkarni, K.M., Loveless, A., Moore, W.S., Oberdorfer, J.A., Oliveira, J., Ozyurt, N., Povinec, P., Privitera, A.M.G., Rajar, R., Ramessur, R.T.,

- Scholten, J., Stieglitz, T., Taniguchi, M. and Turner, J.V. 2006. Quantifying submarine groundwater discharge in the coastal zone via multiple methods. *Science of the Total Environment* 367: 498 - 543.
- Burnett, W. C., Bokuniewicz, H., Huettel, M., Moore, W. S. and Taniguchi, M. 2003. Groundwater and pore water inputs to the coastal zone. *Biogeochemistry*, 66(1 - 2), 3 - 33.
- Burnett, W. C., and Dulaiova, H. 2003. Estimating the dynamics of groundwater input into the coastal zone via continuous radon-222 measurements. *Journal of Environmental Radioactivity* 69: 21 - 35.
- Burnett, W. C., Kim, G. and Lane-Smith, D. 2001. A continuous monitor for assessment of ^{222}Rn in the coastal ocean. *Journal of Radioanalytical and Nuclear Chemistry* 249: 167 - 172.
- Burnett, W. C., Peterson, R., Moore, W. S., Oliveira, J. 2008. Radon and radium isotopes as tracers of submarine groundwater discharge – results from Ubatuba, Brazil SGD assessment intercomparison. *Estuarine, Coastal and Shelf Science* 76: 501 - 511.
- Burnett, W., Chanton, J., Christoff, J., Kontar, E., Krupa, S., Lambert, M., Moore, W., O'Rourke, D., Paulsen, R., Smith, C., Smith, L., Taniguchi, M. 2002. Assessing methodologies for measuring groundwater discharge to the ocean. *EOS Transactions, American Geophysical Union* 83 (11): 117 - 123.
- Burnett, W. C., Wattayakorn, G., Taniguchi, M., Dulaiova, H., Sojisuporn, P., Rungsupa, S., Ishitobi, T. 2007. Groundwater – derived nutrient inputs to the Upper Gulf of Thailand. *Continental Shelf Research* 27: 176 - 190.
- Cable, J. E., Martin, J. B. and Jaeger, J. 2006. Exonerating Bernoulli? On evaluating the physical and biological processes affecting marine seepage meter measurements. *Limnology and Oceanography, Methods* 4: 172 - 183.
- Cable, J. E., Burnett, W. C., Chanton, J. P. and Weatherly, G. L. 1996. Estimating groundwater discharge into the northeastern Gulf of Mexico using radon-222. *Earth and Planetary Science Letters* 144: 591 - 604.
- Cable, J., Martin, J., Swarzenski, P., Lindenburg, M., Steward, J. 2004. Advection within shallow pore waters of a coastal lagoon. *Ground Water* 42: 1011 - 1020.
- Cable, J. E., Burnett W. C., Chanton J. P., Corbett D. R., Cable P. H. 1997. Field evaluation of seepage meters in the coastal marine environment. *Estuarine Coastal and Shelf Science* 45: 367 - 375.
- Capone, D. G. and Slater, J. M. 1990. Inter-annual patterns of water table height and groundwater-derived nitrate in nearshore sediments. *Biogeochemistry* 10: 277 - 288.

- Capone, D. G. and Kiene, R. P. 1988. Comparative of microbial dynamics in marine and freshwater sediments: Contrasts in aerobic carbon metabolism. *Limnology and Oceanography* 33(4): 725 - 749.
- Capone, D. G., and Bautista, M. F. 1985. A groundwater source of nitrate in nearshore marine sediments. *Nature* 313: 214 - 216.
- Caraco, N. F. 1995. Influence of human populations on P transfers to aquatic systems: a regional scale study using large rivers. Phosphorus in the global environment. In: Tiessen, H., Editor. *Transfers, Cycles and Management*. SCOPE, Wiley, New York, pp. 235 - 244.
- Chanton, J. P., Martens, C. S. and Kelley, C. A. 1989. Gas transport from methane – saturated, tidal freshwater and wetland sediments. *Limnology and Oceanography* 34(5): 807 - 819.
- Chanton, J. P., Burnett, W. C., Taniguchi, M., Dulaiova, H. and Corbett, D. R. 2003. Seepage rate variability derived by Atlantic tidal height. *Biogeochemistry* 66: 187 - 202.
- Charette, M. A., Buesseler, K. O. and Andrews, J. E. 2001. Utility of radium isotopes for evaluating the input and transport of groundwater – derived nitrogen to a Cape Cod estuary. *Limnology and Oceanography* 46(2): 465 - 470.
- Chemical Rubber Company, CRC., 1985. *Handbook of chemistry and physics* 65th edition. CRS Press, Inc., Boca Raton, FL, pp. F114 - F120 (1984 - 85).
- Corbett, D. R., Chanton, J., Burnett, W., Dillon, K., Rutkowski, C. and Fourqurean, J. W. 1999. Patterns of groundwater discharge into Florida Bay. *Limnology and Oceanography* 44: 1045 -1055.
- Corbett, R. and Cable, J. E. 2003. Seepage meters and advective transport in coastal environments: comments on “Seepage meters and Bernoulli’s revenge” by Shinn, Reich D. O’Rourke, R. Paulsen, C. Smith, L. Smith and M. Taniguchi 2002. Assessing methodologies for measuring groundwater discharge to the ocean. *EOS Transactions, American Geophysical Union* 83 (11): 117 - 123.
- D’Elia, C., Webb, K. and Porter, J. 1981. Nitrate-rich groundwater inputs to Discovery Bay, Jamaica: a significant source of N to local coral reefs? *Bulletin of Marine Science* 31: 903 - 910.
- Dillon, K. S. and Chanton, J. P. 2005. Nutrient transformations between rainfall and stormwater runoff in an urbanized coastal environment: Sarasota Bay, Florida. *Limnology and Oceanography* 50(1): 62 - 69.

- Dillon, K. S. and Chanton, J. P. 2008. Nitrogen stable isotopes of macrophytes assess stormwater nitrogen inputs to an urbanized estuary. *Estuaries and Coasts* 31: 360 - 370.
- Dillon, K. S., Corbett, D. R., Chanton, J. P., Burnett, W.C. and Kump, L. 2000. Rapid transport of a wastewater plume injected into saline groundwaters of the Florida Keys, USA. *Hydrology* 38: 624 - 634.
- Dulaiova, H., Peterson, R. Burnett, W. and Lane-Smith, D. 2005. A multi-detector continuous monitor for assessment of ^{222}Rn in the coastal ocean. *Journal of Radioanalytical and Nuclear Chemistry* 263: 361 - 365.
- Dyer, K. R. 1973. *Estuaries: A physical introduction*. John Wiley and Sons, London, UK.
- Dyer, K. R. and Taylor, P. A. 1973. A simple, segmented prism model of tidal mixing in well-mixed estuaries. *Estuarine and Coastal Marine Science* 1: 411 - 418.
- Fetter, C. W. 1988. *Applied hydrogeology*. McMillan Publishing Co., NY, 592 p.
- FGS 1985. Florida Geological Survey Open File Report 10: Geology of Sarasota County.
- Fretwell, J. D. and Stewart, M. T. 1981. Resistivity study of a coastal karst terrain, Florida. *Ground Water* 19 (2): 156 - 162.
- Giblin, A., Gaines, A., 1990. Nitrogen inputs to a marine embayment: The importance of groundwater. *Biogeochemistry* 10, 309 - 323.
- Goldharber, M. B., Aller, R. C., Cochran, K., Rosenfeld, J., Martens, C. S. and Berner, R. A. 1977. Sulfate reduction, diffusion and bioturbation in Long Island Sound sediments: Report of the FOAM group. *American Journal of Science* 277: 193 - 237.
- Gorsink, J. P. and Baker, G. C. 1990. Salt fingering in subsea permafrost: some stability and energy considerations. *Journal of Geophysical Research* 95: 9575 - 9584.
- Granier, A. 1985. Une nouvelle methode pour la mesure du flux de seve brute dans troncs des arbres. *Annals of Forest Science* 42: 81 - 88.
- Grasshoff, K., Kremling, K., and Ehrhardt, M. (Eds.). 1999. *Methods of Seawater Analysis*, 3rd Ed., Eds.: Grasshoff, K., Kremling, K., Ehrhardt, M., Wiley-VCH, Weinheim, 600 pp. ISBN 3-527- 29589-5.
- Greenwood, W. J., Kruse, S. and Swarzenski, P. 2006. Extending electromagnetic methods to map coastal pore water salinities. *Groundwater* 44(2): 292 - 299.
- Harrison, W. D., Musgrave, D. and Reeburgh, W. S. 1983. A wave – induced transport process in marine sediments. *Journal of Geophysical Research* 88: 7617 - 7622.

- Hornberger G. M., Raffensperger J. P., Wiberg P. L. and Eshleman K. N. 1998. Elements of Physical Hydrology. Johns Hopkins Univ. Pr. ISBN: 0801858577.
- Howarth, R.W. 1988. Nutrient limitation of net primary production in marine ecosystems. Annual Review of Ecology and Systematics 19: 89 - 110.
- Huettel, M. and Gust G. 1992. Impact of bioturbation on interfacial solute exchange in permeable sediments, Marine Ecology Progress Series 89: 253 - 267.
- Huettel, M., Ziebis, W. and Forster S. 1996. Flow-induced uptake of particulate matter in permeable sediments. Limnology and Oceanography 41(2): 309 - 322.
- Israelsen, O.W., Reeve, R.C. 1944. Canal lining experiments in the delta area, Utah. Utah Agriculture Experimental Station Technical Bulletin No. 313, 52pp.
- Johannes, R. 1980. The ecological significance of the submarine discharge of groundwater. Marine Ecology Progress Series 3: 365 - 373.
- Kelly, R. P. and Moron, S. B. 2002. Seasonal changes in groundwater input to a well – mixed estuary estimated using radium isotopes and implications for coastal nutrient budgets. Limnology and Oceanography 47(6): 1796 - 1807.
- Key, R. M., Guinasso, J. and Schink, D. R. 1979. Emanation of Radon-222 from marine sediments. Marine Chemistry 7: 221 - 250.
- Krest, J. M., Moore, W. S. and Gardner, L. R. 2000. Marsh nutrient export supplied by groundwater discharge: Evidence from radium measurements. Global Biogeochemical Cycles 14: 167 - 176.
- Krupa, S., Belanger, T., Heck, H., Brock, J., Jones, B. 1998., Krupaseep: the next generation seepage meter. Journal of Coastal Research 25: 210 - 213.
- Kulm, L. D. 1988. Potential heavy mineral and metal placers on the Southern Oregon continental shelf. Marine Mining 7(4): 361 - 395.
- Lapointe, B. and O'Connell, J. 1989. Nutrient-enhanced growth of *Cladophora prolifera* in Harrington Sound, Bermuda: eutrophication of a confined, phosphorus-limited marine ecosystem. Estuarine Coastal and Shelf Science 28: 347 - 360.
- Lapointe, B., J. O'Connell, and Garrett, G.S. 1990. Nutrient couplings between on-site sewage disposal systems, groundwater and nearshore surface waters of the Florida Keys. Biogeochemistry 10, 289 - 307.
- Lee D. R. 1977. A Device for Measuring Seepage Flux in Lakes and Estuaries Limnology and Oceanography 22(1): 140 - 147.

- Li, X., Hu, B. X., Burnett, W. C., Santos, I. R. and Chanton, J. P. 2009. Submarine ground water discharge driven by tidal pumping in a heterogeneous aquifer. *Ground Water* 47: 558 - 568.
- Li, L., Barry, D. A., Stagnitti, F. and Parlange, J. Y. 1999. Submarine groundwater discharge and associate chemical input to coastal sea. *Water Resources Research* 35(11): 3253 - 3259.
- Lipp, E. K. and Griffin, D. W. 2004. Analysis of coral mucus as an improved medium for detection of enteric microbes and for determining patterns of sewage contamination in reef environments. *Eco-Health* 1: 317 - 323.
- Lipp, E. K., Kurtz, R., Vincent, R., Rodriguez-Palacios, C., Farrah, S. R., Rose, J. B. 2001. The effects of seasonal variability and weather on microbial fecal pollution and enteric pathogens in a subtropical estuary. *Estuaries* 24: 266 - 276.
- Longworth, G. 1998. *The Radiochemical Manual*. National Measurement System for Ionizing radiation Metrology, AEA Technology, Analytical Services Group, Harwell, UK, 320p.
- Lovely, D.R. and Chapelle, F.H. 1995. Deep subsurface microbial processes. *Reviews of Geophysics* 33: 365 - 381.
- MacIntyre, S., Wanninkhof, R., and Chanton, J. P. 1995. Trace gas exchange in freshwater and coastal marine systems: flux across the air water interface. In *Methods in Ecology: Biogenic Trace Gases: Measuring Emissions from Soil and Water*, eds. P. Matson and R. Harriss. Blackwell Scientific, pp 52 - 97.
- Manheim, F. T., Krantz, D. E., et al. 2004. Studying Ground Water Under Delmarva Coastal Bays Using Electrical Resistivity. *Ground Water* 42(7): 1052 - 1068.
- Martens, C. S. and Klump, J. V. 1980. Biogeochemical cycling in an organic-rich coastal marine – I. Methane sediment – water exchange processes. *Geochimica et Cosmochimica Acta* 44: 471 - 490.
- Mathieu, G. G., Biscaye, P. E., Lupton, R. A. and Hammond, D. E. 1988. System for measurement of ^{222}Rn at low levels in natural waters. *Health Physics* 55: 989 - 992.
- McAulffe, C. 1971. Gas chromatographic determination of solutes by multiple phase equilibrium. *Chemical Technology* 1: 46 - 51.
- McKenna, T. E. and Martin, J. B. 2004. Ground water discharge to estuarine and coastal ocean environments: *Ground Water* 42(7): 957 - 958.

- Meybeck, M. 1993. C, N, P and S in rivers: from sources to global inputs. In: Wollast, R., Mackenzie, F. L., Chou, L. (Eds.), *Interactions of C, N, P and S Biogeochemical Cycles and Global Change*. NATO ASI, Springer, Berlin, pp. 163 - 193.
- Moore, W. 1996. Local groundwater inputs to coastal waters revealed by ^{226}Ra enrichments. *Nature* 380: 612 - 614.
- Moore, W. S. 1999. The subterranean estuary: a reaction zone of groundwater and sea water. *Marine Chemistry* 65: 111 - 126.
- Moore, W. S. 2010. The effect of submarine groundwater discharge on the ocean. *Annual Review of Marine Science*. 2: 59 - 88.
- Mwashote, B. M., Burnett, W.C., Chanton, J., Santos, I. R., Dimova, N. and Swarzenski, P. W. 2010. Calibration and use of continuous heat-type automated seepage meters for submarine groundwater discharge measurements. *Estuarine Coastal and Shelf Science* 87: 1 - 10.
- Neumann, G. and Pierson, W. J. 1966. *Principles of Physical Oceanography*. Prentice-Hall, Englewood Cliffs, 545pp.
- Oberdorfer, J.A., Valentino, M.A. and Smith, S.V. 1990. Groundwater contribution to the nutrient budget of Tomales Bay, California. *Biogeochemistry* 10: 199 - 216.
- Parsons, T. R., Maita, Y., and Lalli, C. M. 1984. *A manual for chemical and biological methods for seawater analysis*. New York: Pergamon Press.
- Paul, J. H., Rose, J.B., Brown, J., Shinn, E.A., Miller, S. and Farrah, S. 1995. Viral tracer studies indicate contamination of marine waters by sewage disposal practices in Key Largo, Florida. *Applied and Environmental Microbiology* 61: 2230 - 2234.
- Paulsen, R. J., Smith, C.F., O'Rourke, D., Wong, T.-F. 2001. Development and evaluation of an ultrasonic ground water seepage meter. *Ground Water* 39: 904 - 911.
- Paytan, A., Shellenbarger, G. G., Street, H. J., Gonness, E.M., Davis, K. A., Young, B.M. and Moore, W. S. 2006. Submarine groundwater discharge: An important source of new inorganic nitrogen to coral reef ecosystems. *Limnology and Oceanography* 51: 343 - 348.
- Peeler, K. A., Opsahl, S. P. and Chanton, J. P. 2006. Tracking anthropogenic inputs using caffeine, indicator bacteria, and nutrients in rural freshwater and urban marine systems. *Environmental Science and Technology* 40: 7616 - 7622.
- Peng, T. H., Takahashi, T. and Broecker, W. S. 1974. Surface radon measurements in the North Pacific Station Papa. *Journal of Geophysical Research* 79: 1772 - 1780.

- Peterson, R. N., Burnett, W. C., Taniguchi, M., Chen, T., Santos, I. R. and Ishitobi, T. 2008. Radon and radium isotope assessment of submarine groundwater discharge in the Yellow River delta, China. *Journal of Geophysical Research* 113: C09021, doi: 10.1029/2008JC004776.
- Petuch, E. J. 1986. The Pliocene reefs of Miami: Their geomorphophysical significance in the evolution of the Atlantic Coastal Ridge, Southeastern Florida, USA. *Journal of Coastal Research* 2(4): 391 - 408.
- Porter, B. 1985. The relationship between Apalachicola Bay water quality and septic system installations in the coastal zone, with application to other estuaries. Dept. of Natural Resources. Shellfish Environmental Assessment Section.
- Portnoy, J. W., Nowicki, B. L., Roman, C. T. and Urish, D. W. 1998. The discharge of nitrate – contaminated groundwater from developed shoreline to marsh – fringed estuary. *Water Resources Research* 34(11): 3095 - 3104.
- Povinec, P. P., Comanducci, J.-F., Levy-Palomo, F. I., and Benjamino O. 2006. Monitoring of submarine groundwater discharge along the Donnalucata coast in the south-eastern Sicily using underwater gamma-ray spectrometry. *Continental Shelf Research Submarine Groundwater Discharge Studies Offshore South-Eastern Sicily* 26: 874 - 884.
- Redfield, A. C., Ketchum, B. J. and Richards, F. A. 1963. The influence of organisms on the composition of seawater, p. 27 – 77. In M. N. Hill (ed.) *The sea*, v.2 Wiley – Interscience.
- Reich, C. D., Shinn, E. A., Hickey, T. D. and Tihansky, A. B. 2002. Tidal and meteorological influences on shallow marine groundwater flow in the upper Florida Keys. In: (Port J. W. and Porter eds.) *The Everglades, Florida Bay, and Coral Reefs of the Florida Keys*. CRC Press, Boca Raton, pp. 659 - 676.
- Robinson, M., Gallagher, D. and Reay, W. 1998. Field observations of tidal and seasonal variations in ground water discharge to tidal estuarine surface water. *Ground Water Monitoring and Remediation* 18: 83-92.
- Rosenberry, D. and Morin, R. 2004. Use of an electromagnetic seepage meter to investigate temporal variability in lake seepage. *Ground Water* 42: 68 - 77.
- Rutkowski, C., Burnett, W. C., Iverson, R. and Chanton, J. 1999. The effect of groundwater seepage on nutrient delivery and seagrass distribution in the northeastern Gulf of Mexico. *Estuaries* 22: 1033 - 1040.
- Santos, I. R., Dimova, N., Peterson, R. N., Mwashote, B. , J. Chanton and W. C. Burnett. 2009. Extended time series measurements of submarine groundwater discharge tracers (^{222}Rn and CH_4) at a coastal site in Florida. *Marine Chemistry* 113: 137 - 147.

- Santos, I. R., W. C. Burnett, J. Chanton, B. Mwashote, B., Suryaputra, I. G. N. A. and Dittmar, T. 2008. Nutrient biogeochemistry in a Gulf of Mexico subterranean estuary and groundwater derived fluxes to the coastal ocean. *Limnology and Oceanography* 53(2): 705 - 718.
- SBEP 2006. Sarasota Bay Environment Program - State of the Bay: Celebrating our greatest natural asset. http://www.sarasotabay.org/pdf/StateOfTheBay_06.pdf.
- Scott, P. J. B., Moser, K. A. and Risk, M. J. 1988. Bioerosion of concrete and limestone by marine organisms: A 13 year experiment from Jamaica. *Marine Pollution Bulletin* 19(5): 219 - 222.
- Shaw, R. D. and Prepas, E. E., 1989. Anomalous, short-term influx of water into seepage meters. *Limnology and Oceanography* 34(7): 1343 - 1351.
- Shaw, R. D. and Prepas, E.E. 1990a. Groundwater-lake interactions: I. Accuracy of seepage meter estimations of lake seepage. *Journal of Hydrology* 119: 105 - 120.
- Shaw, R.D. and Prepas, E.E., 1990b. Groundwater-lake interactions: II. Nearshore seepage patterns and the contribution of groundwater to lakes in central Alberta. *Journal of Hydrology* 119: 121 - 136.
- Shinn E. A., Reich C. D. and Hickey T. D. 2002. Seepage meters and Bernoulli's revenge. *Estuaries* 25: 126 - 132.
- Sholkovitz, E., Herbold, C. and Charette, M. 2003. An automated dye-dilution based seepage meter for the time-series measurement of submarine groundwater discharge. *Limnology and Oceanography, Methods* 1: 16 - 28.
- Shum, K. 1992. Wave-induced advective transport below a rippled water-sediment interface. *Journal of Geophysical Research* 97: 789 - 808.
- Shum, K. 1993. The effects of wave-induced pore water circulation on the transport of reactive solutes below a rippled sediment bed. *Journal of Geophysical Research* 98: 10289 - 10301.
- Slomp, C. P. and Van Capellen, P. 2004. Nutrients inputs to the coastal ocean through submarine groundwater discharge: controls and potential impact. *Journal of Hydrology* 295: 64 - 86.
- Stieglitz, T. 2005. Submarine groundwater discharge into the near-shore zone of the Great Barrier Reef, Australia. *Marine Pollution Bulletin* 51: 51 - 59.

Suzumura, M., Ueda, S. and Sumi, E. 2000. Control of phosphate concentration through adsorption and desorption processes in groundwater and seawater mixing at sandy beaches in Tokyo Bay, Japan. *Journal of Oceanography* 56: 667 - 673.

Swarzenski, P. W., Reich, C., Kroeger, K. D. and Baskaran, M. 2007. Ra and Rn isotopes as natural tracers of submarine groundwater discharge in Tampa Bay, Florida. *Marine Chemistry* 104 (1-2): 69 - 84.

Swarzenski, P.W., Charette, M., Langevin, C., 2004. An autonomous electromagnetic seepage meter to study coastal groundwater/surface water exchange. US Geological Survey Open File Report 2004 – 1369.

Sweeny, R.E. Kahil, E. and Kaplan, I.R. 1980. Characterization of domestic and industrial sewage in S. Cal. Coastal sediments using N, C, and S tracers. *Marine Environmental Research* 3: 225 - 248.

Taniguchi, M. and Iwakawa, H. 2001. Measurements of submarine groundwater discharge rates by continuous heat-type automated seepage meter in Osaka, Japan. *Groundwater Hydrology* 43(3): 271 - 277.

Taniguchi, M. and Iwakawa, H. 2004. Submarine Groundwater Discharge in Osaka Bay, Japan. *Limnology* 5: 25 - 32.

Taniguchi, M. and Fukuo, Y. 1993. Continuous measurements of groundwater seepage using an automatic seepage meter. *Ground Water* 31: 675 - 679

Taniguchi, M., Burnett, W.C., Cable, J. E. Turner, J. V. 2002. Investigations of submarine groundwater discharge . *Hydrological Processes* 16: 2115 - 2129.

Taniguchi, M., Burnett, W. C., Smith, C. F., Paulsen, R. J., O’rourke, D., Krupa, S. Christoff, J. 2003a. Spatial and temporal distributions of submarine groundwater discharge rates obtained from various types of seepage meters at a site in the Northeastern Gulf of Mexico. *Biogeochemistry* 66, 35–53.

Taniguchi, M. and Fukuo, Y. 1993. Continuous measurements of groundwater seepage using an automatic seepage meter. *Ground Water* 31: 675 - 679.

Taniguchi, M., Stieglitz, T. and Ishitobi, T. 2008. Temporal variability of water quality of submarine groundwater discharge in Ubatuba. *Estuarine, Coastal and Shelf Science, Brazil* 76(3): 484 - 492.

Taniguchi, M., Stieglitz, T., Ishitobi, T., Burnett, W. S. and Wattayakorn, G. 2007. Evaluating groundwater – sea water interactions via resistivity and seepage meters. *Groundwater* 45(6): 729 - 735.

- Taniguchi, M., Turner, J.V. and Smith, A.J. 2003b. Evaluations of groundwater discharge rates from subsurface temperature in Cockburn Sound, Western Australia. *Biogeochemistry* 66: 111 - 124.
- Thorstenson, D. C. and Mackenzie, F. T. 1974. Time variability of pore water chemistry in recent carbon sediments, Devil's Hole Harrington Sound Bermuda. *Geochemica et Cosmochimica Acta* 38: 1 - 19.
- TIQ. 2006. A dictionary of quarrying terms'. The Institute of Quarrying. Nottingham, UK, NG15BS.
- Tomasko, D. A., Dawes, C. J. and Hall, M. O. 1996. The effects of anthropogenic nutrient enrichment on turtle grass (*Thalassia testudinum*) in Sarasota Bay, Florida. *19(2B)*: 448 - 456.
- Toth J, 1963. A theoretical analysis of groundwater flow in small drainage basins. *Journal of Geophysical Research* 68: 4785 - 4812.
- Ullman, W. J. and Aller, R. C. 1982. Diffusion coefficients in nearshore marine sediments. *Limnology and Oceanography* 27(3): 552 - 556.
- USGS 2007. Retrospective review of watershed characteristics and a framework for future research in the Sarasota Bay watershed, Florida. Open-File Report 2007 - 1349, pp 49.
- Valiela, I., Costa, J., Foreman, K., Teal, J. M., Howes, B. and D. Aubrey. 1990. Transport of water-borne nutrients from watersheds and their effects on coastal waters. *Biogeochemistry* 10: 177 - 198.
- Visser M. J. 1980. Neap-spring cycles reflected in Holocene subtidal large-scale bedform deposits: a preliminary note. *Geology* 8: 543 - 546.
- Zanini, L., Robertson, W. D., Ptacek, C. J., Schiff, S. L. and Mayer, T. 1998. Phosphorus characterization in sediments impacted by septic effluent at four sites in central Canada. *Journal of Contamination Hydrology* 33(3 - 4): 405 - 429.

BIOGRAPHICAL SKETCH

Personal Information

Name: Benjamin M. Mwashote
Marital Status: Married

Professional Experience

- 1988 to date: Research Scientist (Environmental Chemistry and Chemical Oceanography). Research involved is in Aquatic (Marine and Freshwater) Environmental Studies which include: Biogeochemistry; Nutrient Flux and Marine Pollution Studies within Estuarine and Nearshore Coastal Environments; Groundwater (Submarine Groundwater Discharge, SGD) Measurements and Development of Quantification Techniques (or Instrumentation); Ecological Processes.
- 1988 - 2003: Research Scientist, Kenya Marine and Fisheries Research Institute (KMFRI). Area of environmental research include: Groundwater and Surface Water Quality, Nutrient Flux studies, Marine Pollution (trace or heavy metals).
- 1990 - 1993: Head of Research Division, KMFRI-Sangoro Research Station.
- 1993 - 1995: Research team member, EEC-STD3 Project on “Interlinkages Between East African Coastal Ecosystems.”
- 1996 - 1997: Research team member of the KMFRI/KWS Biodiversity Project on “Ecological Survey of Mida Creek Biodiversity.”
- 1997 - 1998: Principal Investigator in the IOC-UNESCO (WIOMSA MARG I) funded project “The Status of Cadmium, Cd, and lead, Pb, Concentration Levels in Water, Sediment and Some Selected Fish Species in the Kenyan Coast.”
- 1997 - 1999: Research team member of the EEC-INCO project on “Anthropogenically Induced Changes in Groundwater Outflow and Quality, and Functioning of East African Nearshore Ecosystems.”
- 1999 - 2003: Principal Investigator in the project “Assessment of the Water Quality of the Kenya Coastal Waters with Emphasis on Groundwater: Implications to the Health Status of Nearshore Ecosystems and Coastal Communities.”
- 2000 - 2003: Member of the project initiative “IGBP-LOICZ AfriBASINS,” a global assessment effort geared toward addressing coastal change issues and human dimensions from the perspective of nutrients, sediments and other material through the catchment/coast cascade.
- 2004 - 2006: Research Team Member of FSU-DEP SGD Project with Profs. Bill Burnett and Jeff Chanton.
- 2004 - 2007: Research Assistant (RA)/Teaching Assistant (TA), FSU-Department of Oceanography.
- 2006 - 2008: Research Team Member of the NSF-FSUML Project on SGD Study in the Northern eastern Gulf of Mexico.
- 2008: Instructor, Chemistry & Oceanography in RIMS Program, FAMU.

- 2008 & 2010: Participated in the Academy of Teaching, Learning And Success (ATLAS), Adjunct Training Program, 8th Sep -17th Nov 2008 & 22nd Jan – 19th Apr 2010, Tallahassee Community College (TCC), Tallahassee, Florida, USA.
- 2008 - 2009: Appointed into the Program for Instructional Excellence for TA's (PIE - Associate) - FSU.
- 2008 to date: Appointed Adjunct Faculty for Earth Science (Oceanography) and Math Courses at the Tallahassee Community College (TCC), Tallahassee, Florida, USA.
- 2008 to date: Appointed Tutor for Oceanography, Environmental Sciences; Sciences (Chemistry & Physics) and Math at the Center for Academic Retention and Enhancement (CARE) – FSU.
- 2010: Involved in the FSU - Pwani University College (Kenya) Research and Educational Cooperative Agreement - Initiative.
- 2010: Invited Visiting Speaker at Appalachian State University, Geology Department Seminar Series, Fall Term (<http://www.geology.appstate.edu/seminar.htm>).

Academic Awards, Honors and Memberships

- 2003: Distinguished Award of Membership to the American Association for the Advancement of Science (AAAS).
- 2004-2006: IFP Fellow, IFP – Ford Foundation PhD Fellowship recipient. Enrolled for PhD Program at FSU-Oceanography Department.
- 2006: Member of the National Groundwater Association (NGWA), USA.
- 2007: Awarded Exclusive Academic Honor Recognition Membership to The Golden Key International Honor Society (GKIHS).
- 2008: Awarded Exclusive Academic Honor Recognition Membership to The National Scholars Honor Society (NSHS).
- 2009: Awarded Program for Instructional Excellence Recognition Honor (PIE-Teaching Associate Academic Honor) Award for Professional Commitment to Excellence in College Teaching. Florida State University, USA.
- 2009: Appointed Member of The Editorial Board, Journal of Oceanography and Marine Science (JOMS).
- I have authored and co-authored several scientific published papers and reports, many of them in international peer reviewed journals (please see selected examples shown below).

Non-Academic Awards and Honors

Always interested and consider it a great privilege to participate in important activities that are beneficial to society whenever opportunity permits. There are numerous awards and honors within this category.

Education/Training

Institution & Location	Degree	Year(s)	Field of Study
University of Nairobi, Kenya.	B. Sc (hons)	1984-1987	Chemistry
University of Nairobi, Kenya.	M. Sc	1993-1997	Environmental Chemistry
Florida State University, USA.	PhD	2004-2010	Chemical Oceanography

Selection of Recent Publications (2002 - 2010)

1. **Mwashote, B. M.** 2010. Submarine groundwater discharge: its measurement and implications for nutrient inputs and biogeochemical processes in the nearshore coastal zone. *PhD Dissertation in Chemical Oceanography, Florida State University, USA (defended, graduation in Fall, 2010). Pp. 173.*
2. **Mwashote, B. M.**, Burnett, W. C., Chanton, J., Santos, I., Dimova, N. and Swarzenski, P. W., 2010. Calibration and use of continuous heat-type automated seepage meters for submarine groundwater discharge measurements. *Estuarine Coastal and Shelf Science, 87: 1- 10.*
3. **Mwashote, B. M.**, Murray, M., Burnett, W. C., Chanton, J., Kruse, S and Harrison, A. 2010. Submarine Groundwater Discharge in the Sarasota Bay System: Its Assessment and Implications for the Nearshore Coastal Environment (in prep).
4. **Mwashote, B. M.** and Burnett, W. C. 2010. Assessment and Elimination of Environmentally Induced Artifacts in Submarine Groundwater Discharge Measurements Using Benthic Chamber Based Seepage Meters (in prep).
5. **Mwashote, B. M.** 2010. Submarine Groundwater Discharge: Its Importance and Quantification. *SciTopics*.
http://www.scitopics.com/Submarine_Groundwater_Discharge_Its_Importance_and_Quantification.html.
6. **Mwashote, B. M.**, Ohowa, B. O. and Wawiye, P. O. 2005. Spatial and temporal distribution of dissolved inorganic nutrients and phytoplankton in Mida Creek, Kenya. *Journal of Wetland Ecology and Management, 13: 599 - 614.*
7. **Mwashote, B. M.** 2003. The Status of Cadmium, Cd, and Lead, Pb, Concentration Levels in Water, Sediment and Some Selected Fish Species in The Kenyan Coast. *Western Indian Ocean Journal for Marine Science, 2(1): 25-34.*
8. **Mwashote, B. M.**, Mwangi, S. N., Mwaluma, J. M., Mitto, C. K. and Emuria, J. E. 2003. The Status of Water Quality in the Kenya Coastal Waters With Emphasis on Groundwater. *KMFRI Technical Series Report. Pp. 48.*

9. **Mwashote, B. M.** and Jumba, I. O. 2002. Quantitative aspects of inorganic nutrient fluxes in the Gazi Bay: Implications for coastal ecosystems. *Marine Pollution Bulletin*, 44(11): 1194-1205.
10. **Mwashote, B. M.** and Ohowa, B. 2002. Nutrient Dynamics. In J. Uku and J. Kitheka (eds) Mida Creek: The Physical and Biological Aspects. *KWS Technical Series Report*. Pp. 10-11.
11. Santos, I. R., Dimova, N., Peterson, R. N., **Mwashote, B. M.**, Chanton, J. and Burnett, W.C. 2009. Extended time series measurements of submarine groundwater discharge tracers (²²²Rn and CH₄) at a coastal site in Florida. *Marine Chemistry* 113: 137 – 147.
12. Santos, I., Burnett, W. C., Chanton, J., **Mwashote, B. M.**, Suryaputra, I G. N. A., and Dittmar, T. 2008. Nutrient Biogeochemistry in a Gulf of Mexico Subterranean Estuary and Groundwater-Derived Fluxes to the Coastal Ocean. *Limnology and Oceanography*, 53(2): 705-718.
13. Burnett, W. C., Chanton, J. P., **Mwashote, B. M.** and Fuleky, P. 2005. Simplified Approach to Estimating Groundwater Discharges. DEP Project Final Report, 12p.
14. Kitheka, J. U. and **Mwashote, B. M.** 2002. Estuarine Systems of Kenya: Gazi Bay Mangrove Creek. In Dupra, V., Smith, S. V., David, L. T., Waldron, H., Marshall Crossland, J. I. and Crossland, C. J. (eds.). Estuarine Systems of Africa (regional Workshop II): Carbon, Nitrogen and Phosphorus Fluxes. LOICZ Reports & Studies No. 20, i+81 pages, LOICZ, Texel, The Netherlands. Pp. 52-58.